CADMIUM SELENIDE NANOCRYSTALS FOR SPECIFIC INTERACTIONS WITH BIOMOLECULES

PAR

Isabelle GEISSBÜHLER

chimiste diplômée de l'Université de Lausanne
de nationalité suisse et originaire de Lützelflüh (BE)

acceptée sur proposition du jury:

Prof. H. Vogel, Prof. M. Grätzel, directeurs de thèse
Prof. H. Hofmann, rapporteur
Prof. G. Schmid, rapporteur
Prof. M. Textor, rapporteur

Lausanne, EPFL
2005

Table of contents

6

Abstract

The goal of this work was to produce water-soluble fluorescent semiconductor nanocrystals suitable to interact specifically with biomolecules and thereby creating hybrid supramolecular structures composed of nanocrystals and proteins.

Hydrophobic TOPO-coated cadmium selenide (CdSe) nanocrystals (NCs) were synthesized using published protocols (TOP/TOPO method). The challenge was to find a novel procedure to solubilize and functionalize the NCs in water for further specific interactions with biomolecules. We therefore coated the NCs with a lipid mono-layer (lipid-NCs) in a one-step process. The lipid monolayer made the NCs water soluble and simultaneously allowed to decorate the NCs surface with different functional groups. The resulting lipid-NCs are functionalized, fluorescent and stable; they can thus be used for further interaction with biomolecules.

The ability of the functionalized lipid-NCs to bind specifically to biomolecules was demonstrated for His_6-NCs, biotin-NCs and NTA-NCs (hexahistidine, biotin and nitrilotriacetic acid NCs) using fluorescence resonance energy transfer (FRET). Multi-functional NCs were also produced by decorating the NCs with biotin and NTA simultaneously; these NCs showed specific interactions toward to the complementary partner molecules.

The properties of the lipid monolayer coat on the NCs surface were characterized by investigating its interaction with the peripheral membrane protein cytochrome c. This protein bound to the lipid-NCs only in the presence of negatively charged lipids, very similarly as in the case of lipid vesicles and mitochondrial membranes.

The functionalized-NCs could also be immobilized on micro-patterned surfaces for creation of a photostable, fluorescent patterned surface for biosensor applications. We could observe via FRET the specific binding of a fluorescent protein on the NCs patterns.

Version abrégée

Le but de cette thèse était la production de nanocrystaux (NCs) fluorescents et leur utilisation pour la création d'assemblage hybride entre les NCs et des molécules biologiques comme des protéines.

Cette recherche s'est orientée dans la modification de la surface des NCs de semi-conducteur CdSe par recouvrement d'une couche lipidique. Pour obtenir des NCs ayant des propriétés optiques intéressantes, leur synthèse se fait en milieu organique (oxyde de trioctylphosphine, TOPO) à haute température et résulte donc en la formation de colloïdes solubles dans les milieux organiques. Le problème était alors de trouver un moyen de les solubiliser dans l'eau et de les fonctionnaliser pour permettre des interactions spécifiques avec des biomolécules. Nous avons ainsi développé un moyen efficace et versatile de solubiliser et fonctionnaliser simultanément les NCs en les enveloppant avec une monocouche de phospholipides comprenant des lipides fonctionnalisés (lipide-NCs).

Ces lipides-NCs fonctionnalisées interagissent spécifiquement avec les biomolécules complémentaires, ceci a été démontré par transfert résonnant d'énergie de fluorescence en solution (FRET) avec des biomolécules complémentaires fluorescentes.

L'adsorption d'une protéine périphérique, ici le cytochrome c, sur la surface des lipide-NCs a été étudiée, démontrant la possibilité pour la monocouche de mimer une biomembrane. L'interaction de la protéine périphérique avec la monocouche de lipides concorde avec les observations qui ont été faites auparavant sur des vésicules ou sur la membrane interne des mitochondries.

Les lipide-NCs fonctionnalisées ont été spécifiquement immobilisées sur des surfaces micro-structurées résultant en des micro-domaines fluorescents et photostables applicables à des biosenseurs. L'attachement spécifique d'une protéine fluorescence est également démontré par FRET.

1 Introduction

1.1 Small is beautiful

The research described in this thesis focuses on the use of nanomaterials within biology. The nanometer world is a particular domain in which the dimensions of the materials reach the nanometer regime, where their behavior, characteristics and physico-chemical properties change drastically from those of bulk materials [1, 2] approaching the molecular features. It neither possesses the bulk properties nor those of the molecules [3].

Nanomaterials enclose all materials within a large domain of sizes, which scales from a nanometer to particles as large as hundreds of nanometers. We can classify them into nanostructured materials and nanoparticulate materials, the former group is about condensed bulk materials that contain grains or composites with sizes that are in the nanometer range, the later are dispersed or colloidal nanoparticles (NPs).

Nanotechnology has become a key word in scientific research as well as in the public interest in the 1990's. It is considered as the technology of the 21st century, following the microtechnology development. It has already taken a remarkable part in our daily lives, even if we do not realize it yet. These particular and interesting properties make the NPs applicable in a variety of fields like miniaturized devices [4], light-emitting diodes [5-7], photovoltaic [8], lasers [9], optical memory [10, 11] or as fluorescent probes for diagnostic markers in biology [12-16].

Nanoparticles can be considered as a single "crystal" of a typical size of a few nanometers consisting of 100's to 1,000,000's of atoms, which preserve some of the attributes of the bulk material but exhibit in addition very interesting properties due to the **size quantization effect**. The nanoparticles can be in a variety of state from pure or mixed solid materials to the state

of powder, thin films or colloidal solutions. The name nanoparticle (NP) states for all colloidal materials in the nanometer range, as the designation nanocrystal (NC) is used mostly for semiconducting highly crystalline nanoparticles, as in our case. The name quantum dot (QD) is also often used for highly fluorescent NCs [14] and newly commercially available fluorescent nanoparticles (Qdots from Quantum Dot, Quantum Dots from Biopixel or Evidots from Evident).

The following list enumerates some examples of materials, which can be produced in the nanometer range, giving rise to nanoparticles:

- Metals: gold [17], silver [18], palladium, platinum, cobalt.
- Oxides: ZnO [19], TiO_2.
- Semiconductors: silicon [20], II-VI [21] (CdS [22], CdSe [21, 23], CdTe [24], ZnS [19], ZnSe [25]), III-V [26, 27] (GaAs [28, 29], GaP, GaN, InAs, InP [30]) and the IV-VI group (PbS [31], PbSe, PbTe).

The nanoparticles possess a variety of properties depending on their chemical composition. Metal nanoparticles such as gold or silver exhibit plasmon absorbance bands in the visible spectral region that are controlled by the size of the particles. Numerous studies reported on the labeling for bioassays and staining of biological tissues using those metal nanoparticles as means to analyze and visualize biological processes [32-38]. These metal nanoparticles (especially gold) are commercially available and produced in a size range of 5 to 100th of nanometers (nm) and in very monodispersed way.

Oxides are mostly used as nanostructured materials, or nanoparticulate films in e.g. the well-known nanocrystalline films of titanium dioxide for dye-sensitized solar cells developed by Professor M. Graetzel [39, 40]. Zinc oxide was also produced as colloidal solutions, their emission and absorption spectra lie in the UV to blue region. Doping these NPs with different metals as e.g. manganese or lithium [41, 42] can shift the emission bands of ZnO to larger wavelengths.

For this thesis, the synthesis was concentrated on production of CdSe nanocrystals, the advantages being: First, they have been intensively studied and produced with well-developed synthesis routes giving rise to nearly-monodispersed solutions [21, 23]; Second, they feature attractive optical properties as bright fluorescence emission and wide absorption band

in the visible region, wavelengths depending on the NCs size (figure 1.1.1), sharp emission peaks and high photostability [43].

Figure 1.1.1: Fluorescence photograph of solutions containing CdSe nanocrystals of different sizes, from blue the smallest to red the biggest ones. This illustrates well the variation of the emitting domains with increasing sizes. This image is taken from the Biopixel website.

The interesting properties of these nanocrystals motivated a lot of research on their exploitation in biological imaging. The utilization of NCs with different sizes allowed multicolor imaging or multiplexing on living cells with a single excitation wavelength [44-46]. Figure 1.1.2 illustrates a multicolor image of specific parts of cells using functionalized NC from Qdot Corporation.
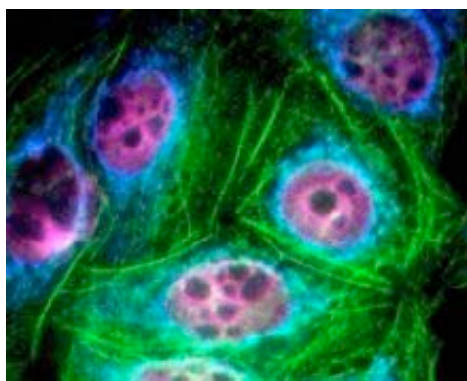
Figure 1.1.2: Fluorescence image of HepG2 cells stained with Qdot 655 Goat F(ab')2 anti-Mouse IgG Conjugate (H+L) (blue), Qdot 605 Protein A Conjugate (red) and Qdot 565 Streptavidin Conjugates (green). This image is an application example from Qdot Corporation products (www.qdots.com).

The photostability of the NCs allowed Dahan et al. [47] to use QDs to track individual glycine receptors and analyze their lateral dynamics in the neuronal membrane of living cells for

periods ranging from milliseconds to minutes. The long photostability allowed as well Dubertret et al. to observe embryogenesis of NCs stained *Xenopus* embryos [13].

Here, work concentrated on the surface modification to obtain fluorescent water-soluble NCs and their biological applications, through bio-functionalization and specific interactions with biomolecules.

1.2   Quantum size effect

Although the Egyptians knew of the "metaphysical" and healing powers of gold nanoparticles, and the use of colloidal particles of different materials was known and used by the Romans toward the middle age (for e.g. staining of glass), it was the great alchemist Paracelsus who first prepared gold colloid solution in modern times. But serious study on gold colloids did not start until the mid-19th century by Faraday, who prepared colloidal gold in 1857, and many uses were found for his solutions of "activated gold". These colloidal solutions were the first contacts with size effects.

When we move from bulk material toward smaller and smaller aggregates, we realize that reaching certain dimensions one begins to enter a new regime where the particles start to experience changes in their properties compared to the bulk material. The properties difference in between the bulk material and the isolated molecules is already known. In fact the nanomaterial domain is a bridge in between the two, implying that their properties lie between those of the bulk and the isolated molecules.

About size quantization effect, the passage from bulk to nanomaterials is manifested when their size get small enough that the charge carriers inside the particle start to feel the volume limitations, the "walls" of the particles. As we know from elemental quantum mechanics, when the electronic particles or charge carriers (electrons and holes) are confined in a volume limited by potential barriers that are comparable or smaller than the deBroglie wavelength of the particle, their allowed energy states become discrete (quantized) rather than continuous as in the bulk material.

In semiconductor materials, the electric current is carried by electrons and holes [48]. There is an energy gap or band gap (Figure 1.2.1) between the allowed energies of the electrons in the material that separates the normally filled energy levels of the valence band (where missing

electrons behave like positively charged current carriers called "holes") and the conduction band (where electrons behave like a gas of free negatively charged carriers). The band gap width in between the two bands depends on the nature of the material, but also on temperature and pressure. The absorption of energy can elevate electrons to the conduction band leaving a hole in the valence band. In bulk semiconductors, the two charge carriers are separated by the energy of the band gap. At low temperature, these two charge carriers form a weak coupled pair, which is called **exciton**. The energy of the exciton lies below the energy of the band gap of the semiconductor crystal because of the electrostatic Coulomb interaction. Quantization depends on spatial confinement and can be classified in three different regimes: confinement in one, two or three dimensions. Confinement in one dimension produces quantum films, in two dimensions quantum wires and confinement in three dimensions produces quantum particles, often referred to as quantum dots, nanoparticles or nanocrystals. Fundamental differences exist between the three different quantization regimes, for example the density of states (DOS) as a function of the energy is quite different for each quantum system (Figure 1.2.1 B). For quantum films the DOS is a step function while for the quantum dots it is a series of discrete values resembling that of a molecule or an atom. Quantum wires have a DOS distribution that is intermediate between the quantum films and the quantum dots.
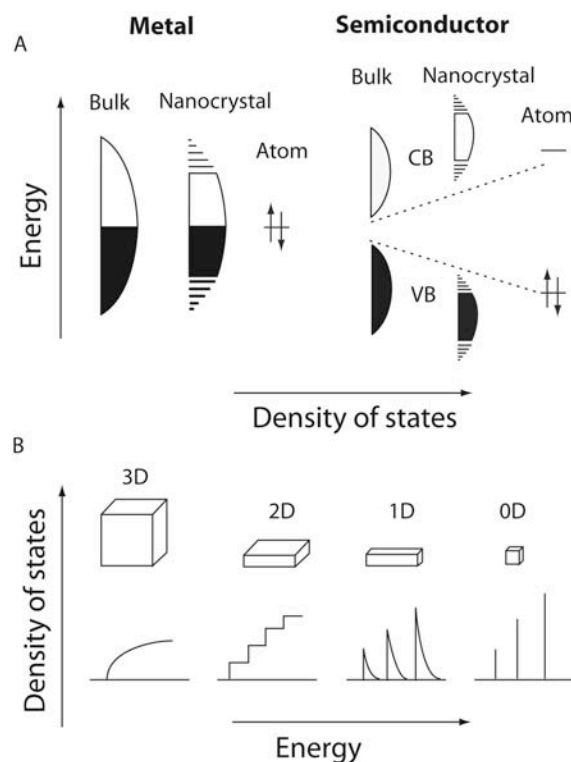
Figure 1.2.1: A) Schematic illustration of the density of states in metal and semiconductor clusters according to Alivisatos [14]. For semiconductors, the dashed lines are showing the increasing band gap separations for bulk toward molecule, between valence band (VB) and conduction band (CB). B) Density of states in one band of a semiconductor as a function of the dimensional freedom. 3D represents the bulk, 2D quantum films, 1D quantum wires or fibers and 0D the zero dimensional quantum dots.

The great interest in these materials is mostly due to the optical, electrical and photoredox properties of the semiconductor and which can be tuned and manipulated in many ways, just by controlling the shape and dimensionality of the material.

The following discussion will be focused on the semiconductor quantum dots or nanocrystals that were used for this thesis. When the size of the bulk material is reduced in all 3 dimensions and approaches the value of the Bohr radius (a_B) of the bulk material, we then deal with a zero-dimension electronic system [49]. The Bohr radius for CdSe is $a_B = 56$ Å.

The most easily observable effect is the blue shift of the optical absorption and emission of the semiconductor quantum dot with decreasing size resulting from the increasing band gap. For example, bulk CdSe has a band gap of 1.74 eV or 714 nm, but when it is produced as quantum dots with average diameter of 1, 2 or 3 nm absorption onset will become 400, 480 or

540 nm (3.10, 2.58 or 2.29 eV) respectively, and emission spectra will be similarly shifted. Relation between eV and nm units is

$$E(eV) = \frac{1.2398 \cdot 10^3}{\lambda(nm)}$$

1.1

Moreover interband optical transitions will appear in the absorption spectra, as the valence and conduction bands separates into a number of discrete energy states. This phenomenon is a manifestation of the size quantization effect at these dimensions; meaning the spacing between allowed energy levels becomes sensitive to the size of the NC (charge carriers start to feel the energy barrier of the walls of the quantum dot).

Quantum size effect on small particles in suspension was first reported in the early 1980s by Ekimov [50], Efros [51] and Papavassiliou [52]. Shortly later, Brus et al. [53, 54] laid out the proper framework for understanding the observed effects from the point of view of molecular quantum chemistry. Other models have been developed as well [55, 56], but here, the effective mass approximation was used as it gives a good sentiment of the phenomenon [53, 54]. Taking the radiative recombination of photogenerated electron-hole pair, before thermalization or trapping, the pair is called a Wannier exciton and is assigned as a single particle in an excited state in which the electron and hole are coupled by attractive Coulomb forces and no net charge is present. Electronic particles diffract off the periodic lattice of the crystal and behave as if they have an inertial mass different from the free-electron mass. This mass is designated as the effective mass m* [57, 58].

In II-VI and III-V semiconductors, excitons are considered to be similar to a hydrogen atom and can be well described by a hydrogenlike model incorporating the effective mass and the screening described by the dielectric constant. Brus et al. [54] considered that unlike in bulk materials where the electron-hole pair is free to move, in small quantum dots they can become physically confined. Strong confinement leads to a rising of the electronic energy in the same way as would be expected from the simple particle-in-a-box model of quantum mechanics.

If we take a simple example of quantum chemistry as the one-dimensional problem of a particle subjected to a stepped potential energy function infinite everywhere except for a finite line segment of length L. The explicit form of the Schrödinger equation under these conditions is as following

$$\frac{\partial^2 \Psi}{\partial^2 x^2} = \frac{8\pi^2 m}{h}\left(E - \infty\right)\Psi = 0 \qquad\qquad 1.2$$

where Ψ outside the box is zero and inside the box $\Psi = c_1 e^{i\theta} + c_2 e^{-i\theta}$, where $\theta = (2mE)^{1/2}(2\pi x/h)$. Solving the equation yields to the energy equation

$$E = n^2 \frac{h^2}{8mL^2}, n = 1,2,3,... \qquad\qquad 1.3$$

which satisfies the boundary condition of continuity at $x = L$. The boundary condition allows only quantized energy levels, in other words the spectrum of eigenstates is discrete. In comparison the energy of a free particle could have any value. We should notice also that the energy E is inversely proportional to the square of L meaning that the energy increases quadratically as the size of the "box" is reduced. This treatment can be applied easily to the problem of excitonic energy levels of the semiconductor clusters, with some minor modifications. Mohan et al. used the quantum Monte Carlo (random walk) method to calculate the energies of the Wannier excitons in clusters of varying shapes and sizes and reported the results for spheres, cubes and rectangular parallelepipeds of semiconductors CdS and ZnO [59]. Using these results, calculation was made for a spherical quantum dot by Dwayne Miller et al. [60], they used the bulk values of m^*_e and m^*_h, and approximated the wave function by a few configurations of $\Psi_i(r_e)\Psi_j(r_h)$ of the particle-in-a-sphere wave functions. Schrödinger equation for the quantum dot could be written as

$$\left[\frac{-h^2}{8\pi^2 m^*_e}\nabla^2_e \frac{h^2}{8\pi^2 m^*_h}\nabla^2_h + V_0(\xi_e,\xi_h)\right]\Phi(\xi_e,\xi_h) = E\Phi(\xi_e,\xi_h) \qquad\qquad 1.4$$

where the new parameters ξ_e and ξ_h represent the position of the two charges of magnitude e inside the sphere. Then following Weller et al. [61], the energy difference between the lower edge of the conduction band of the cluster and the vacuum level (wall of the sphere, with $V_0 = \infty$ outside) is in fact not infinite but $V_0 = 3.8$ eV [62] for aqueous environment. In reality the potential barrier is not infinite and results in a surface polarization of the NP. This may influence self-trapping of the charge carriers at the surface of the dot, the effect being more pronounced for heavier holes (see part 1.5) [63].

This implies that the expected quantum size effect will be lower, implying that to see a high effect smaller sizes should be reached. By using the wave functions for the particles in a sphere

$$\Psi_n = \frac{C_n}{r} \sin\left(\frac{n\pi}{R}\right) \qquad\qquad 1.5$$

where r is the radial position, C_n are normalization constants and R is the radius of the sphere, and

$$E_n = \frac{h^2 n^2}{8mR^2} \qquad\qquad 1.6$$

The size dependence of the energy of the first excitonic transition upon radius R can then be estimated. By using the wave function $\Phi = \Psi_i(r_e)\Psi_j(r_h)$, the energy of the lowest excited state becomes.

$$E_n = \frac{h^2}{8mR^2}\left[\frac{1}{m_e^*} + \frac{1}{m_h^*}\right] - \frac{1.8e^2}{\varepsilon_2} + \left\langle \frac{e^2}{R}\sum_n \alpha_n \right\rangle \qquad\qquad 1.7$$

where the $\langle\ \rangle$ means an average over Ψ_n. The second term is the Coulomb attraction and the third term is the solvation energy loss, where

$$\alpha_n = \frac{(\varepsilon + 1)(n + 1)}{\varepsilon_2(\varepsilon n + n + 1)} \qquad\qquad 1.8$$

and $\varepsilon = \varepsilon_2/\varepsilon_1$. The terms ε_2 and ε_1 are the dielectric coefficients of the sphere and the medium (solution), respectively. If we do the calculation for CdS, $E_g = 2.42$ eV, $m_e^* = 0.21$, $m_h^* = 0.8$, and $\varepsilon = 5.4$ [64], the energy shift for a 4.5 nm diameter cluster is 2.58 + 0.38 = 2.96 eV or 418 nm (for CdS, the third term of equation 1.7 is less than 0.05 eV for NPs greater than 2 nm, thus neglected). An illustration of the size quantization effect is shown for a range of cluster sizes for different semiconductor particles in figure 1.2.2.
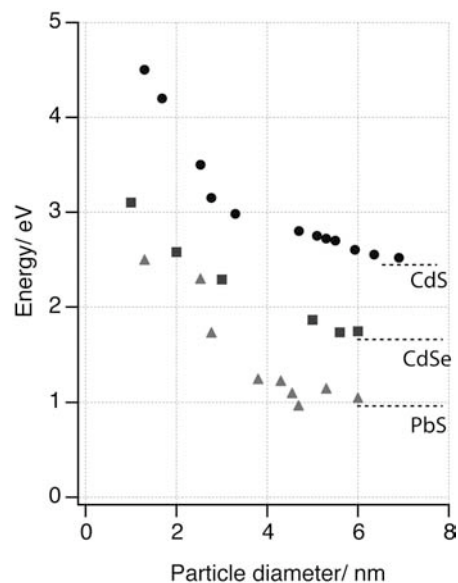
Figure 1.2.2: Illustration of the band gap energy changes in function of semiconductor nanoparticle diameter taken from Weller [2] for PbS (grey triangles) and CdS (black circles), and calculated for CdSe (black squares).

While some researchers assume the applicability of the effective mass approximation for small clusters sufficiently adapted for approximative estimations, others claim that it is not really appropriate and gives rise to large deviations (errors) for very small particle sizes, implying generally a overestimation of the band gaps [55, 65, 66]. Calculations using pseudopotentials or tight-binding calculations provide much better agreement between predicted and experimental band gaps for CdS and CdSe quantum dots at very small clusters sizes (diameter smaller than 3 nm).

Another approach to the problem can then be an adjustment of the effective mass for the very small particles. An elaborated calculation that relates oscillator strengths to the effective mass was used to calculate the change in effective mass as a function of two-dimension confinement in superlattices (this for the very small sizes) [67]. For example, the effect is significant only below 3 nm for CdTe, with $E_g=1.6$ eV, where the effective mass increases gradually as the lateral dimension is reduced, peaking at +15% of the bulk value at 3 nm, and after that precipitously decreases to near zero as the radius approaches zero.

In semiconductors with very small carrier effective masses, the effective mass approximation breaks down even for bulk materials. A rigorous solution to this problem would be to add a correction term to the equation 1.7 to account for the band nonparabolicity that causes this effect [54, 60].

1.3 Thermodynamic Changes

While the size quantization effect is mainly considered to describe physical properties, the surface or interface induced effect, plays an eminent role for chemical processing, in particular in connection with heterogeneous catalysis. The later effect can be experienced by measurement of thermodynamic properties [68]. One particular interesting phenomenon is the size-dependent melting point depression in nanomaterials; the smaller particles possess a lower melting point than the bulk. This can be understood via the two following explanations. First, the cohesion energy of the crystal comes from the sum of the pair-wise interactions between the atoms. In a very small crystal the number of surface atoms is large and therefore the cohesion energy per atom has not yet converged to the bulk values. From a thermodynamic point of view, as a solid is heated, melting takes place at the temperature when the chemical potential of the solid and liquid are equal. For very small crystal, a term for the surface energy is added to the usual chemical potential. As a consequence, the smaller the nanocrystal the lower its melting temperature will be, dependent on the surface to volume ratio or inversely proportional to the nanocrystal radius. This effect is illustrated in figure 1.3.1.
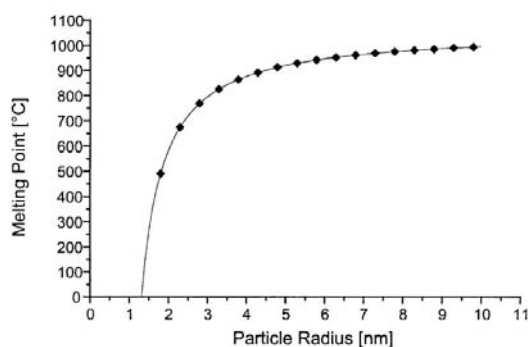

Figure 1.3.1: Relation between the size of gold particles and their melting point temperature [69].

To illustrate the great importance of the surface atom ratio in the nanoscale range, table 1 is illustrating different cluster sizes and the consequences on surface atom to total atom ratio, taken from Prof. H. Hofmann lecture on nanoparticulate materials (EPFL).
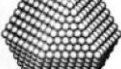
	1 shell	2 shells	3 shells	4 shells	5 shells	7 shells
Full-shell clusters						
Total N° of atoms	13	55	147	309	561	1415
Surface atoms (%)	92	76	63	52	45	35

Table 1: The relationship between the total number of atoms in full-shell clusters (metal) and the percentage of surface atoms. Idealized representation of hexagonal close packed full-shell "magic number" clusters according to Prof. H. Hofmann.

1.4   Absorption mechanisms of NCs

There is a close relation between the electronic structure, the optical properties and the nanocrystal size. Optical spectroscopic methods probe the energy differences between electronic states as well as the lifetimes of excited states and their respective energy relaxation channels using time-resolved techniques. The decrease of particle size shifts the onset of absorption from the infrared to the visible region of the electromagnetic spectrum as the band gap energy of the semiconductor increases (Figure 1.4.1). From a molecular point of view it corresponds to an energy decrease of the highest occupied molecular orbital (HOMO) and increase of the lowest unoccupied molecular orbital (LUMO) due to the spatial confinement of the charge carrier wavefunctions. By changing the size of the semiconductor quantum dots one can tune the color of the NCs as well as their oxidation-reduction properties.

1.4.1   Absorption spectra

If we take the example of CdSe quantum dots, reducing the size of the NCs induces a shift of the absorption onset toward higher energies and the development of different discrete bands (quantization) in the absorption spectra due to the different possible transitions. These features are familiar from the "particle-in-a-box" model.

Typical absorption spectra of CdSe NCs synthesized during this thesis work (chapter 2) are depicted in Figure 1.4.1 together with the calculated energy level and transitions.
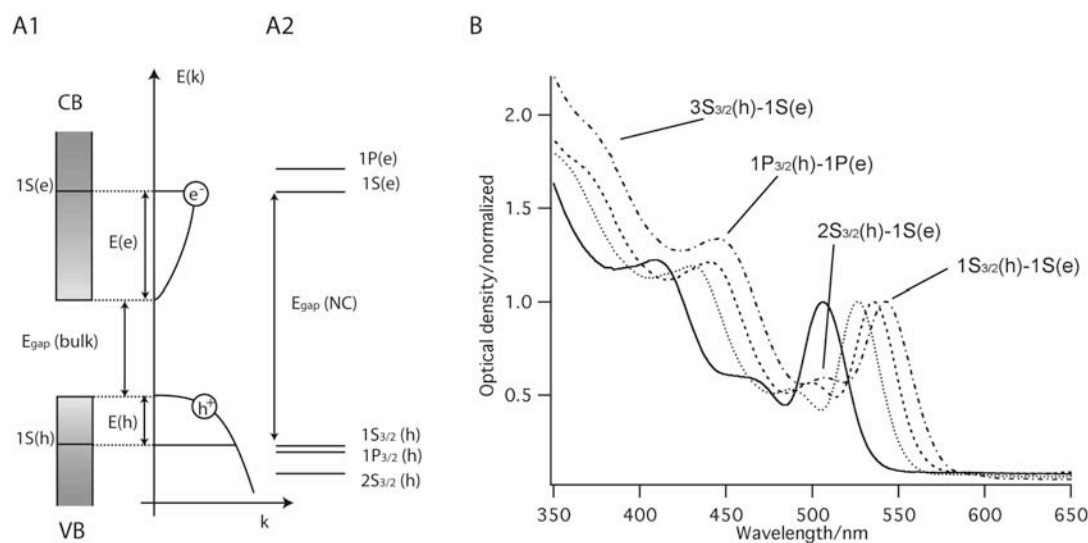
Figure 1.4.1: A1) Energy E(k) of the electron (e⁻) and hole (h⁺) states of CdSe bulk as a function of their the wave vectors in the strong confinement regime. A2) Corresponding electron and hole states for CdSe nanocrystals in a strong confinement regime, here for example $1S_{3/2}(h)$. B) Typical absorption spectra for CdSe NCs solutions in toluene synthesized as indicated in chapter 2, with method 4. The different spectra correspond to NCs of different diameters: left to right: 2.5, 3.1, 3.3 to 3.5 nm. The discrete bands in the spectra correspond to the indicated transitions.

The absorption spectra are sensitive to various physical and chemical effects, as listed here:

- Line broadening in the spectra mostly comes from the polydispersity of the ensemble of NCs, thus absorption spectra do not show discrete lines at the different maxima as it would be expected for a single nanocrystal [70]. Even the best methods of preparation do not give NCs with less than 2% deviation from the average size [23]. It also depend on the shape fluctuation of NCs [71], the crystalline defect concentration and the environmental inhomogeneities.

- The absorption spectra can be influenced by the crystal structure of the NCs. For example if CdSe NCs can form an hexagonal Wurtzite structure or cubic Zincblend structure [71].

- Solvatochromic shifts of colloidal CdSe nanocrystals absorption spectra were observed when passing from a diluted solution to a densely packed film, an effect presumed to be due to a change in dielectric environment [72].

- Doping with electrons leads to a smoothing of the band related to the first excitonic peak, and a new intraband transition in the mid-IR occurs [73].

- Covering the surface of the NCs with inorganic or organic shells also modifies the absorption spectra.

24

1.4.2 Evaluation of colloidal CdSe solutions concentration

The correlation between the peak position of the first excitonic transition and the size obtained from TEM pictures provides reliable optical sizing of the NCs as shown by Schmelz et al. [74]. Using these data allowed us to get an estimation of the size and size distribution of the synthesized samples. Absorption spectra also give an evaluation of the concentrations, the absorption cross-section and extinction coefficient of the NCs [75-77]. This was very useful for experimental purpose, particularly for the concentration determination. A table was created with experimental values of Schmelz et al. [78] correlating the first excitonic peak absorption and the concentration of the solution for optical density (OD) of 1 (figure 1.4.2). This allowed us to estimate the concentrations by measuring absorption spectra optical density at the first excitation band.
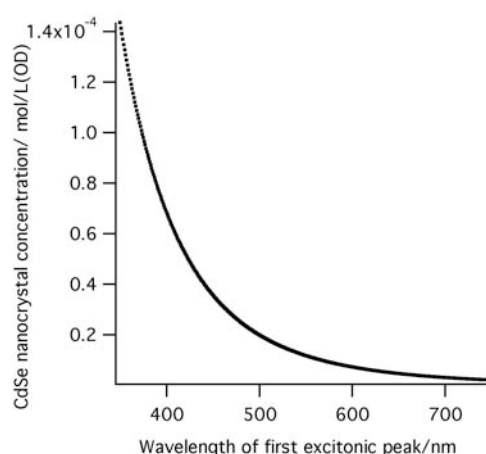
Figure 1.4.2: Dependence of the concentration on the first excitonic maximum of the absorption spectra (cuvette of 1 cm thickness and OD=1) for TOPO coated NCs in toluene. Extrapolated from our data.

1.5 Fluorescence spectra

The emission observed for CdSe NCs is a sharp peak with only a small Stokes shift corresponding to the band gap or near band gap emission resulting from the recombination of the electron-hole pair. A much broader band at longer wavelength can be observed for particles with many surface defects states, and originates from the trapped charge carrier recombination. The recombination or relaxation of the charge carriers can follow different

process as, radiative recombination (band gap emission), recombination via trap states or annihilation of the exciton or Auger processes.

1.5.1 Relaxation process

On absorption of a quantum of light, an electron is excited to energy levels over the band gap (excited states). This is followed by a very fast (picoseconds regime) nonradiative vibrational relaxation process, which brings the electron to the lowest excited state. This process can be followed by fluorescence emission (with lifetime in the nanosecond regime), the system emits a photon (fluorescence) and relaxes to the ground state [9]. But there are alternative ways for the relaxation of the electron due to trapping of electrons and/or holes by trap states within the band gap of the NC followed by weak red shifted fluorescence or nonradiative relaxation (figure 1.5.1).
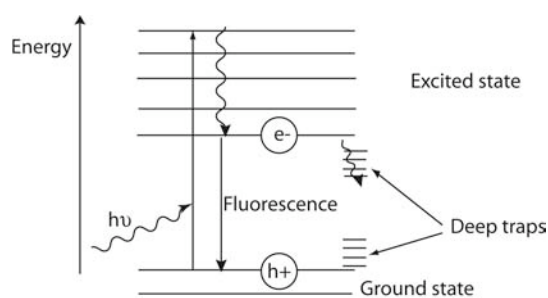
Figure 1.5.1:Schematic path for absorption of light, vibrational relaxation which occur at the picoseconds regime, and radiative recombination (fluorescence emission) or relaxation through trap states.

When the surface consists of many defect states, this leads to quenching of the band gap emission and appearance of weak deep trap long-wavelength emission. However, it has been shown that a good passivation of the surface by an organic or inorganic shell gives rise to quantum yields approaching unity at room temperature. On the other hand, extrinsic surface states can be brought by other materials in a close vicinity to the surface as ligands for example, this results in quenching of the emission. The origin of photoluminescence of semiconductors and the lifetimes longer than nanoseconds has been a subject of great interest during the last years. The long fluorescence lifetimes are in contrast with those of carrier recombination processes occurring in the picoseconds domain. It has been suggested that shallow and deep traps are responsible for the long lifetime as trapping (slow) can compete with radiative recombination. Alternatively, it has been proposed that the long-lived emission

can result from the presence of an optically nonradiative triplet state, the band gap recombination being then a spin-forbidden transition and this would explain the observed long emission lifetime.

1.5.2 Surface states in the nanocrystals

Atoms at the surface of NCs or bulk material show coordinative unsaturations, which lead to spatially and energetically localized electronic states (surface states or defects states) [79]. The so-called intrinsic defects reflect the aperiodic termination of the lattice on the surface. Adsorbates can occupy the vacant coordination sites on the surface; this can induce adoption of near-bulk coordination geometry leading in some cases to removal of the intrinsic surface states. In turn, new extrinsic surface states are created, which arise from unsaturated coordination bonds of adsorbates, and may lie within the band gap or in environment continuum bulk states. Photooxidation is an example via oxide formation on the surface of the NC that leads to extrinsic surface states.

An alternative description by Brus et al. [80] explained surface defects by introducing two different sorts of traps: deep traps and shallow traps. Deep traps are essentially localized at the lattice site defects and lie in the middle of the gap. Shallow traps lie within a few millivolts of the corresponding band edge and are delocalized over several unit cells (Cd-Se). The surface energy gap of NCs is dominated by the quantization of the material, thus the energy levels of the traps depend on the size of the NCs. A decrease in size induces splitting of the energy levels more dramatically for the shallow than for deep traps. Thus for the strong confined regime of NCs, the distinction between shallow traps and the electronic states of the cluster disappears. The energy range between deep traps and delocalized states from the cluster is illustrated in figure 1.5.2.
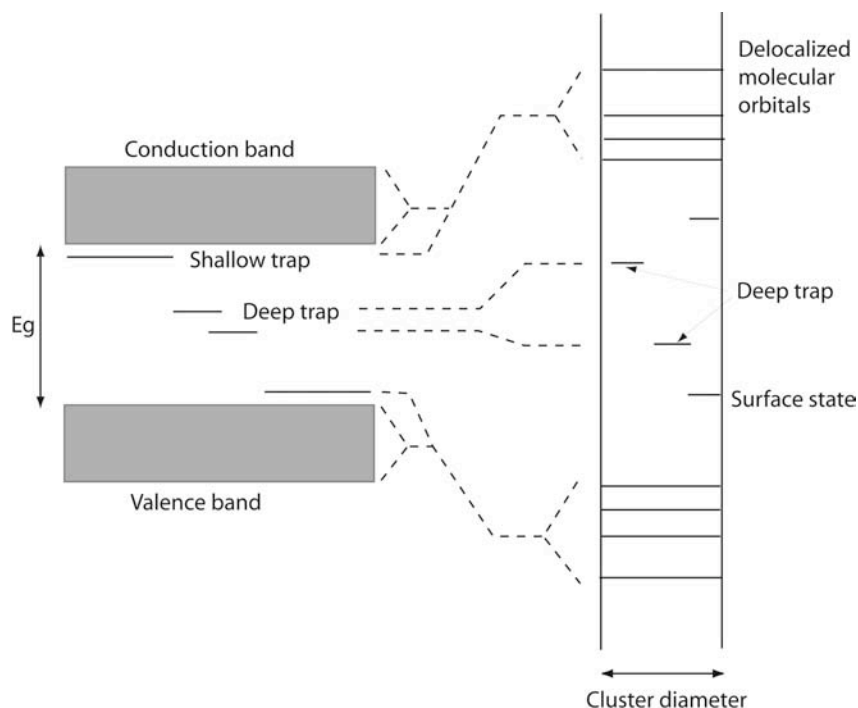
Figure 1.5.2: Schematic diagram of the shallow and deep traps in the bulk as well as in a semiconductor cluster, for the bulk material (left) and the corresponding nanocrystal (right) [80].

1.5.3 Auger processes

Under strong illumination, as for example in confocal microscopy investigations, the absorption of light can induce excitation of more than one electron, leading to the formation of more than one exciton in a single NC. "Auger processes" can occur by interaction between the exciton pairs and can lead to non-fluorescent "dark states". The internal Auger process leads to fluorescence suppression because the recombination energy of one pair is transferred to the other with promotion of the electron to higher energy levels (hyper excited state) leading to non-radiative relaxation [9, 81, 82].

The external Auger process leads to the formation of an ionized NC. Here the recombination energy of one pair will eject an electron from the NC interior rendering the NC ionized. Surface trap states can participate to this process and hold the electron for a certain time, but this phenomenon is mostly reversible and thus can be observed by the blinking of the single NC in single molecule imaging (SM). Blinking means the fluorescence intensity fluctuation with time between on (bright) and off (dark) states. The blinking of the NC is also sensitive to the surrounding, pointing out the surface trapping processes for the fluorescence of NCs [83].

28

1.5.4 Fluorescence and Stokes shift

Figure 1.5.3 shows typical absorption and fluorescence spectra of CdSe nanocrystals solution. The fluorescence emission spectrum is shifted by 10 nm towards lower energy transition compared to absorption maximum. This shift is called the Stokes shift, it is mostly due to two different processes (Figure 1.4.1): the resonant Stokes shift is due to the singlet-triplet state splitting due to asymmetry of the Wurtzite structure of the NCs and electron-hole interaction [84]; the non-resonant Stoke shift, is larger than the resonant one, and is due to the size polydispersity within the sample and exciton-phonon coupling, which leads to broadening of the spectra. The weighted average of the absorption and emission maxima are shifted to higher and lower energies respectively, expanding the Stokes shift value.
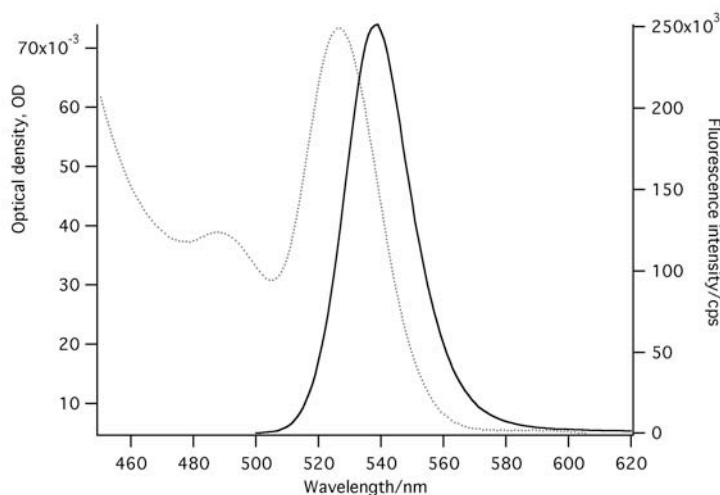
Figure 1.5.3: Absorption and fluorescence emission spectra of CdSe nanocrystals dispersed in toluene (first excitonic peak at 529 nm; emission maximum at 539 nm). Excitation wavelength was 490 nm, FWHM = 26 nm, QY=54%. (NCs from method 4 chapter 2).

Recent investigations have shown that not only the crystalline structure but also the shape of the NC had also an effect on the Stokes shift. For CdSe nanorods, it has been shown that bigger Strokes shift are expected, with increasing aspect ratio of the rods [85].

1.5.5 Photooxidation

The stability of the NCs is limited by photochemical processes, in particular by photooxidation [86]. The absorption of light produces charges, electrons and holes, which are spatially separated inside the NC core. Electrons are mobile and can be found on the surface.

The holes can react with electrons of dangling electron bonds of selenium atoms to form highly reactive selenium radicals. An excess of holes h^+, due to Auger processes for example, can activate the following reaction leading to photooxidation.

$$h^+ + Se^{2-}{}_{surface} \longrightarrow Se^-$$
$$Se^- \xrightarrow{O_2} SeO_2^- \xrightarrow{O_2} SeO_4^{2-}$$
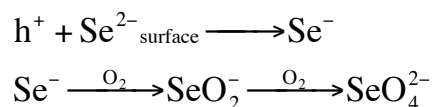
Oxygen is adsorbed at the surface due to electrostatic interactions. XPS measurements [86] confirmed the formation of selenium oxide on the surface of the NC. Desorption of the oxide may lead to shrinking of the NC size and formation of surface defects. A blue shift in the absorption and fluorescence spectra of the NC solution after exposure to oxygen was observed by Potapova et al. and attributed to shrinkage of the NC size [87].

1.6   Scope of the thesis

The motivation of this project was the preparation of NCs possessing high fluorescence quality and photostability, the surface of which should be easily and rapidly modulable to possess functionalities and properties of any kind. The surface modification should be easy and rapid compared to the existing procedures. These modified-NCs should be used for supramolecular assemblies with biomolecules producing powerful functionalized and fluorescent tools for binding applications.

Macromolecular assemblies of functionalized-nanocrystals and biological compounds are of high interest and under intensive investigations now-a-days [15, 16, 88-90]. These complexes use the capability of molecular recognition, engendering highly specific interactions. Coupling this with the nice properties of the NCs would end up with modulable fluorescent systems as illustrated in figure 1.6.1.
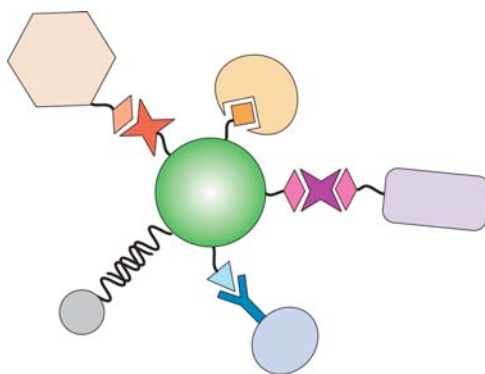
Figure 1.6.1: Scheme of the decoration of NCs with different functional group for further specific interaction with biomolecules. Many approaches are possible for the NC surface modification.

When this work started, the synthesis of highly fluorescent and photostable nanocrystals e.g. CdSe was well developed using the highly toxic precursor Cd(Me)$_2$ [23]. These NCs were passivated with a layer of trioctylphosphine oxide (TOPO) rendering them hydrophobic. At this time the water-solubilization was achieved by ligand exchange using thiols, giving rise to NCs with poorer optical properties and stability [91]. An additional covalent linkage enabled the binding of a biomolecule. Another way of solubilization was followed by A.P. Alivisatos research group [92-94], they were building a silane shell around the NCs, then followed by a conversion of functional group on the surface by addition of a functionalized ligand [12]. The successive steps were time consuming and giving rise to much bigger NCs (tens of nm).

We thought of using the hydrophobic layer of the initial NCs instead of multi-step ligand exchange and functionalization. In biology, membrane proteins for example are partly hydrophobic and often need lipids as co-solubilizing agents alone or together with detergent molecules. Inspired by this, we developed a method for coating the TOPO-NCs with phospholipids, giving lipid-coated NCs (named lipid-NCs). The advantage of this method is the rapidity, the versatility as a mixture of lipid of our choice should be possibly used for coating. The lipid mixture should contain functionalized lipids to add functional groups on the NC surface. The solubilization and functionalization of the surface is made in an efficient, rapid and easy one step method.

The next chapter will focus on synthesis methods and growth mechanism especially for CdSe nanocrystals. The synthesized NCs being soluble in organic solvent, an alternative method is developed in chapter 3 for their water solubilization using amphiphiles. The decoration of the NCs with functionalized lipids allowed us to simultaneously functionalize the NCs with the

desired functionality or multiple functionalities. Specific interactions with proteins were investigated using Fluorescence Resonance Energy Transfer (FRET) and are shown in chapter 4.

To test the membrane-like properties of the lipid-layer around the NCs, we investigated the interaction between a peripheral protein, cytochrome c, and a negatively charged lipid-NC in chapter 5.

The functionalized-NCs allowed us to specifically immobilize them on micropatterns surfaces as shown in chapter 6.

2   Synthesis of nanocrystals

2.1   Structure of the nanocrystals

The nanoparticles are formed by a core such as cadmium selenide in our case, and often are surrounded by a capping layer of another material that protects the core from the environment. This layer might be composed of organic molecules, so-called **ligand** molecules that bind to surface atoms of the NCs. The organic layer can chemisorb or physisorb onto surface atoms, preventing further growth of the nanoparticles during synthesis and avoiding aggregation. The ligands interact with the surface through functional groups e.g. phosphine, phosphine oxide, thiol and amine. They not only passivate the surface but also influence the solubility, the optical properties and stability of the NCs. The ligands are usually introduced during the synthesis and they influence the reaction mechanism, the size distribution and quality of the resulting NCs. **Ligand-exchange** can be achieved after synthesis resulting in modification of the properties such as solubility of the NCs.

Concerning optical properties, even the best organic ligand used for surface passivation cannot fully prevent the photooxidation and environmental "quenching" of the fluorescence; to minimize this effect, a uniform inorganic shell with crystalline lattice matching the core possessing a higher band gap (e.g. ZnS, ZnSe or CdS for CdSe core NC) can be grown on the NC surface [95]. This **core-shell** NCs structure is schematically depicted in figure 2.1.1.
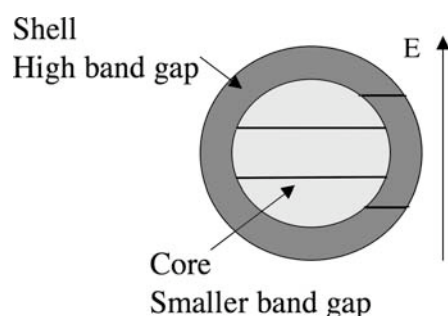
Figure 2.1.1: Scheme of a core-shell system, the shell material possess a higher band gap seating outside of the core CdSe confining the charge carriers inside the core.

This shell confines the charge carriers inside the core due to the energy gap existing between the two materials, and thus yields in general large fluorescence quantum yields up to almost unity and enhanced chemical as well as photo-stability. This improvement is also due to the reduction of crystalline defects on the surface of the emitting core (by lattice matching of the two materials). The core-shell systems are also surrounded by an organic ligand layer, but it influences less intensely the optical properties of the NCs compared to the core NCs.

This work focuses on nanocrystals made of cadmium selenide produced by the so-called "TOP/TOPO" method (hot amphiphilic media made of trioctylphosphine oxide (TOPO) and trioctylphosphine (TOP)), resulting spherical or nearly spherical NCs possessing narrow size distribution and good optical properties (high quantum yield, narrow emission peak). We will describe briefly some synthetic methods developed so far, and in more details the synthesis in hot amphiphilic solvent introduced by Murray et al. [23], and then modified by Peng et al. [21]. Here the growth mechanisms will be explored and the optical properties and shapes of synthesized NCs will be presented.

2.2 Preparation of nanocrystals

The main obstacle for practical applications is the controlled and reproducible production of NCs showing uniform size and properties. To produce nanocrystals, one should bring the reagents into contact under suitable conditions for continuous and homogeneous chemical reaction.

Summarizing the different methods and mechanisms for nanoparticles synthesis would be impossible as numerous methods and modifications thereof have been accomplished the last

two decades. For example, the nanoparticles can be synthesized in water, in organic media, in micelles or solid matrixes. A good historical review of synthetic methods was made by Prof. G. Schmid [96], giving a good overview of the field (see also [97]).

By simplifying, there are two methods for NPs synthesis [98]. First, reaction in a microscopically homogeneous bulk (e.g. solution, molten glass [99]); this was historically the first method to produce semiconductor nanocrystals. The mechanism is a controlled precipitation, involving the formation of a stable sol from the mixture of the ionic precursors. The stability of the NPs is achieved by the presence of "stabilizers" in solution (e.g. polymer, surfactants). This method encounters many drawbacks such as a wide size distribution, and difficulty in isolation of the NC from the matrix in certain cases.

The reaction in a coordinating bulk containing nanometer-sized compartments prior to the injection of precursors is another way. Their volumes and diffusion within these "templates" are the limiting parameter determining the size and sizes distribution of the resulting NPs. The compartmentalization can be formed by reverse micelles or microemulsion droplets [61, 100-103], by a bicontinuous cubic phase of a lipid [104] or by pores, cavities in zeolite or in sol-gel matrix [105].

For the synthesis of CdSe nanocrystals, we used a method involving a thermal treatment of the initial hot amphiphilic matrix containing the Cd and Se precursors, leading to a burst of nuclei formation and a further growth up to the desired size and shape. Pyrolysis of organometallic precursors in hot TOPO (360°C) became the standard method [23] to produce series of e.g. CdS, CdSe, CdTe NCs of different sizes in a nearly monodispersed way. Peng et al. [21] modified this synthetic route by changing the initial Cd precursor dimethyl cadmium (Cd(Me)$_2$) with a less toxic and less expensive one, cadmium oxide (CdO) or other Cd salts, resulting in NCs with similar qualities.

To understand the role of the precursors, temperature and coordinating solvent for the synthesis of NCs of desired optical and structural properties, the growth mechanism is discussed in the following part [98].

2.3   Growth mechanism of CdSe NCs

Precursors of Cd and Se coordinated in trioctylphosphine (TOP) or tributylphosphine TBP are kept at a temperature below the reaction threshold before injection in the preheated TOPO

matrix. The matrix serves to engulf the precursor droplets and promotes the subsequent chemical reaction into it between the Cd and Se ions forming seeds of NCs (nucleation). Little is known about the type and size of the amphiphile compartments or micelles hosting the precursors in the hot matrix, which prevents us from totally understanding the growth mechanism and especially the initial nucleation.

As a model reaction path, the following figure illustrates the growth of the CdSe NCs with addition of coordinated Cd and Se ions on the surface.
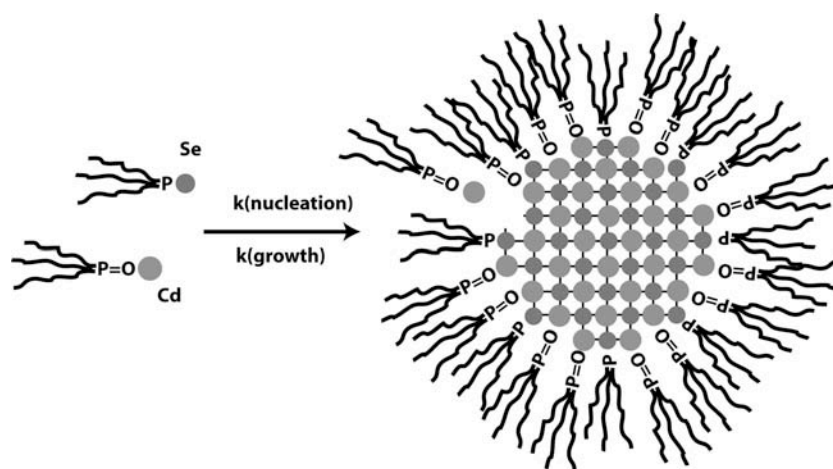
Figure 2.3.1: Model of a CdSe nanocrystal growing in a TOPO matrix due to the influx of Cd and Se ions selectively bound to an amphiphile molecule (TOPO and TOP). Selenium is assumed bound to TOP whereas cadmium is assumed bound to TOPO, inspired by Dushkin et al. [98].

La Mer and Dinegar showed that the production of monodispersed colloids requires a temporally discrete nucleation event followed by a slower controlled growth of the existing nuclei [106]. In brief, rapid injection of reagents to the reaction vessel raises the precursor concentration above the nucleation threshold. A short nucleation burst partially relieves the supersaturation. As long as the consumption of precursors by the growing colloidal NCs is not exceeded by the rate of precursor addition to the vessel, no new nuclei will form.
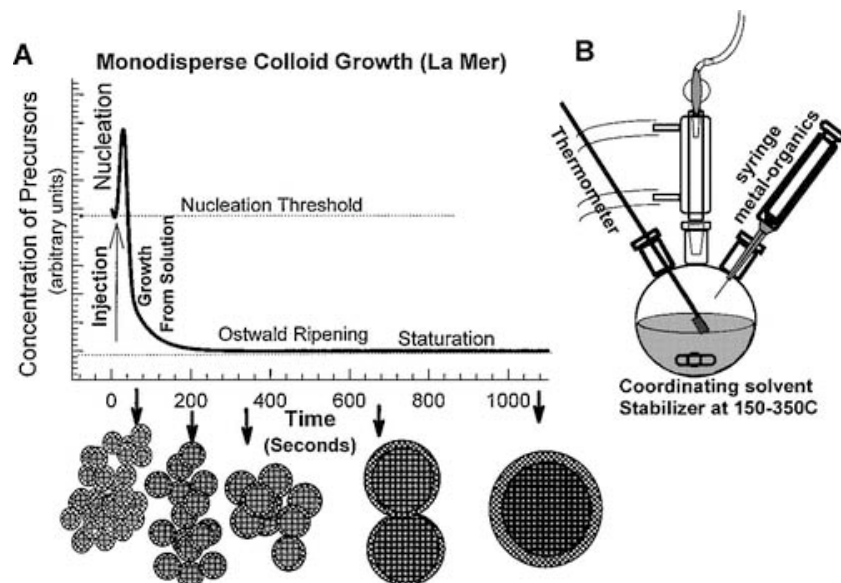
Figure 2.3.2: A) Scheme showing the stages of nucleation and growth for the preparation of monodispersed NCs with the La Mer model [106]. As NCs grow with time, a size series of NCs may be isolated by periodically removing aliquots from the reaction vessel. B) A representation of the synthetic apparatus employed in the preparation of nearly monodispersed NC samples.

Many systems exhibit a second, distinct, growth phase called Ostwald ripening [107, 108]. In this process the high surface energy of the small NCs promotes their dissolution, where new material is deposited on the larger ones. The average NC size increases over time with a concomitant decrease in NC number. Exploiting these effects can greatly simplify the preparation of a size series of NCs [23].

Since the growth of the NCs is relatively uniform, the initial size distribution is largely determined by the time over which the nuclei are formed and begin to grow. If the percentage of NC growth during the nucleation period is small compared to the subsequent growth, the NCs can become more uniform over time [109]; this phenomenon has been referred to as "focusing" of the size distribution as smaller NCs grow faster than larger ones [110, 111].

Taking a particular example from Peng et al. [110] for CdSe NC synthesis, after swift injection of the precursors (Cd(Me)$_2$ and Se in TOP) into the hot solvent (TOPO at 360°C), CdSe nucleation take place. The NCs are then growing in the focusing regime, the size distribution is focusing (0-22 min from figure 2.3.3); at this regime, the reaction mixture is cooled down to stop the reaction and obtain nearly monodispersed NCs. For the production of larger monodispersed particles at the same temperature, a multi-injection scheme can be used: when

38

the defocusing is reached, the size distribution of the NCs is broadened (from 22-190 min in the graph for CdSe), an additional injection of the precursors suppresses Ostwald ripening and refocusing gives rise to a decrease of the size distribution. A similar process was observed for InAs [110].
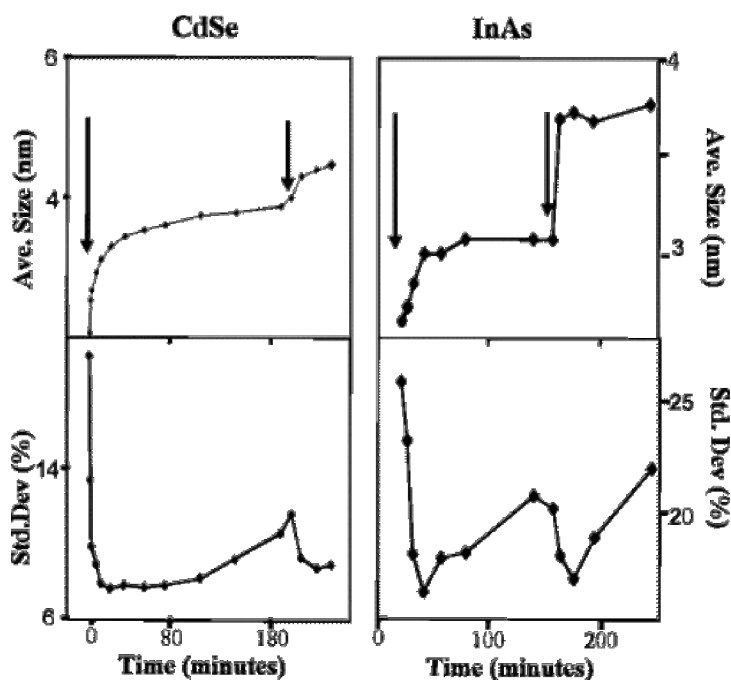
Figure 2.3.3: (Left) Average size and size distribution of CdSe NCs as a function of growth time, (from [110]). The arrows indicate the injection of fresh precursors, the first time at the beginning and the second time when defocusing occurs. The bottom graph shows that refocusing is accompanied by the reduction of the size distribution. (Right) Same phenomenon is shown for InAs NCs growth.

According to Peng et al. [110], the kinetic of nucleation are difficult to study, whereas the subsequent growth stage is more readily examined. At fixed monomer concentration, assuming diffusion limited rate, the size dependent growth rate can be obtained by considering the Gibbs-Thomson equation

$$S_r = S_b \exp\left(\frac{2\sigma V_m}{rRT}\right)$$
2.1

where S_r and S_b are the solubilities of the NCs and the corresponding bulk solid, respectively; σ is the specific surface energy; r is the NC radius; V_m is the molar volume of the material; R is the gas constant and T the temperature.

The coefficient in brackets is called the "capillary length" and is of the order of 1 nm. This equation describes well the colloidal regime for radii larger than 20 nm. However for CdSe with radii comprised between 1-10 nm, the value of the capillary length is approaching the particle radius, and the particle solubility becomes nonlinear against 1/r. Therefore, the particle growth can be described as a diffusion controlled process instead [112].

$$\frac{dr}{dt} = K\left(\frac{1}{r} + \frac{1}{\delta}\right)\left(\frac{1}{r^*} - \frac{1}{r}\right)$$

2.2

where dr/dt is the growth rate, K is a constant proportional to the diffusion constant of the monomer; δ is the thickness of the diffusion layer and r^* is the critical radius for which the NC solubility is exactly the concentration of the monomer in solution (zero growth rate). If we plot this equation for a fixed high monomer concentration, we obtain:
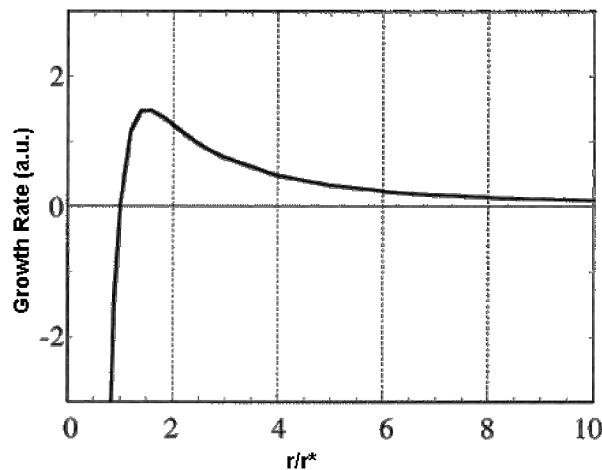
Figure 2.3.4: Variation of the growth rate versus size, according to a model of Sigimoto, taken from Peng et al [110].

This graph shows that very small particles have negative growth rate, i.e. smaller NCs are dissolving while larger ones have a positive growth rate and are growing. Focusing to a particular size distribution occurs when r is slightly larger than r* because smaller NCs grow faster than the larger ones but only when the monomer concentration is high and therefore constant. When the monomer concentration is depleted, Ostwald ripening (defocusing) takes place because the smaller NCs are shrinking while larger ones are growing.

2.4   Controlling synthesis of NCs

2.4.1   The precursors

Temperature and precursor concentration are not the only parameters to be considered for obtaining good NC preparations. The reactivity of a particular precursor is also important. Thus $Cd(Me)_2$ was used as a Cd source for a long time, because it is highly reactive compared to other Cd compounds. Then Peng et al. [21] proposed other precursors such as CdO, $CdCO_3$ and other cadmium salts, which are stable and much less toxic than $Cd(Me)_2$. Activation of these "new" Cd precursors was achieved via their complexation with acids such as phosphonic acids (e.g. hexadecylphosphonic acid (HPA), octylphosphonic acid (OPA) or tetradecylphosphonic acid (TDPA)) or fatty acids (e.g. stearic acid (SA)). At high temperature these acids react with the Cd precursor forming complexes where the Cd^{2+} is in an active state because solubilized in TOPO. These PA-Cd complexes react with TOP complexed Se to produce the CdSe NCs. In this "greener" synthetic method the Cd and Se precursors are separately delivered to the reaction vessel, which allows a better control over the concentration of the monomers, an important factor for monodispersity.

2.4.2   The coordinating solvent

The coordinating solvent plays an important role in synthesis and influences the final properties of the NCs. It has to fulfill the following tasks:

• Coat the NC with a uniform layer.
• Remove the maximum of dangling electron bonds/surface states responsible for fluorescence "trapping" and photooxidation.
• Solubilize the NCs.
• Allow synthesis at high temperatures (280-300°C).

The required high temperature limits the choice of ligand; TOPO is considered as one of the best coordinating solvents as it has a high boiling point of 365°C and a good ability to coordinate surface atoms on the NCs. A mixture of TOPO with alkylamines (hexadecylamine (HDA)) was shown to yield even improved fluorescence properties of the synthesized NCs and uniformity of the sample [111]. This result can be explained by the high affinity of amines towards Cd on the surface, higher packing order of the mono-alkyl chains as well as the

higher complexation level of the surface atoms due to the thinner hydrophobic part as compared to TOPO which possesses a more conical shape due to its three octyl-chains.

All these ligands give rise to hydrophobic NCs. If hydrophilic properties are needed, further processing of the NCs is possible by exchanging TOPO with hydrophilic ligands or by coating the hydrophobic NC surface with a lipid monolayer, as it will be introduced in the following chapter.

2.4.3   Size and shape of NCs

Size and shape of the NCs critically depends on the reaction conditions. In hot amphiphilic solvent, Wurtzite structured CdSe NCs are produced. Therefore different facets of a NC have different reactivity. At high growth rate, growth is generally faster along the c axis, resulting rod-like or prolate NCs. However, at low growth rate more spherical NCs are formed (the shape that minimize the surface area is favored).

The reaction rate can be controlled by the use of specific surfactants. In pure TOPO very fast reactions are observed yielding long rods, which are often insoluble. Impurities frequently present in technical grade TOPO, can drastically reduce the rate of the reaction and thus produce spherical NCs. Among the impurities found in TOPO are phosphonic acids, which bind strongly to the NC surface hence slowing down the NC growth.

We unintentionally also obtained nanorods instead of dots when we started to use CdO as cadmium precursor. The following deductions were made according to observations made by Peng et al. with $Cd(Me)_2$ [85]. They obtained the rods visible in figure 2.4.1.

If the concentration of PA was more than 5%, and consequently rods were synthesized. If less than 3% PA relative to TOPO would then dots or prolate dots would be more likely produced. In this context it is important that the amount of PA should be small enough if dot shaped NCs should be synthesized, but high enough to solubilize the CdO by complexation. Such conditions can be obtained if the precursors are diluted with additional TOPO.

42
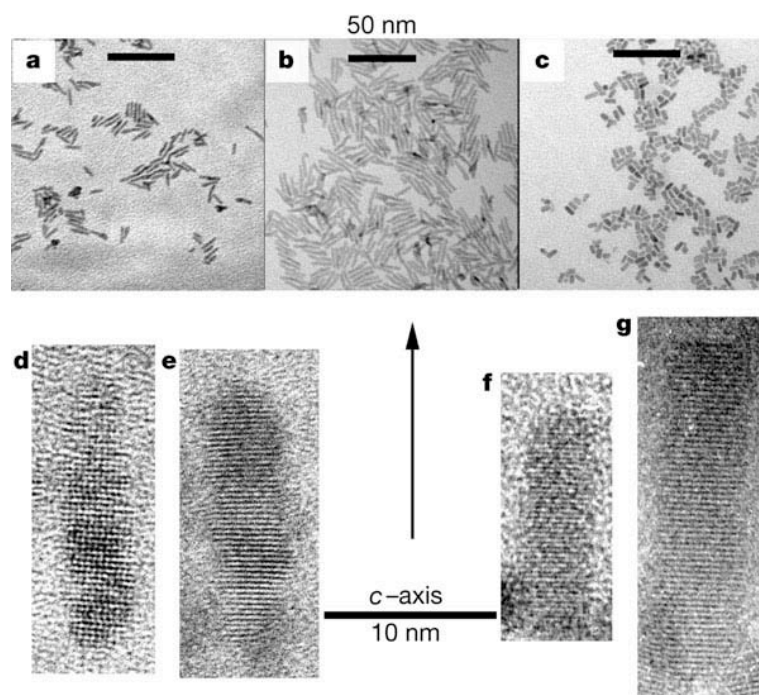
Figure 2.4.1: a–c Low-resolution TEM images of three quantum-rod samples with different sizes and aspect ratios taken from Peng et al. [85]. d–g High-resolution TEM images of four representative quantum rods. d and e are from the sample shown in a; f and g are from the sample shown in c.

2.4.4 The passivating layer

The standard synthetic procedures deliver CdSe nanocrystals surrounded by a TOPO layer, which passivates the NC surface. TOPO is bound to the NC surface through cadmium atoms in a coordinative manner, the oxygen of the phosphonic oxide directing toward the cadmium atom on the surface, as depicted in figure 2.4.2.
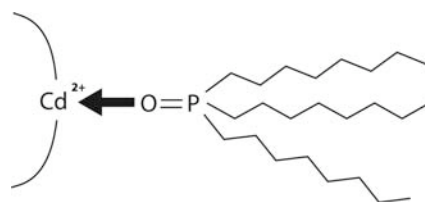
Figure 2.4.2: The TOPO is assumed to coordinate the Cd atoms of the surface in a "dative bond" way. The oxygen lone pair occupy the empty orbital of the cadmium in a coordination way.

The amount of TOPO molecules per NC was estimated from XPS measurements by Katari et al. [86]. A percent coverage of ligands was obtained by calculating the number of CdSe units in

the NC and on the NC surface for a given diameter. The obtained surface coverage estimations varied from 60 to 30% for the smaller to larger NCs. The percentage corresponds to the number of Se and Cd atoms on the surface, which are coordinated by TOPO. The lower percentage coverage of TOPO with bigger NCs can be explained by sterical considerations, TOPO being assumed as a conical shaped ligand and thus possessing a large lateral dimension [86] avoiding compact packing if less curved surfaces.

2.4.5   Controlling solubility of NCs by ligand exchange

There are two main approaches to obtain water-soluble NCs: First nucleation of the NCs inside stabilizing micelles in water [24, 113], and second via an exchange of the hydrophobic ligands coming from synthesis [114-116]. The NCs obtained by the first route possess generally poor fluorescence quality and broad size distribution. The molecules that cap the NC surface (such as TOPO or HDA, for example) can be substituted by another ligand through ligand exchange. The NCs are exposed to an excess of the competing ligand, e.g. an amine or a thiol, and mixed for several hours. Heating can be required for certain amines. This is followed by isolation of the NCs (centrifugation or precipitation with methanol). Dissolving the NCs e.g. in toluene and repeating this cycle several times completes the ligand exchange. This method can be used for a wide range of ligands, even if the new ligand binds less favorably than the original one. For TOPO capped NCs, the exchange give rise normally to a 90% TOPO exchange if using pyridine or thiols.

To get hydrophilic NCs, hydrophilic ligands have to be chosen, which are typically not soluble in the initial NC solution. A two-phase reaction is then required with the TOPO-capped NCs in chloroform and an excess hydrophilic ligand in an aqueous phase. The two non-miscible liquids are stirred and a transfer into the aqueous phase is visible after some time. This reaction can be performed at room temperature within short mixing times and high yields. Dialysis or precipitation-redispersion cycles can be used for purification and washing out of the excess ligands.

2.5   Experimental section

2.5.1   Materials

TOPO (technical grade 90%) and tetradecylphosphonic acid (TDPA, 98%) were purchased from Alfa Aesar, Switzerland. CdO and Selenium powder were from Aldrich, Switzerland. Tributylphosphine (TBP, 95%), trioctylphosphine (TOP, 90%) and hexadecylamine (HDA, 90%) and all solvents were used as received from Fluka, Switzerland.

2.5.2   Synthesis

The synthesis of the CdSe NCs possessing high optical properties (fluorescence, stability) requires an inert atmosphere system. For this, we used a typical home made Schlenk system (see figure 2.5.1). The inert gas used for synthesis was argon.
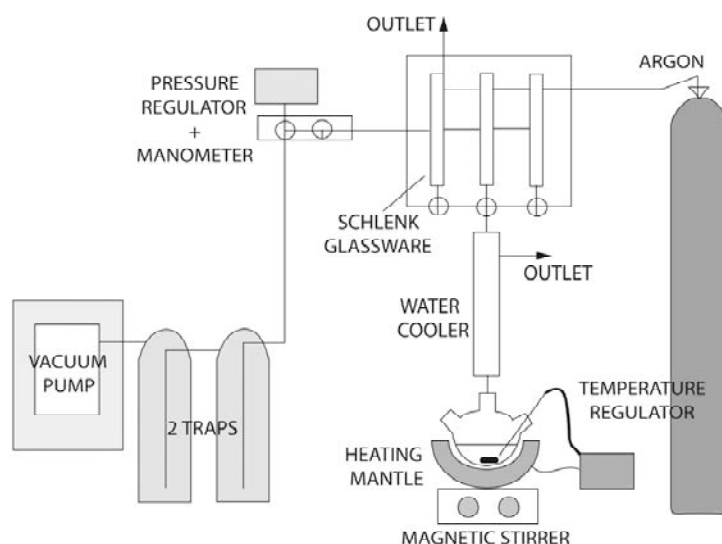
Figure 2.5.1: Scheme of the Schlenk system used for the air free synthesis of CdSe nanocrystals.

During the last 4 years, the synthesis of CdSe nanocrystals has evolved continuously allowing me to adapt to the new improved conditions of security and NCs quality.

Different protocols were investigated for the synthesis of CdSe nanocrystals and gave rise to different kinds of NC solutions. **Method 1**: $Cd(Me)_2$ served as cadmium precursor in TOPO. **Method 2**: CdO was used together with 5 (wt)% of TDPA in TOPO. **Method 3**: CdO dissolved in TOPO and 3 (wt)% TDPA. **Method 4**: same as method 3 but using a mixture of TOPO/HDA 2:1 as solvent. Details on the synthesis protocols are as following.

Method 1: [23, 117] Dimethylcadmium[a] (CdMe$_2$) and selenium powder were co-dissolved in a tri-alkyl phosphine solvent (-butyl or -octyl) in a glove box (stock solution: 20 g TBP or TOP, 0.197 g Se, 0.534 g CdMe$_2$). This solution (2 ml) was injected in one shot using a glass syringe into hot (340-360°C) TOPO (6 g) under Argon flow (previously evacuated for 1 hour at 100°C and few mbars). The temperature dropped to 270°C. Nucleation occurred rapidly followed by growth at 280-300°C. The reaction time depended on the size required and can vary from 1 second to several hours. At the end of the reaction, the solution was quickly cooled down by removing the heating mantle and blowing air on the flask, and the NCs were precipitated from solution by adding methanol, isolated by centrifugation and redispersed in toluene, chloroform or hexane.

Method 2-3-4: [21] TDPA (5 or 3 weight %) and TOPO (6 g or TOPO/HDA 2:1 mixture) were put into the reaction vessel together with CdO (51.4 mg) and evacuated for 1 hour. The temperature was increased to 300°C to allow cadmium complexation by the phosphonic acid to get a reactive Cd species; this can be optically observed by a color change from turbid violet-red to a pale yellow clear homogeneous solution. Now the proper reaction temperature was selected (from 270 to 300°C), before swift injection of 4 ml of Se in TOP stock solution (in glove box: 158 mg into 4 ml). When the required NC size was reached (estimation via the solution color), the solution was quickly cooled to 60°C, then precipitated with methanol, isolated via centrifugation and washed with methanol 3-4 times (see next part) before redispersion in toluene.

2.5.3   Purification and size selective precipitation

As prepared, the TOPO coated NCs are dispersed in an organic solvents such as toluene and chloroform. The capping layer provides an energetic barrier against aggregation of the NCs, which depends strongly on the energy of mixing between the tethered groups and the solvent. Addition of a nonsolvent such as methanol, which is miscible with the initial dispersing solvent, destabilizes the NCs and make them precipitate. Then the NCs can be collected by centrifugation and thus separated from synthetic side-products and non-reacted precursors.

---

[a] Dimethylcadmium is a highly reactive and highly toxic compound, and must be handled in a secure and well-maintained glove box (absence of moisture and oxygen). The solution of the precursors in TOP are prepared in the glove box, the flask is sealed and handled with gloves.

The NC can be redispersed in hydrophobic solvents such as toluene. This process can be repeated few times to get higher purities.

If the size distribution of the NCs is not satisfactory, size selective precipitation can be used to obtain NCs with narrower size distribution [78, 106]. By titration with a non-solvent like methanol, the bigger NCs tend to precipitate prior to the smaller ones due to the greater attractive Van de Waals forces. If we allow only a partial precipitation of the NCs, the larger particles can be separated by centrifugation, keeping the smaller ones in solution. To narrow the distribution further, this procedure can be repeated with the aggregated NCs redispersed in toluene or chloroform. A chemical yield of 95% is obtained. Although the size selective precipitation narrows the size dispersion of the NCs considerably, the negative effect is that multiple precipitation/redispersion cycles leads to a partial "washing off" of the capping molecules from the NC surface, leading to less stable NC solutions. Moreover TOPO molecules bound to the NC surface slowly exchange with free molecules in solution. In order to restabilize the purified NCs in solution a small concentration of TOPO is added to prevent aggregation. Under these conditions the NC solutions are stable for years.

For completeness we also mention other techniques used for separation of different size-fractions of nanoparticles. For example, the preferential evaporation of a solvent from a mixed solvent/nonsolvent system resulting in a gradual flocculation can be used [78, 106]. Gel permeation or size exclusion chromatography was employed to narrow size distributions of CdS NCs; however this method is slow and the yield is low [118, 119]. Gel electrophoresis was used by Zanchet et al. for DNA conjugated Au colloids [120, 121] and CdSe NCs [122, 123]. Standard dialysis was also used for purification from excess capping molecules, this was tried here as well but aggregation resulted sometimes from dialysis, so precipitation-redispersion method was preferred.

2.5.4   Optical properties

Absorption spectra were acquired on a HP 8453 UV-visible spectrometer (Hewlett Packard, DE). Diluted NC solutions were placed in a 1 cm thick quartz cuvette. The spectra were taken against the respective pure solvent reference. Solution concentrations were estimated from absorption spectra according to Schmelz et al. [78].

Photoluminescence spectra were recorded on a SPEX Fluorolog II (Instruments S.A., Stanmore, U.K.), using quartz cuvettes of 1x1 cm^2 (Hellma, Müllheim, DE). The spectra were

taken for solutions having an optical density below 0.05 at excitation wavelengths. Room temperature fluorescence quantum yields QY were determined by comparing the integrated emission band of the NC solution to the integrated emission band of reference dyes such as peryleneimide solution in toluene [124] or rhodamine B, which have a known quantum yield and absorb and emit in the same region as our NCs. The equation used is

$$QY_{NC} = \frac{I_{NC}}{I_{Dye}} \times \frac{OD_{Dye}}{OD_{NC}} QY_{Dye} \qquad\qquad 2.3$$

QY_{NC} and QY_{Dye} for the quantum yield of the NC and the dye respectively. I_{NC} and I_{Dye} are the integrated emission band, and OD_{NC} and OD_{Dye} the optical densities at the excitation wavelength of the NC and the Dye respectively.

2.5.5 Confocal microscopy CM

Single molecule measurements were performed at the CSEM, Neuchâtel, using a homemade instrument [125]. The laser light source is an Argon-laser (principal laser line: 488 nm/100 mW; ION Laser Technology, Utah, USA). The samples are mounted on a glass coverslip. The fluorescence light is collected by the objective lens and reflected by a dichroic beam splitter into a polarizer cube (Newport, USA) where it is slit into two perpendicularly polarized beams. Finally, the fluorescence light is focused by a lens onto the core of a multi-mode fiber connected to a single photon counting avalanche photodiode (EG&G, Canada).
For sample preparation, a very diluted solution of CdSe NCs in toluene (nanomolar range) were spin-coated onto a cleaned glass slide, which was then covered with a thin polymer film of Poly(methylmethacrylate) (PMMA).

2.5.6 Transmission electron microscopy (TEM)

Samples solutions in toluene with an optical density of 0.1 were loaded on a holey carbon film copper grid (300 mesh) from Plano, Germany. The grid was then dried with a light argon stream. The images were taken either on an Hitachi HF2000 transmission electron microscope, equipped with a field emission gun operated at 100 kV and a GATAN PEELS 666 spectrometer, or a Philips CM 20 with a LaB6 source, accelerating voltage operating at 200 kV, having a point resolution of 2.8 Å.

2.6 Characterization of synthesized NCs

Absorption spectra of the NCs in solution give information on the size of the particles (first excitonic band position), their size distribution with the profile of the absorption spectra (different bands visible referring to monodispersity) and an estimation of the concentration (optical density at first excitonic peak). The width of the fluorescence spectra also gives information of the size distribution of the NCs. The Stoke shift value seems to be related to the shape of the NC. It is normally less than 15 nm for dot-shaped NC and increases for small aspect ratio rods of NCs [85, 126]. TEM is useful for determining sizes and size distribution NCs. Different protocols for the synthesis of CdSe nanocrystals were tested as listed in the experimental part. The following table summarizes the optical properties and shapes of the CdSe nanocrystals synthesized with the different methods.

Method	Abs max Emission [nm]	Stoke shift [nm]	FWHM [nm]	Quantum yield	Shape (from TEM)	Aspect ratio (from TEM)	Size distribution
1. Cd(Me)$_2$, TOPO	500/580 510/600	10-15	25-30	0.2-0.35	Dots	1	5-10%
2. CdO, 5% TDPA, TOPO	524/555 540/575	16-20	30	0.15-0.2	Rods	3	≥10%
3. CdO, 3% TDPA, TOPO	524/565 540/575	9-13	27-30	0.17-0.6	Dots	1	10%
4. CdO, 3% TDPA, TOPO/HDA	507/543 520/553	9-13	26-28	0.4-0.54	Dots	~1	5%

Table 2: Resume of the optical properties of the nanocrystals obtained from different synthesis procedures. The shape of the NCs was determined by TEM.

The nanocrystals produced have a range of absorption from 500 to 580 nm (first excitonic peak) and a maximum in the fluorescence spectrum ranging from 520 to 600 nm. NCs

emitting more in the red can be synthesized using the multi-injection method but this was not used here [110].

The **FWHM** of the fluorescence spectra of the different batches of NCs are all reasonably small indicating a nearly monodispersed solution of NCs. For example, the largest observed FWHM is 30 nm, which refers to 10% size distribution. A FWHM of 30 nm is still considerably smaller than that of typical organic fluorophores [127]. The values depicted in the table refer to NCs directly obtained from synthesis without size-selective precipitation.

Also the fluorescence **quantum yields** of the NCs are influenced by the applied synthesis protocol. The replacement of 1/3 of TOPO with HDA resulted in brighter NCs, with quantum yields up to 50%, which is very high for core CdSe nanocrystals in toluene. It is believed that alkyl-amines are more favorable ligands for the NC surface as they have a much smaller cross-sectional area (one alkyl chain) compared with TOPO (three alkyl chains), thus more surface atoms can be coordinated by the ligands and thus less surface traps are present [111, 128] which in turn influences the fluorescence properties of the NCs.

Typical **absorption** and **florescence spectra** of NCs in solution obtained by the different synthesis methods are shown in the figure 2.6.1. Of particular interest is the position of the first excitonic peak in absorption spectra that gives a good estimation of the NC size. The resolution of the different bands at higher energies in the absorption spectra also illustrates the size distribution (the more distinct they are, the smaller the size distribution and higher crystallinity are supposed to be).

If we consider the absorption spectra of the NCs produced with Method 1, we can see a relatively symmetric first excitonic peak, and well-defined bands towards the blue, describing a nearly homogeneous solution of dot-shaped NCs. The absorption bands are clearly visible and we can count 3 different ones here. The Stokes shift of the fluorescence spectra is less than 15 nm for all cases.

The absorption spectra resulting from the second synthetic method 2 show a first excitonic peak that is not symmetric anymore. A kind of plateau appears on the higher energy side, but higher energy bands are still vaguely visible supposing reasonably homogeneous solutions.

The number of visible bands is 3 to 4. The Stoke shift of the fluorescence spectra are range from 16 to 20 nm, but are still smaller than those reported for long nanorods [126]. TEM images of the NC preparation confirmed the presence of nanorods (figure 2.6.3).

For the synthetic Method 3, less phosphonic acid was used and gave rise to CdSe nanodots of appreciable quality, but absorption spectra were not as clearly defined as before, indicating that this particular NC preparation was less homogeneous than method 1 with respect to NC sizes. The number of visible bands is 2. The Stokes shifts of the fluorescence spectra are smaller than 15 nm.

Method 4 gave rise to the NCs with the best optical properties, as the distinct absorption bands are well defined. QY of around 50% were calculated. The first excitonic peak in the absorption spectra is much more defined and symmetric, as compared to the absorption spectra of the NCs obtained by the other methods. We can see much more bands than for the cases before and they are very well defined. The number of visible bands is 4. Here we can conclude from the spectra that the NC solution is very homogeneous and the NCs are spherical. This latter statement was confirmed by TEM measurements.

For the **fluorescence spectra**, all show nearly symmetric and narrow emission bands with FWHM ranging between 25 and 30 nm, which corresponds to a size distribution of the NCs between 5 to 10%. The spectra also show no deep trap emission band in the red spectral region, except for the NCs obtained with Method 2 where a slight emission onset is visible. This is not observed for the other methods.

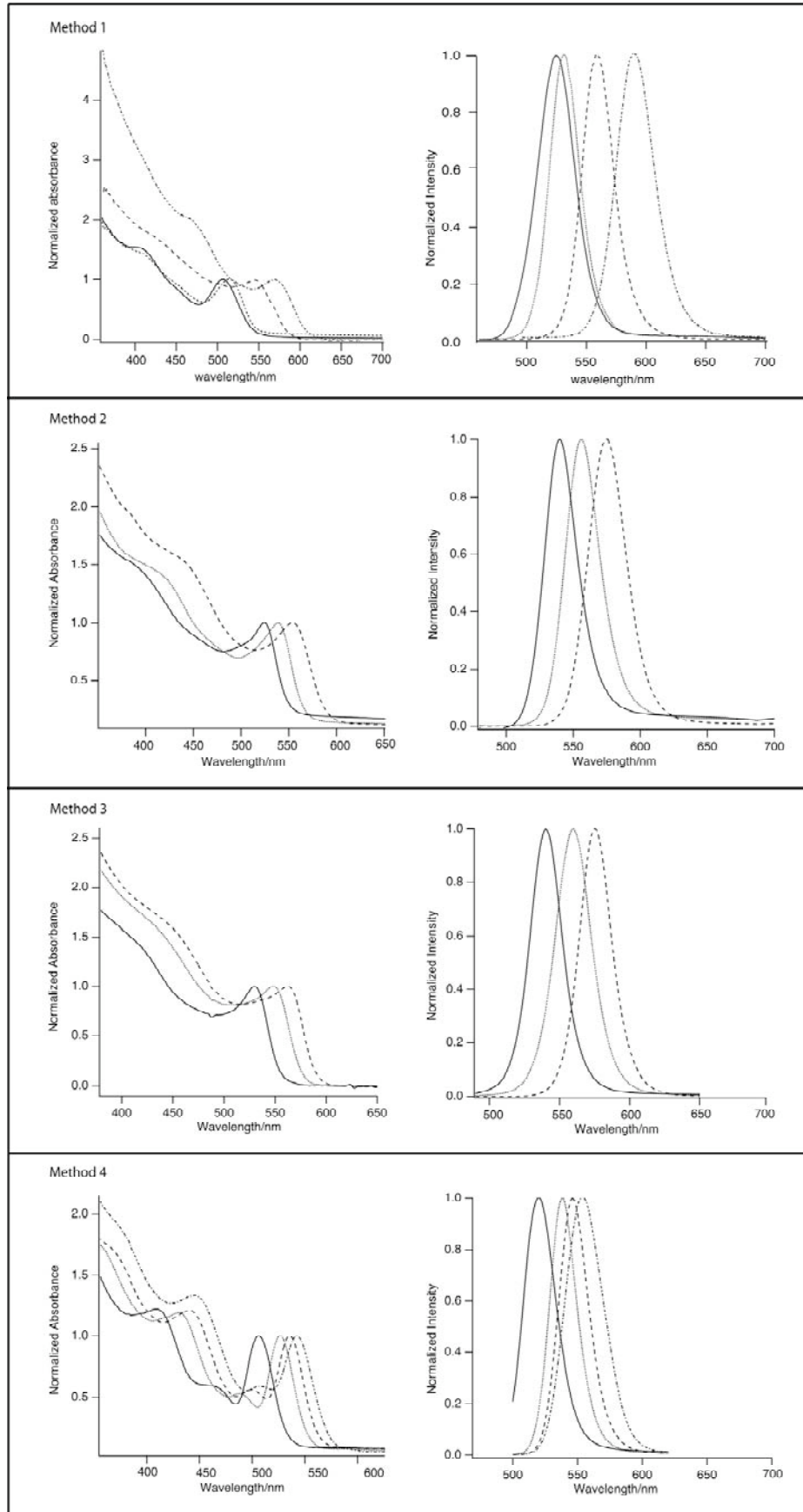Method 1

Method 2

Method 3

Method 4

Figure 2.6.1: Absorption (left) and fluorescence (right) spectra of CdSe NCs of different diameter batch. The different preparations of CdSe NC solutions resulting from synthetic **Method 1 to 4** are shown one under the other.

Method 2 resulted in the synthesis of CdSe with a nanorod or "peanut" **shape** as confirmed by TEM images (figure 2.6.3). This was due to elevated concentration of PA used for the synthesis as explained by X. Peng et al. [85]. The other methods of synthesis gave rise to spherical NCs (see figure 2.6.2).

Some representative **TEM images** of different NC preparations are presented below to show the presence of the two different kinds of particles produced. For regular spherical NCs synthesized via Method 1 using $Cd(Me)_2$ and then Method 2 using CdO and more than 5% TDPA, giving rise to rod-like or "peanut" shaped NCs. The figure 2.6.2 represent the NCs from Method 1.
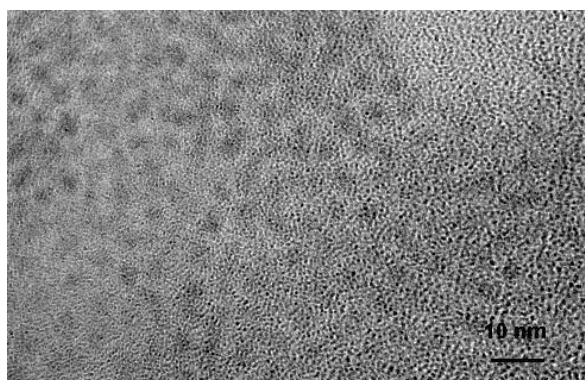
Figure 2.6.2: TEM image of a batch of CdSe NCs produced with Method 1. The dot-like structures possess diameters of about 3nm and are nearly monodisperse).

The small dots visible in figure 2.6.2 give an estimation of the size and size distribution of the particles. The NCs are not as regularly organized as reported sometimes in the literature, this being due to the kind of copper grid used here. Indeed with holey carbon film lower organization is observed compared to the use of carbon films without holes (personal communication: Dino Tonti, due to more irregular structure and thicker films). The film is much thicker on the holey carbon film grids (except around the holes) compared to the other ones.

The TEM image in figure 2.6.3 shows NCs with an elongated shape, resembling rods or more precisely peanut shapes. This can be obtained if too much PA to TOPO ratio is used for the synthesis, as explained by Peng et al. [85]. The preparation was obtained from Method 2 and appears rather homogeneous. The peanut shaped structures seem to be a result of aggregation of individual NC dots. This particular NC preparation was not further investigated within this thesis and the NCs not used.
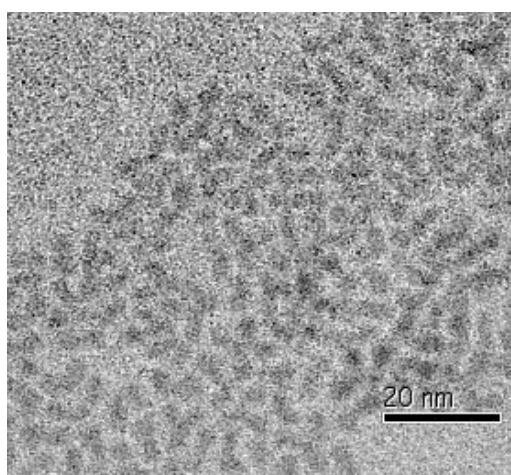
Figure 2.6.3: TEM image of rod-like or "peanut" shaped CdSe NCs, synthesized by Method 2. The structures possess an aspect ration of 3 for average dimensions of 3/9 nm.

Single molecule spectroscopy. Caterina Minelli (CSEM in Neuchâtel, Switzerland) did measurements on single nanocrystals. Single nanocrystal emission is characterized by fluorescence blinking and bleaching, and also depends on the polarization of the excitation beam [83, 129-133]. For this the NCs obtained from Method 2 were spin-coated in PMMA on a glass slide producing thin polymeric film comprising NCs, which are protected from air. Measurements were performed on a conventional optical microscope. More technical details can be found in the thesis work of Caterina Minelli, EPFL, 2004.

A typical image of single NC is shown in figure 2.6.4, where the bright spot correspond to fluorescence of a single NC.

(a)   (b)
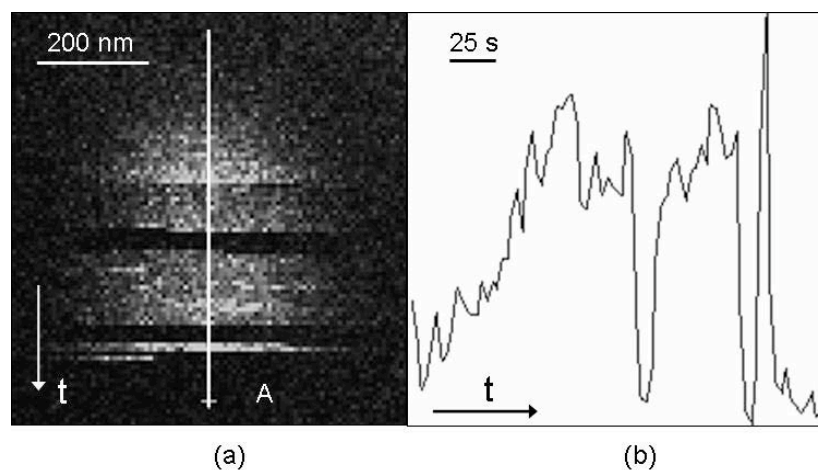
Figure 2.6.4: Confocal optical image of a CdSe nanocrystal, (with scanning direction: right-left, up-down); the nanocrystal exhibit typical blinking and bleaching behavior. (b) Emission intensity profile along the section A, we can see here the on and off states. Excitation at 488nm, NCs produced with Method 2.

As we can see from the figure, the single NC exhibits bleaching and blinking behavior. Also visible in the graph on the right is the cross section representing the emission intensity profile along the scanning direction. Analyzing the on and off states, (off states of less than 3 pixels were not resolved), one can observe off states of 5.07s 4.55s and 1.71 s. Then bleaching occurred.

In the next experiment, she made the same measurements but this time observing emission in two different and perpendicular polarizations. This time with this sample they observed a difference in intensity depending on the emission polarization changing by 90° (figure 2.6.5). Thus the intensity of the fluorescence emission was found to depend on the polarization.
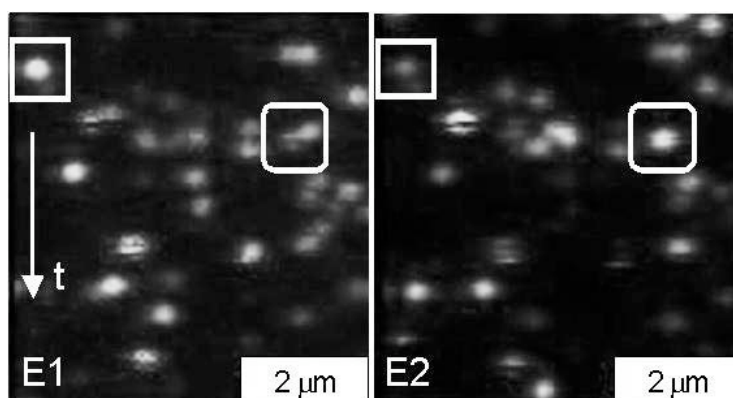
Figure 2.6.5: CdSe NCs were excited with a linearly polarized light, into two components E1 and E2 of the emitted field. TEM images of this sample indeed confirmed the rod shape of the NCs.

The fluorescent spots could be positively identified as single NC due to the blinking and bleaching behavior of their emission. These single NCs exhibit a highly polarized emission. For example the NC indicated by squares showed a strong emission component E1, while a limit visible one for E2. Analogous phenomena were observed for the emission of other single crystals of the same synthetic batch. This characteristic is well known for nanorods [134], and indeed TEM images confirmed that those NCs were in fact nanorods coming from a batch of the NCs synthesized with method 2.

2.7 Conclusion

Different protocols for NCs synthesis were used in this thesis. The use of CdO as cadmium precursor allowed us to avoid the use of dimethylcadmium, which is highly toxic, reactive and sensitive to air and moisture. We could obtain fluorescent quantum dots of narrow size distribution, which could be used for the following experiments. The fluorescence is not as high as core-shell systems, but enough for testing new surface modification to render them water-soluble.

NCs were characterized by absorption and emission spectra, as well as TEM images to get information on the size, homogeneity and optical properties of the synthesized nanocrystals.

The synthesis of fluorescent TOPO-CdSe nanocrystals resulted in NCs possessing good optical properties in toluene. As water-soluble NCs were needed for our purpose, we developed an original one step coating strategy to render them water-soluble and functionalize their surface simultaneously with different functionalities. These functionalities allow them to specifically bind to a complementary protein. Mostly the NCs made with method 1,3 and 4, were used for experiments in the following chapters. The use of different batches did not show variations in the following binding experiments, so no specific mention will be made on which NC preparation was used for a particular experiment.

3   NC surface modification

3.1   Surface modification of NCs

Here, we report on experimentation on modifying the surface of NCs such that they become water-soluble and functionalized for further specific interactions with biomolecules such as proteins or DNA. For few years now, researchers have linked NCs to biomolecules in a wide variety of ways reviewed elsewhere [15, 16, 88-90].

NCs become water-soluble, if they comprise polar or charged groups on their surface [135, 136]. Much work has been done by exchanging hydrophobic ligands as TOPO or pyridine by hydrophilic thiols on the NC surface [114-116, 136]. Because this procedure generally results NCs with poor fluorescence properties and because further chemical modifications were still necessary for attachment of biomolecules, other routes were taken for NC solubilization. Silanization of the NC surface was widely used in particular by the Alivisatos group [92-94]. This method requires multiple, time consuming steps. Moreover, the final modified NC reach a quite big size of tens of nm due to the silane shell, avoiding any FRET interactions.

More complex shells on the surface of the NCs were developed as well by adsorbing layers of protein [44, 137, 138], polymers [139-141, 142, Wu, 2003 #300] or lipids [13] for example.

Figure 3.1.1 taken from Chan et al. [127] summarize and illustrates the different approaches for obtainment of water-soluble NCs via surface modification of the nanocrystals, suitable for further binding to biomolecules.
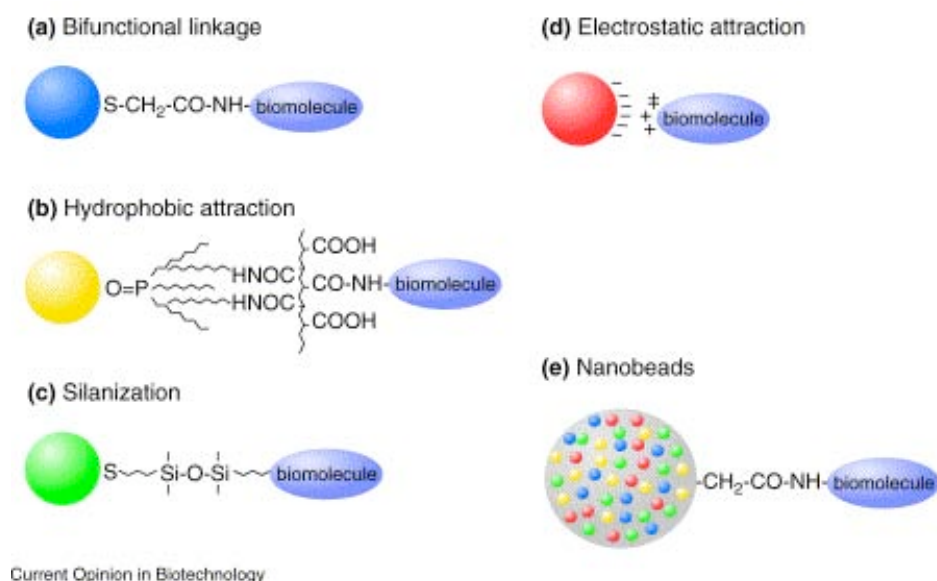
58

(a) Bifunctional linkage
S-CH$_2$-CO-NH- biomolecule

(b) Hydrophobic attraction
O=P ∼∼∼ HNOC { COOH
∼∼∼ HNOC { CO-NH- biomolecule
{ COOH

(c) Silanization
S∼∼ Si-O-Si ∼∼ biomolecule

(d) Electrostatic attraction
biomolecule

(e) Nanobeads
-CH$_2$-CO-NH- biomolecule

Current Opinion in Biotechnology

Figure 3.1.1: Schematic illustration resuming the different bioconjugation methods. (a) Use of a bifunctional ligand such as mercaptoacetic acid for covalent linkage of NCs to biomolecules [135]. (b) TOPO-capped NCs bound to a modified acrylic acid polymer by hydrophobic interaction. Then biomolecules are covalently attached. (c) NC solubilization and bioconjugation by exchanging TOPO against mercaptosilane, additional silanization and finally covalent linkage to a biomolecule [12]. (d) Creation of negatively charged NCs through ligand exchange, then adsorption of biomolecule via electrostatic interactions [137]. (e) Incorporation of NCs into nanobeads, then linkage to biomolecules [143]. Image taken from Chan et al. [127].

Exchange of TOPO by charged ligands such as thiolactic acid [137, 144] and subsequent electrostatic adsorption of biomolecules is an interesting method for exposing various functional groups on the NC surface. Presently, it is difficult to analyze and quantify such adsorbed biopolymers at the NC surface. Furthermore problems with non-specific binding were observed on the biopolymer coat. Many other approaches of surface modification and binding of NC to biomolecules were performed using strategies present in figure 3.1.1 [44, 138, 145-150].

Monolayers of ligands around the NCs can often result in unstable colloidal solutions. In contrast, NCs coated by multilayers of ligands and/or adsorbed molecules show higher stability, but the procedure to obtain modified NCs is time consuming and often difficult to control.

In the present work, we self-assembled lipid monolayers on TOPO-coated NCs (scheme b in the figure 3.1.1) via hydrophobic interactions. For this purpose, mixtures of lipids and

different functionalized lipids were used to obtain water-soluble functionalized-NCs. Different functionalities were tried to get different functionalized-lipid-NCs so-called functionalized-NC. Specific binding was then shown for the functionalized-NCs as well as for multi-functionalized NCs (chapter 4).

3.2 Amphiphile coating methods and lipid choice

3.2.1 Goal to be reached

We believe that coating TOPO-NCs with lipids offers certain advantages. First, by varying the lipid polar headgroups in the lipid mixture, it is possible to introduce a variety of physical (switchable electrical charges, structures, entropic shielding) and chemical (reactive groups, biological recognition elements) properties. In addition, if functionalized lipids (e.g. biotin, NTA, hexahistidine, amino group, carboxylic acid, DNA) are added to the mixture, functionalized NCs are produced. Many functionalized-lipids can be purchased, and if necessary, the addition of a desired functionality on a lipid is relatively straightforward [151]. The amount of functional groups on a NC can also be controlled easily by varying their initial ratio of functionalized-lipids in the lipid mixture. In addition, the water-solubilization step and the functionalization step are achieved simultaneously.

Another important advantage of the lipid coating is the small size of the resulting coated NCs, which allow observation of FRET interactions (see chapter 4). Indeed the lipid coating increases the TOPO-NC radius of approximately 2 nm, a thin layer compared to proteins or polymer adsorption.

For structural size concern, a lipid-NC is typically composed of the core, the CdSe semiconductor NC, which is surrounded by a 1 nm thick TOPO layer and finally by the lipid shell (figure 3.2.1).
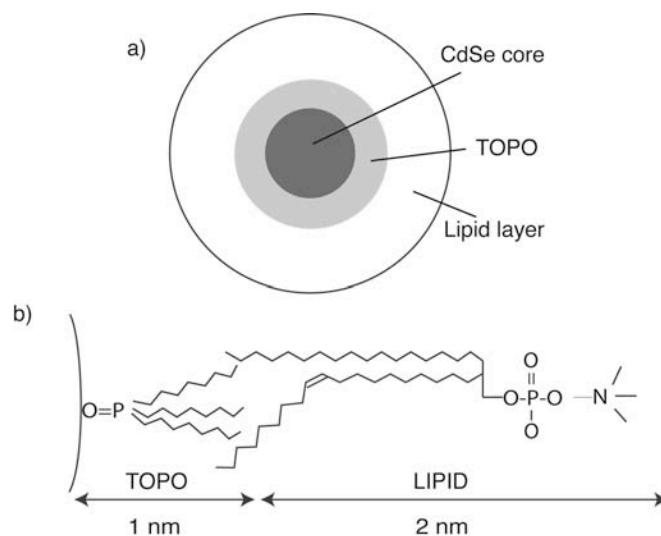
Figure 3.2.1: Schematic representation of a lipid-NC. a) The CdSe core (dark grey) is surrounded first by a TOPO layer (faint grey) via coordination of the P=O group toward the Cd atoms of the surface. The TOPO-NC is then surrounded by a lipid monolayer (white). If the lipid monolayer comprises functionalized lipids, we obtain a functionalized-NC. b) Chemical structure and orientation of TOPO and the lipid with respect to the NC surface (bent line).

3.2.2 Solubilization method and lipid composition

For the lipid coating of NCs, two different methods were used. Different protocols were developed by varying systematically experimental conditions, such as the use of detergent, the mixture of lipid and their relative concentrations. The goal was to obtain solubilized NCs suitable for further specific binding of biomolecules.

Methods:

- *Method 1*. A solution in chloroform of lipids and TOPO-NCs is dried first in a rotary evaporator, then in high vacuum overnight. Hydration of the film is achieved by addition of water and agitation. If indicated detergent was added in the aqueous solution. The way of dispersing (sonication or smooth vortexing) the NC together with lipids in water can influence the resulting solution.

- *Method 2*. We start with two phases, a chloroform solution containing the TOPO-NCs and the lipid mixture and a second water solution containing the detergent. The mixture is slowly rotary evaporated until total evaporation of the chloroform (chloroform has a lower boiling temperature) ending up with an aqueous solution of the solubilized NCs containing lipids and detergent.

Selection of lipids:

A wide variety of different lipids exist, but not all of them are suitable for covering the nanometer-curved NCs (approximately 3 nm). We selected the lipids according to the following considerations:

- The head groups should be negatively charged (e.g. phosphatidic acid, serine, glycerol, inositol, cardiolipin), positively charged (DOTAP-Cl) or zwitterionic (choline, ethanolamine). Negatively charged lipids are known to form small vesicles in solution. At low ionic strength of solutions dispersions of negatively charged lipid vesicles are stabilized via electrostatic repulsions between vesicles. The area per lipid headgroup in a lipid mono- or bilayer depends on its electrical charge and of course on its geometrical size, which in turn determines the structures of the lipid aggregation in water.

- The lipid can have a single (lysolipids, micelle forming lipids) or two hydrocarbon chains. The alkyl chain length and saturation can be selected as well. All these parameters influence the transition phase temperature and the shape of the lipid.

A summary of the shape-structure concept considered for the lipid choice is illustrated in the figure 3.2.2.

When using a lipid mixture of differently shaped lipids instead of a single sort of lipid, the packing mode can be changed. Looking at figure 3.2.2, we can conclude that for NC solubilization, only lipids belonging to the first and second category or mixtures thereof would be suitable for NC coating.
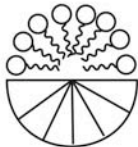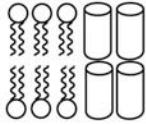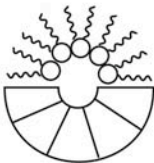
Figure 3.2.2: A model of geometrical packing of various amphiphiles into colloidal aggregates. Illustration taken from [152].

The phase transition temperature should be also considered. It will be shown below that a rigid lipid such as DPPC can give rise to lipid coated NCs as well, with a similar stability as lipids with phase transition below room temperature.

Other parameters to be considered are: the ionic strength, pH, buffer used, as well as the temperature of the aqueous phase.

3.3   Fluorescence photo-brightening effect

Fluorescence photo-brightening (FPB) is observed within some batches of NCs and is an annoying effect for quantitative experiments. But it might be interesting to increase the QY of the fluorescent NCs if required. With FPB effect, an increase of the fluorescence quantum yield of the NCs is observed during illumination, and a reversible decrease in the dark. This effect is impressively illustrated in figure 3.3.1, taken from Jones et al. They observed this effect with CdSe/ZnS core-shell systems instead of core CdSe like us, but this experiment illustrates well the FPB effect.
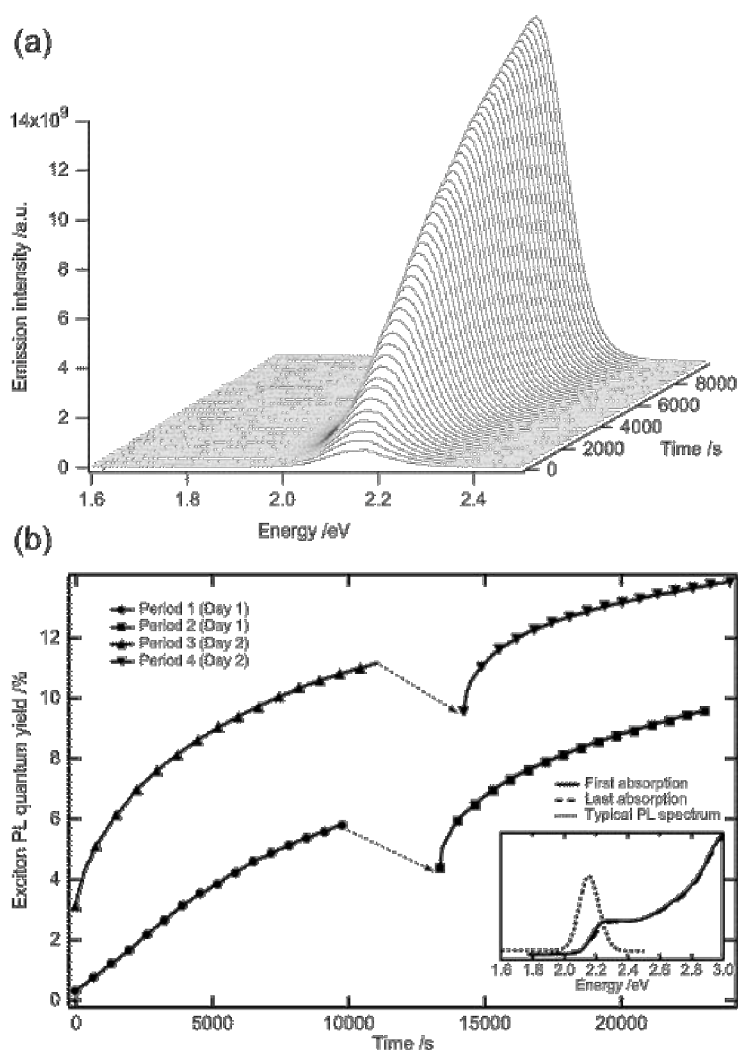
Figure 3.3.1: Representative series of fluorescence spectra (a) and the relative fitted exciton emission intensities for CdSe/ZnS core-shell in toluene 0.01M illuminated with 488 nm light. The insert depicts typical spectra with two adsorption spectra taken before the first and after fourth illumination period. Image taken from Jones et al. [153].

This effect was not observed with the first batch of NCs synthesized, so TIRF immobilization could be measured without problems (see chapter 6), but with the later samples, this effect perturbed us first without knowing it origin. We could illustrate this effect by taking a simple time base scan of the fluorescence intensity and observed the continuous increase of the fluorescence intensity with illumination time.

Similar effect was observed by Maenosono et al. on CdSe NC in polymer films [154, 155] as an increase in photoluminescence (PL) with illumination. It was reversible and accompanied by

a slight blue shift, and the initial explanation was referred to excited electron accumulation in the NC organic environment as depicted in figure 3.3.2.
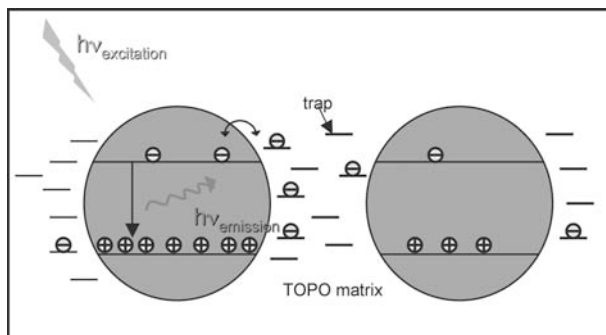
Figure 3.3.2: Illustration of the electron accumulation through illumination of a polymer film containing NCs. Taken from Maenosono et al. [154].

Cordero et al. [156] made different experiments on this photo-enhancement of photoluminescence PL or fluorescence, and observed as before a slight blue shift and quasi-reversibility of the phenomenon. But they found out that this effect was much less pronounced for core-shell CdSe/ZnS NCs. They observed that under dry gas atmosphere, no FPB effect occurred, as opposed to a "wet" atmosphere. They explained these observations by photo-passivation of the surface due to adsorbates, especially water molecules, which are responsible for the luminescence activation according to them. Molecular adsorption paths are represented in the figure 3.3.3.
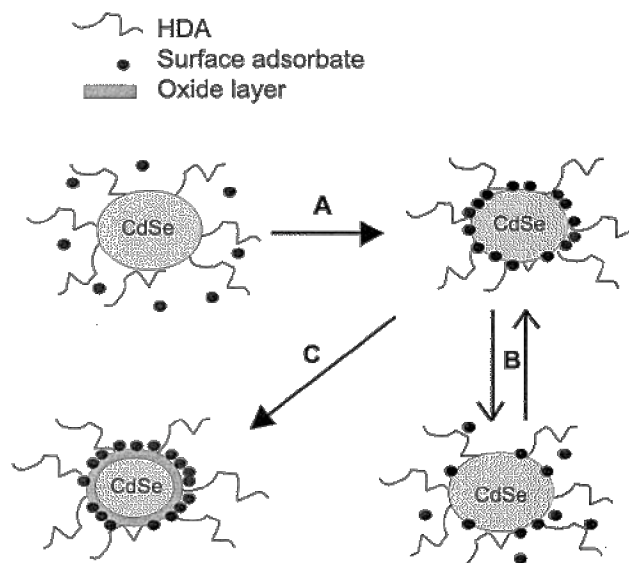
Figure 3.3.3: Simple illustration of the proposed adsorption model for fluorescence activation. Nearby water molecules adsorb to the surface of the quantum dot upon illumination with above band edge light (path A). The adsorption is pseudo-reversible shown by path B. Here, the adsorbates are removed during illumination by opening the sample to vacuum, or likewise by shutting off the illumination source. Path C shows the eventual outcome of extended excitation in air. Consequently, the formation of an oxide layer leads to a decrease in the luminescence, and a smaller dot (blue shift in the exciton spectrum). The product of path C can continue to undergo path B, but is not illustrated here. Taken from Cordero et al. [156].

Only recently, Jones et al. [153] further studied this effect during darkening periods where the PL decreased, the fluorescence spectra showed a blue shift and FWHM changed. PL decay-kinetics before and after illumination and increase of PL in the absence and presence of methanol in the organic solution were also studied: The FPB could yield a 42-fold increase of the initial PL intensity (figure 3.3.1). The slight blue shift observed for emission and absorption peak could be explained by a charge accumulation on the NC surface resulting in a Stark effect energy shift. An increase of the fluorescence lifetime was also observed. After illumination followed by a dark period, a second illumination was carried out, and they observed that the initial rise was faster the second time than the first time; as if the sample was "sensitized" by the first illumination. This sensitization decreased with the time spent in darkness. The authors interpreted these data as the nonradiative decay of excitons to the trap states that exist long enough to ensure that there is a significant possibility for their thermalization back to spin-allowed states S1. They also speak about photo-induced

rearrangement of TOPO molecules on the NC surface or the addition of surfactant molecules as methanol that could stabilize these traps and increase their lifetime and finally PL.

Asami et al. [157] reported investigations on the surface changes of TOPO coated CdSe NCs thin films by X-rays photoelectron spectroscopy (XPS) and time of flight secondary ion mass spectroscopy (ToF-SIMS). XPS measurements showed a slight decrease of the Se content and a increase in the selenium oxide peak, indicating that Se oxidation occurred on the NC surface; it also revealed a decrease of P and C which might be attributed to decomposition of TOPO and desorption from the surface. ToF-SIMS experiments showed that during brightening period an increase in TOPO-Se fragment ions was observed which was not existent in the initial solution before illumination. They explain that this would indicate that a part of the TOPO migrated from the Cd atoms to the Se during illumination as the quantum efficiency of PL is deeply correlated to surface states in NCs. This effect is qualitatively explained by the degree of passivation of surface traps by selenium oxide formation and TOPO migration.

3.4   Experimental section

3.4.1   Materials

Octyl-β,D-glucopyranoside (OG) and phosphate buffered saline (PBS) were purchased from Aldrich, Switzerland. All solvents came from Fluka, Switzerland. Non-labeled lipids as DPPC (dipalmitoylphosphatidyl choline), DOPC (dioleylphosphatidyl choline), POPC (palmitoyloleylphosphatidyl choline), POPG (palmitoyloleylphosphatidyl glycerol), mPPG (mono-palmitoylphosphatidyl glycerol) and mMG (mono-mysistoyl glycerol) and DOGS-NTA-Ni (1,2-dioleyl-sn-glycero-3-(N(5-amino-1-carboxypentyl)iminodiacetic acid)succinyl (Nickel salt)) were from Avanti Polar-lipids, USA. Biotinylated lipid DHPE-X-biotin (N-((6-(biotinoyl)amino)hexanoyl)-1,2-dihexadecanoyl-*sn*-glycero-3-phosphatidyl ethanolamine, triethylammonium salt) were from Molecular Probes, USA. Water used was of MilliQ purity. All products were used without further purification.

3.4.2   Lipid-coating of the NCs

NCs were precipitated from 1 ml of a 10 μM toluene solution by addition of 4 ml of methanol, pelletted by centrifugation (4000 rpm (rotor), 5 min), and dispersed in 2 ml of a

lipid solution (1 mg/ml) in chloroform. A typical lipid mixture used for preparing lipid-NCs consisted of 90 m% POPC and 10 m% POPG to produce lipid-NCs, or of 80 m% POPC, 10 m% POPG and 10 m% of the functionalized lipid (e.g. DHPE-X-biotin, DOGS-NTA-Ni), to produce biotin-NCs or NTA-NCs. 4 ml of 26.4 mM OG in water was added and then the mixture was slowly concentrated by evaporating the chloroform using a rotary evaporator. The resulting solution containing the coated NCs was dialyzed for 12h at room temperature against (2000 volume) water or PBS buffer for detergent removal.

3.4.3 Vesicles solution preparation and incorporation of NCs

4 mg DOPC in chloroform is rotary evaporated and dried under high vacuum overnight. The rehydration of the lipid film is done with 1 ml PBS buffer. Giant vesicles are formed. The solution is then sonified for few minutes to get small vesicles ranging from 30 to 100 nm.

3.4.4 Optical properties

See chapter 2 for material and apparatus.

The calculation of room temperature fluorescence quantum yields QY were determined by comparing the integrated emission band of the NC solution to the integrated emission band of reference dyes such as peryleneimide solution in toluene [124]. But here we have to count for the change of solvent from toluene to water (thus a change in refractive index). The equation used is

$$QY_{NC} = \frac{I_{NC}}{I_{Dye}} \times \frac{OD_{Dye}}{OD_{NC}} QY_{Dye} \frac{n_{NC}^2}{n_{dye}^2} \qquad 3.1$$

QY_{NC} and QY_{Dye} for the quantum yield of the NC and the dye respectively. I_{NC} and I_{Dye} are the integrated emission band, and OD_{NC} and OD_{Dye} the optical densities at the excitation wavelength of the NC and the Dye respectively. The values n_{NC} and n_{Dye} are the refractive index of the solvent solubilizing the NCs and the dye respectively (1.495 for toluene and 1.33 for water).

3.4.5 Cryo-TEM

For cryo-TEM a drop of lipid-NPs in water (approx. 1mg/ml) was deposited on an amorphous holey film carbon-coated 200-mesh copper grid. After removing excess solution

by blotting with filter paper, the grid was plunged into liquid ethane at – 180°C for immediate vitrification to obtain a thin film of amorphous ice containing lipid-NCs. The frozen grids were mounted under liquid nitrogen in a cryospecimen holder and measured at approximately –172°C in a Phillips CM12 electron microscope, operating at 80 kV. The pictures were collected on Kodak 4489 electron image film (Eastman Kodak Co.) at a nominal magnification of 45000.

3.4.6   Protocols

Density-gradient ultracentrifugation was performed to separate the lipid-NC from lipid vesicles present in solution. A density-gradient was created by layering up CsCl solutions of different densities; 1.5 (4M), 1.3 (2.4M) and 1.1 (0.78M) g/ml were selected. On the top layer, 500 µl of the lipid-NC solution was carefully loaded. The resulting gradient was ultracentrifuged at 55000 rpm (rotor) for 4 hours at 22°C. The lipid-NC migrated as a colored band between 1.3 and 1.1 density fraction. The collected lipid-NC solution was dialyzed against water or PBS to remove the CsCl.

Determination of phosphorus content using Fiske-Subbarow method [158] was done on ultracentrifuged and dialyzed lipid-NC solution. It allows estimation of the average lipid quantity surrounding a NC, if the quantity of TOPO (phosphorous containing molecule) per NC is known. Following Bowen Katari et al. [159] we estimated the amount of TOPO for a 3 nm CdSe NC to be 80. Known volumes (20 µl, 50 µl, 200 µl, 500µl and 1ml) of lipid-NP solution of 0.5 µM was dried out in a tube and 300 µl of $HClO_4$ was added, then sample was heated for 2-3 hours at 180°C in a destruction block, a marble placed on top of the tube. After cooling down, 3 ml of ammonium molybdate solution and 120 µl of Fiske-Subbarow reagent solution were added. Color was developed for 20 min in a boiling water-bath. Absorption spectra of the solutions were taken to determine the content of phosphorus, by calibration with solutions of known concentrations (90 nmol P_i gives an OD (830 nm) of about 0.7). The resulting amount was divided by the concentration of NCs and substracted by 80 to result in the amount of lipids as we have one P per lipid.

FTIR Spectra were collected on a 7000 FTIR spectrometer, DigiLab, Switzerland. The ATR data were acquired with the "Golden gate" diamond anvil ATR accessory (Graseby-Specac, U.K.) using typically 64 scans at a resolution of 2 cm^{-1}. A drop of the sample was deposited

on the diamond base and let to dry under nitrogen. Spectra were collected from 500 to 4000 cm^{-1}. Atmospheric water vapor bands were systematically subtracted from all spectra.

3.5   The amphiphile coating of NCs

Initially, we chose the zwitterionic DPPC as a rigid lipid with a phase transition of 41°C, i.e. above room temperature. We also opted for POPC as a fluid lipid, and POPG, which possesses a negative charge, and thus a larger head group favoring curved bilayers and avoiding aggregation, and finally a lysolipid to see its effect on coated NCs. The two methods introduced before were tried for different lipid mixtures and gave very different results, shown below.

3.5.1   Method 1: lipid/NC film
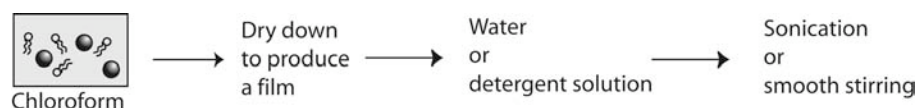
In this protocol, a chloroform solution of the TOPO-NCs and the desired lipids were totally dried down. The lipid mixture chosen were 100% DPPC, a mixture of POPC 90% and POPG 10% or POPC 70%, POPG 10% and 20% mPPG (lysolipid). On the dried NC/lipid film water or Octyl-β,D-glucopyranoside (OG) detergent solution was added. To assist the solubilization, smooth vortexing or sonication for 5 minutes were tried. The results for the dry film rehydration method are summarized in the table of the following page.

When clear solutions were obtained, fluorescence spectra and cryo-TEM images of NCs were taken. The cryo-electron microscopy picture (figure 3.5.1) show representative result of the lipids and NCs initially dried down and then rehydrated with detergent followed by sonication. The use of PBS pH 7.4 instead of water, gave no significant changes.

Sample	DPPC	POPC	POPG	mPPG	Detergent OG	Stirring method	Clear solution?	Stability	Average Quantum yield
1	100%	-	-	-	0	Stirring	NO	-	-
					0	Sonication	NO	-	-
					1.2 CMC	Stirring	NO	-	-
					1.2 CMC	Sonication	YES	Few days	0.03
2	-	90%	10%	-	0	Stirring	NO	-	-
					0	Sonication	NO	-	-
					1.2 CMC	Stirring	NO	-	-
					1.2 CMC	Sonication	YES	Few days	0.04
3	-	70%	10%	20%	0	Stirring	NO	-	-
					0	Sonication	NO	-	-
					1.2 CMC	Stirring	NO	-	-
					1.2 CMC	Sonication	YES	1-2 days	0.02
4	-	-	-	-	Only OG 2.4 CMC	Stirring	NO	-	-
					Only OG 2.4 CMC	Sonication	NO	-	-

Table 1: Results of trials using different lipid mixtures, with or without detergent, by stirring or sonication method. The average stability and quantum yield of the resulting solutions are given on the basis of repeated experiments. If the solution was not clear, and the NCs not solubilized, the fluorescence spectra could not be measured.
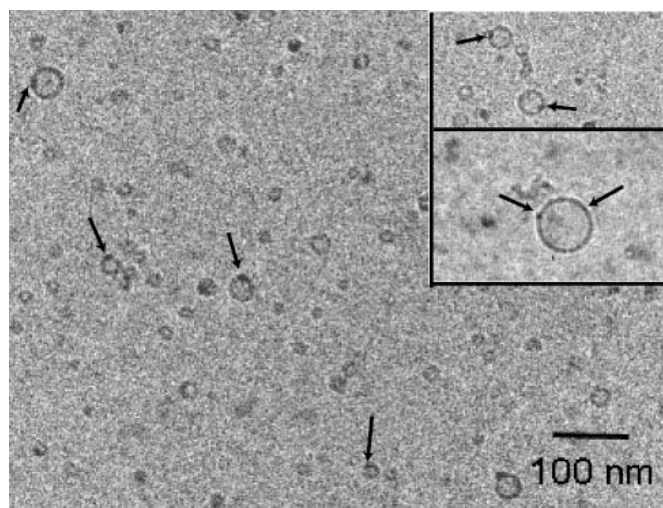
Figure 3.5.1: Representative cryo-EM image of samples from clear solutions summarized in the table (sample 2). The nanocrystals, visible as black dots, have more contrast than the organic lipid part and background. Small lipid-NCs coated by a lipid shell can be seen but many vesicles (with diameters smaller than 100nm) and NCs incorporated in the lipid bilayer of the vesicles. Upper right: two parts of different areas showing NCs incorporated into vesicles membranes (same scale).

It can be seen from the cryo-EM images taken from the different resulting clear solutions, that they consist of a mixture of structures such as NCs embedded in vesicle membranes and some lipid-NCs. The vesicles obtained are smaller than 100 nm. This result shows that it is possible to stain vesicles or cell membranes with the NCs, incorporated inside of the bilayer. (This is tried later with detergent-coated NCs).

By smooth stirring of the lipid and NC film with water, a procedure which in the absence of NCs yields giant vesicles, no clear solution could be obtained even after extended stirring overnight, with or without detergent. We believe that with this method giant vesicles are produced without incorporation of NCs. The NCs indeed stay in form of an insoluble orange film on the wall of the flask.

In conclusion, the method of drying the lipids and NCs into a film does not seems to be a good way to prepare single lipid-NCs, but gives interesting results as the NC can incorporate into the lipid membrane of a vesicle. Dubertret et al used this method for solubilizing NCs using PEG-lipids, drying a film and rehydration in water. They obtained good homogeneous solutions, but this could not be achieved with the lipid mixture chosen here. The use of polyethylene glycol (PEG) lipid mixture resulted in cloudy solutions.

3.5.2 Method 2: Smooth evaporation
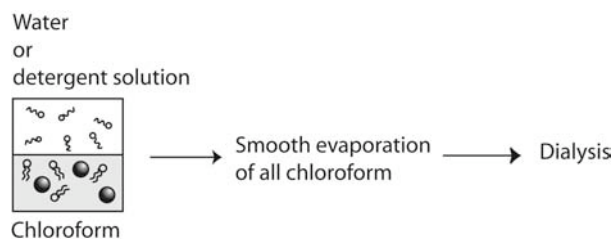
In this method, the chloroform solution containing the lipid mixture and the TOPO-NCs is added to an aqueous solution containing OG or not. This double-phase is then slowly evaporated to a 1/4 of the initial volume, avoiding drying of the mixture and forcing the hydrophobic species to solubilize into the water phase slowly during evaporation of the chloroform. Characterization via cryo-TEM, fluorescence and stability measurements (stability with time) were carried out and resumed in the table.

Samples	DPPC	POPC	POPG	mMG	Detergent OG	Clear solution?	Stability	Average Quantum yield
5	100%	-	-	-	0	NO	-	-
					1.2 CMC	YES	1 week	0.10
6	-	90%	10%	-	0	NO	-	-
					1.2 CMC	YES	Weeks	0.10
7	-	85%	10%	5%	0	NO	-	-
					1.2 CMC	YES	Few days	0.05
8	-	-	-	-	2.4 CMC	YES	Weeks	0.10

Table 2: Results of trials using different lipid mixtures, with or without detergent. The average stability and quantum yield are given on the basis of repeated experiments. Critical micellar concentration (CMC) of OG is 21 mM.

If no detergent was used, no clear solution could be obtained by gentle rotary-evaporation; irrespective which lipid mixture was used only turbid solutions were obtained.

Using OG solutions, different results were obtained depending on the lipid mixture. For the following lipid mixtures: 100% DPPC or POPC–POPG mixtures similar results were obtained. Increasing the percentage of POPG from 10 to 30% enhanced slightly the stability of the solution. This was most probably due to the negative charges on the surface. Similar lipid-NC structures and homogeneity were obtained for these lipid mixtures. A representative resulting solution is characterized by cryo-EM in figure 3.5.2 (sample 6).
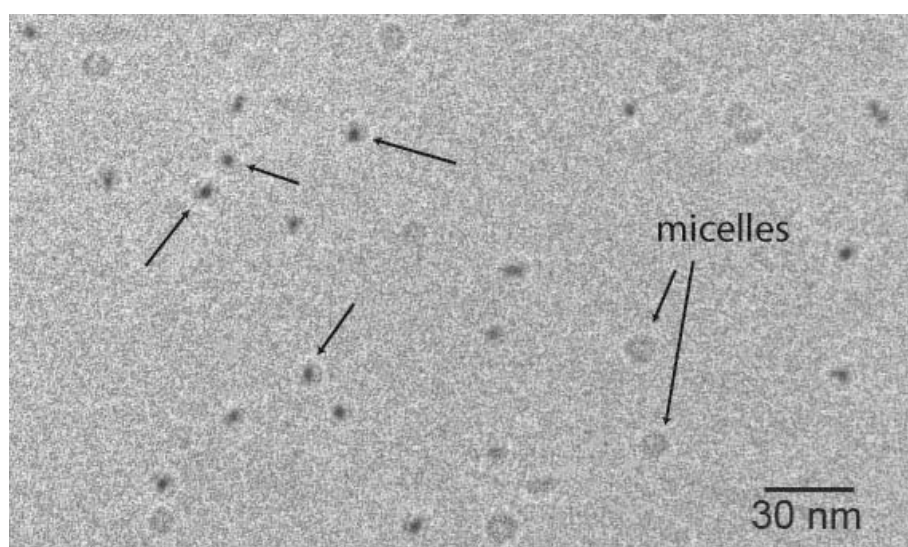
Figure 3.5.2: Representative cryo-EM image of a resulting solutions from method 2 sample 6. A more homogeneous solution can be seen here. We should point out the presence of few empty micelles as well, of similar sizes as the lipid-NC nanostructures. More than 80% are single NCs surrounded by a lipid shell, 18% are two NCs per lipid shell, and very few show more than 2 NCs.

In this figure 3.4.2, we can see that the solution is quite homogeneous. The NCs appear as black spots coated by a lipid monolayer (lipid-NCs). Few empty micelles could also be seen, but in a negligible amount and containing no NC thus not fluorescent. This protocol resulted in lipid-NCs, the structures we were interested to get for further production of functionalized lipid-NCs (functionalized-NCs), which are used in the next chapters.

If the lipid mixture was composed of POPC 85%, POPG 10% and mMG 5%, the resulting solutions were less stable, and the cryo-EM revealed the presence of aggregates in the form of filaments as illustrated in figure 3.5.3.
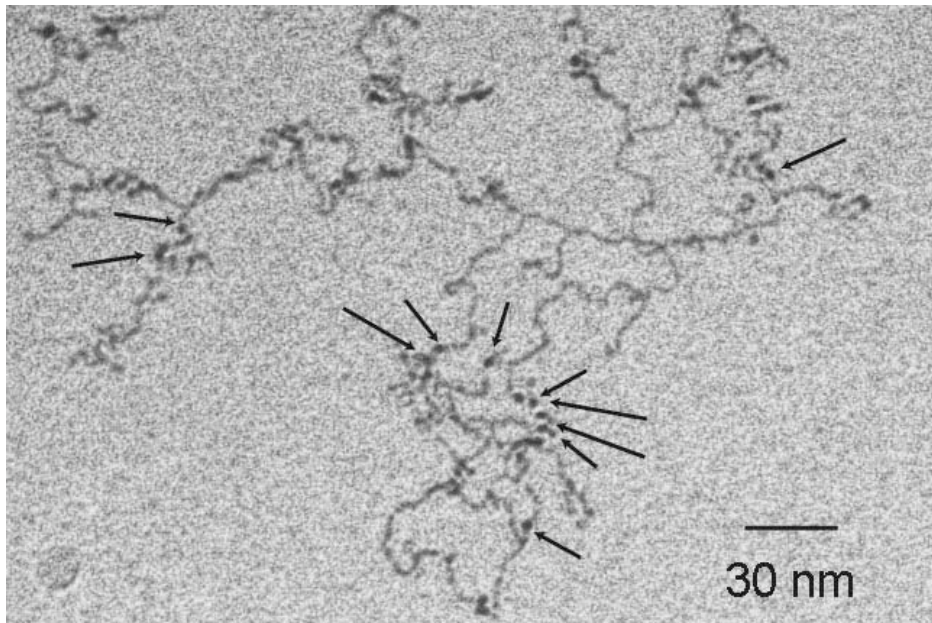
Figure 3.5.3: Representative cryo-EM image of a resulting solutions from method 2 sample 7. The NCs, black dots, are embedded in a network or filaments of lipid bilayers.

Taking a mixture of POPC, POPG 10%, with addition of 10, 20 or 30% PEG2000-lipid, it resulted in huge aggregates and the solution becoming instable.

If only detergent was used without lipids (sample 8), a clear and fluorescent solution of detergent-NCs was obtained with comparable QY to lipid-NCs, the long stability being slightly higher. The cryo-EM images revealed the presence of many vesicles together with small detergent-coated NCs (figure 3.5.4).
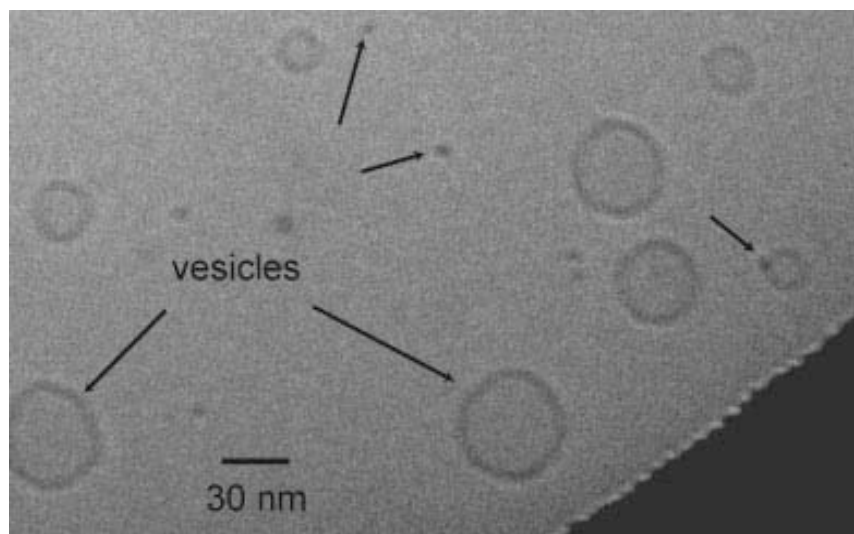
Figure 3.5.4: Representative cryo-EM image of a resulting solutions from method 2 (sample 8). The NCs (black dots) are surrounded by a detergent shell, but are also present in vesicles membranes. Here many vesicles of diameter ranging from 30 to 200 nm are present in the solution.

Subsequently we tried to incorporate the NCs into preformed lipid vesicles. If this would be feasible, we then would be able to incorporate the NCs also into cell membranes using a detergent-NCs solution. The NCs would be exploited like a hydrophobic membrane dye.

In order to realize this goal we first injected 200 µl of detergent-NCs (2.4 CMC in 0.5 mg/ml NCs in PBS) into a 400 µl solution of DOPC vesicles (4mg/ml in PBS at room temperature). During this procedure we quickly diluted the detergent-NCs below critical micellar concentration of OG, and thus remove (part) of the detergent monolayer surrounding the remaining TOPO-NCs. The hydrophobic TOPO-NCs are then forced to partition into the core of the vesicular lipid bilayers, as can be seen in the cryo-EM images in figure 3.5.5.
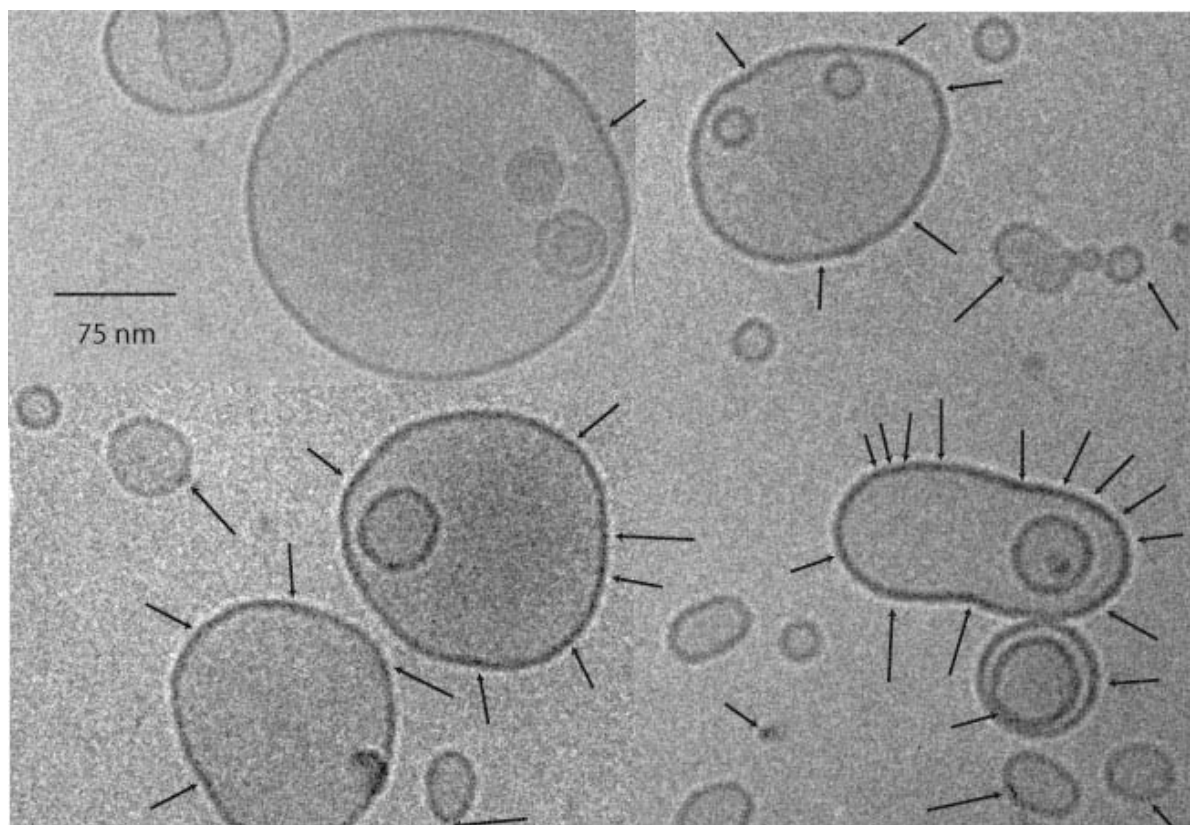
Figure 3.5.5: Cryo-EM images of DOPC vesicles after addition of detergent-NCs. NCs can be seen in central part of the vesicular lipid bilayer (arrows).

This positive result encouraged us to further test the incorporation of the NCs into cell membranes, but this gave rise to adhesion of patches of NCs on the cell membranes (aggregation). Moreover the presence of detergent disturbed the cell, as vesicles formed rapidly around the membrane (the cell bubbles). This was not further studied, as it was not the main goal of the thesis, but will be followed up by another PhD student.

Summarizing the data from the above results, the presence of detergent is important for the formation of homogeneous lipid-NCs colloidal solutions. The composition of the lipid mixture does not influence the resulting solution so much, apart from the presence of lysolipids and PEG2000 lipids. The use of detergent only was not suitable for production of small single NC structures, but is encouraging for the incorporation of NCs as membrane dyes in vesicles or cells.

Method 2, avoiding total drying was finally chosen for production of lipid-NCs, as it gives rise to reasonably homogeneous solutions of mostly single NCs surrounded by a lipid monolayer (lipid-NC), if using DPPC or mixtures of POPC and POPG. Adding

functionalized lipids to the lipid mixture allowed the formation of functionalized-NCs. The presence of 10% functionalized lipids together with POPC and POPG did not modify the homogeneities of the lipid-NCs solutions.

In an optimized protocol we used POPC 80%, POPG 10% and 10% of a functionalized-lipid to prepare functionalized-NCs as stable and fluorescent nanocomposites for specific interactions with biomolecules and subsequent immobilization.

3.6 Characterization and behavior

3.6.1 Optical properties

In this part we investigated the lipid-NCs absorption and emission spectra, followed by calculation of quantum yields and photostability measurements.

The optical properties of the lipid-NPs in water were compared to those of the original NPs in toluene. Transferring the NPs from organic solvent to aqueous phase by coating them with a phospholipid layer yielded no significant changes in the absorption and emission spectra shapes except for a slight diminution of the band visibility in the absorption spectra profile. The fluorescence emission maximum and the stability against photobleaching in solution were comparable to the initial ones. However, the modification of the microenvironment of the NP upon lipid coating is revealed by a modification of the fluorescence quantum yield.

Quantum yields of 10% on average were obtained for the different clear lipid-NC solutions. The QY of the initial preparation of TOPO-NCs in toluene is approximately 30-50%. Others [13, 150] have observed as well that the transfer of fluorescent organic shell-coated quantum dots from organic solvents to water via surface modification is accompanied by a reduction of the fluorescence quantum yield. However, a detailed investigation of this effect is still missing in the scientific literature. But it is known that the surface of the NC is critical for the fluorescence characteristics of the NC (see chapter 1 and 2). The amount of ligands on the surface, the position and structure of the ligand layer, the lipid layer influence on TOPO molecules and presence of water are potentially influencing parameters. In that sense, Wuistler et al. [160] made interesting observations recently. These authors have shown that the fluorescence of QDs responds upon changes of the structure of self-assembled alkylamines coating the nanoparticles. This demonstrates that the organic coating layer plays an active role on the creation or prevention of fluorescence quenching surface states of QDs.

The use of core-shell systems could resolve the problem of low quantum yield in water. These core-shell NCs give rise to QY of around 30% in water for lipid-coated CdSe/ZnS NCs (the core-shell were a sample given by I. Potapova from University of Mainz; the lipid-coating was made with method 2 using POPC-POPG mixtures). Only core CdSe lipid-NCs where used for the experiments described in the following chapters.

3.6.2   Results on fluorescence photo-brightening effect

Looking at our NCs behaviors, we observed a similar FPB effect as increase of fluorescence with illumination, as well as a faster increase upon second illumination after pre-illumination and darkness. In our case, the reversibility was not total; the final QY after long periods in the dark was still slightly higher than the initial one. The blue shift observed in our illuminated samples reached a maximum 5 nm, which is less than some published values for comparable increases (figure 3.6.1).

We could observe as well that the FPB effect was dependant to the illumination intensity. Illuminating with different laser power, we observed higher intensities reached with higher laser power for illumination.
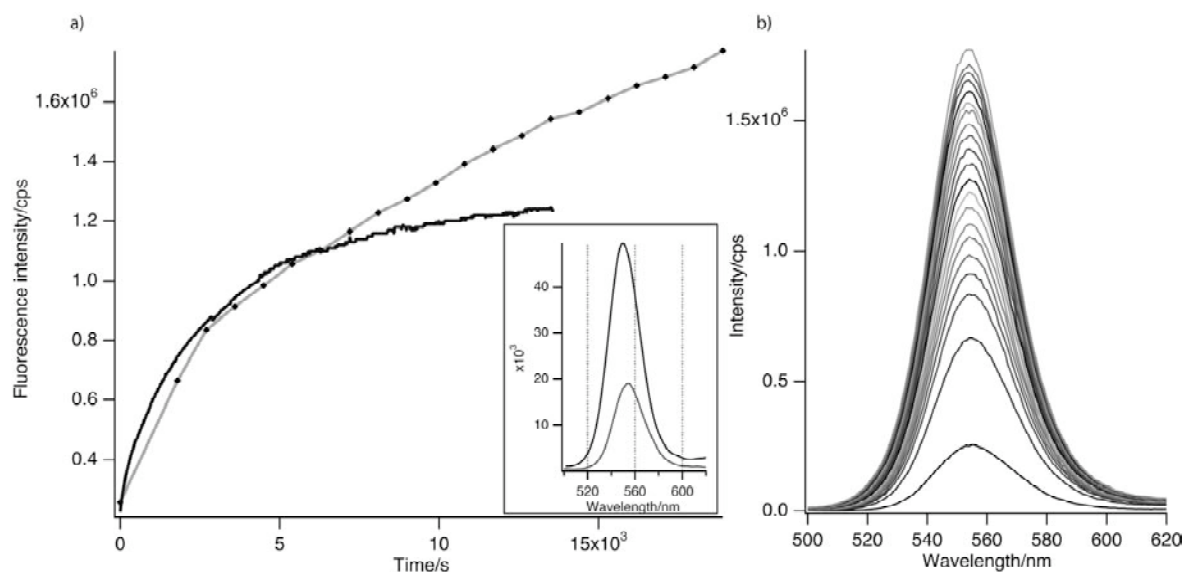
Figure 3.6.1: Results from FPB effect on our NCs (synthesis method 2, lipid-coated sample 6). a) Intensity increase with illumination time for two different laser powers, 200mW for the black continuous line and 400mW for the dotted-grey line. The insert representing the emission graph before grey and after illumination, a slight blue shift of 5 nm is visible. b) represent the emission spectra with progressive illumination time, corresponding to the grey curve in a. Increasing intensities corresponding to increasing illumination time. The batch used for this experiment had a initial QY lower than usual, around 3%.

Different batches were tried to find a correlation between the FPB effect observed and some samples, but no concrete conclusions could be made on the parameters influencing the FPB. We had the impression that the NCs produced with the synthesis method resulting in larger aspect ratio showed a more pronounced effect than dots. We also remarked a bigger increase for the lipid-NCs with the lowest QYs. But this was not further studied.

Another interesting finding was that TOPO-NCs in toluene did not show much FPB, the same NCs coated with lipids in water had a lower QY but showed a great FPB effect, the final fluorescence sometimes reaching values comparable to the NCs in toluene. The QY decreased reversibly in the dark without reaching the initial value (bottom right insert from figure 3.6.1 a). These findings can be correlated with the results from Asami et al., the presence of water in the surroundings being higher than in toluene.

This effect disturbs quantitative measurements based on fluorescence intensities. For our own experiments the FPB was checked if present and if so it was avoided by taking a new sample of the solution for each measurement for interaction with proteins. The quantum yields reported in this PhD work refer to the initial NC solution without illumination. The positive

aspect of FPB remains for microscopic imaging to enhance the fluorescence intensity of NCs. Pre-illumination can be done on the sample to increase the brightness.

3.6.3 Fourier Transform Infrared spectroscopy

FTIR was used to probe the presence of the different components of the lipid-NCs as shown in figure 3.6.2.
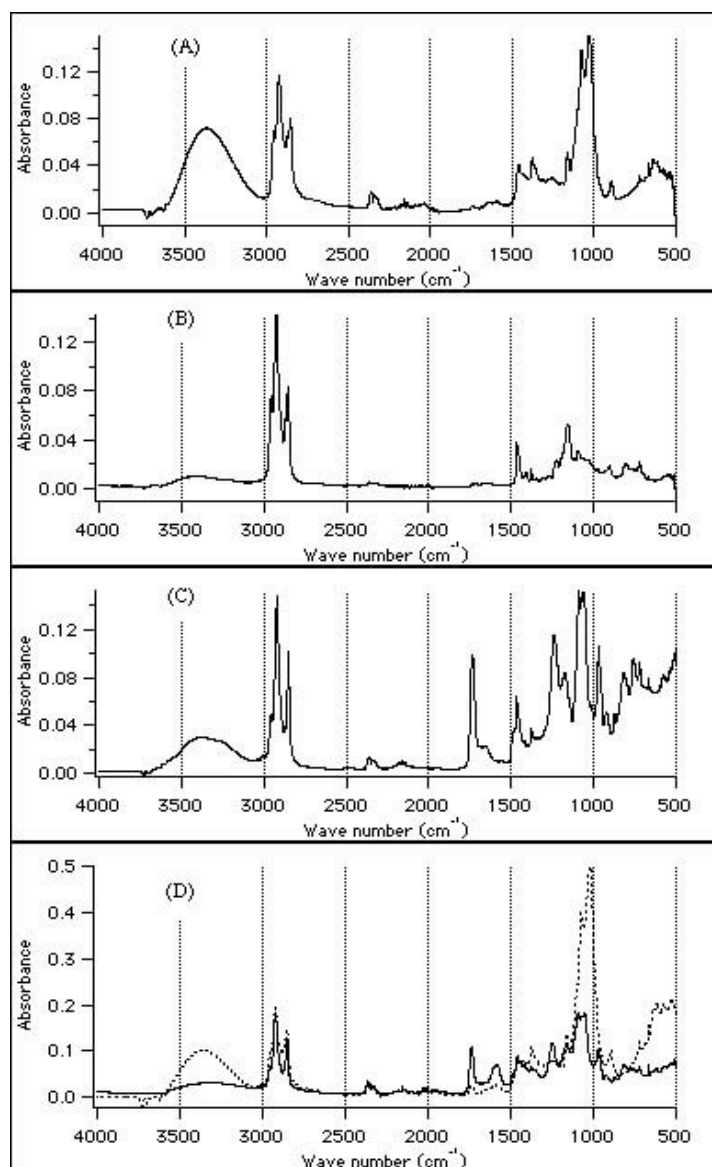

Figure 3.6.2: FTIR spectra of compounds. (A) detergent OG, (B) TOPO ligand, (C) lipid mixture and (D) the resulting lipid-NC solution before (dashed line) and after dialysis (black line). We can see that majority of the OG detergent is removed.

The comparison of the non-dialyzed and dialyzed lipid-NCs spectra demonstrate that most of the OG detergent used during lipid coating is removed by dialysis.

3.6.4   Amount of lipid per nanocrystal

Determination of phosphorus content using Fiske-Subbarow method [158] was performed on ultracentrifuged lipid-NC solutions (eliminating the small amount of micelles present). This allowed estimation of the lipid quantity surrounding the NCs, knowing the quantity of TOPO per NC [159]. The resulting ratio of NCs: Lipids was 1: 70, assuming 80 TOPO molecules per NC of 3 nm (diameter). This ratio seems to be too low for the size of the particle as a geometrical estimation gave results of 100-120 lipids per NC (depending on packing considered). These measurements were done on ultra-centrifuged samples, which are maybe different from the initial. A certain amount of lipid is maybe washed out during this process. The amount of functionalized lipids was determined by producing lipid-NCs including 10% of a fluorescent lipid (Rhodamine-DHPE, absorbing between 500 and 600 nm) instead of functionalized lipids. After lipid coating, we could estimate the amount of fluorescent-lipid to NCs with the absorption spectrum and obtained 5-6 fluorescent-lipids per NC. This values compared to the amount of 70 lipids indicates that the composition on the NC reasonably reflects that of the initial mixture used for coating.

3.6.5   Effect of buffer composition

Prior to use lipid-NCs, it is important to evaluate their fluorescence properties in different buffers. We tested the pH-dependence of the fluorescence of lipid-NCs (all solutions 5 μM) in the following buffers: sodium citrate pH 5, PBS pH 7, HEPES pH 7.4, borax pH 9; deionized (MilliQ) water was used for comparison. The results are summarized in figure 3.6.3.
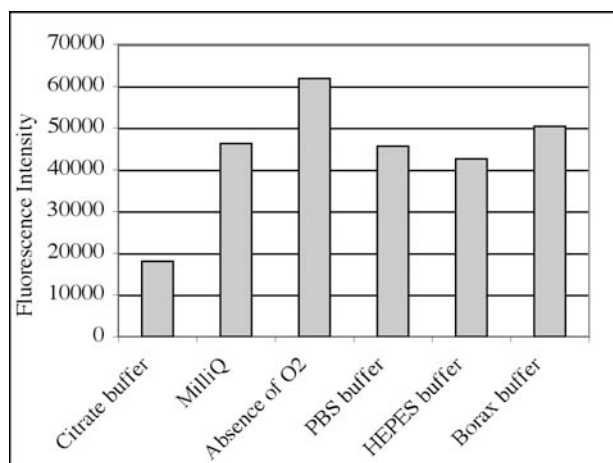
Figure 3.6.3: Fluorescence of the lipid-NCs in different buffers. The lipid-NCs (90% POPC, 10% POPG) were dissolved in different buffers and their fluorescence intensities are shown in the graph.

Lipid-NPs showed no significant difference in fluorescence intensity between pH 7 and 9 in different buffers, however, a decrease by 1/3 at pH= 5. These measurements show that lipid-NPs are not very sensitive to the environment and can be applied to a variety of experimental conditions.

3.7 Conclusions

We introduced an easy-one-step method to solubilize the TOPO-coated NCs through coating with lipids.

A huge choice of functionalities is available for preparing functionalized-NCs. We can control the average amount of functionalities needed on the NC surface by adjusting their percentage of the initial lipid mixture for coating. This is not straightforward with other existing methods.

We can produce an adjustable surface, which properties could vary from negative to positive surface charges or other physical properties by varying the lipids of the mixture. The lipid-NCs possess good optical properties and photostability, and remain stable in solution for weeks. Certain samples showed fluorescence photobrightening FPB effect. This was circumvented by the use of new solutions for each fluorescence measurements.

Thus it is easy to produce NCs with any fluorescent "color" bearing any needed functionality. In the following chapters the properties and functionalization of the lipid-NC were exploited to demonstrate specific interactions, first for different functionalities with complementary

biomolecule, for multi-functionalized-NCs and for the absorption of a peripheral membrane protein. Functionalities were used as well to specifically immobilize the NCs in predefined structures of micropatterns.

4   Specific interactions of functionalized-NCs

As well described in recent reviews [15, 16, 90] and the book entitled "Nanobiotechnology" [161], **hybrids** of nanomaterials and biomaterials are in the focus these years. Modified biomolecules such as nucleic acid, proteins or anti-bodies are put into contact with inorganic nanoparticles, and supramolecular complexes of these components are produced to create nanostructures possessing the desired properties and function.

The unique properties of the two classes of building blocks are of interest here: The size dependant optical, electrical, magnetic and electrochemical properties of the nanomaterials (depending on the material they are made of, their size, their structures), while the biomolecules, such as proteins and nucleic acids, reveal perfect binding properties and biochemical functionalities.

Research in this field today is concentrated in two major directions. First, the fabrication of self-assembly of inorganic nanoparticles and biomolecules, e.g. for the design of useful artificial nanometer structures using biological molecules or micropatterning on surfaces [34, 137, 162, 163]. Second, they are used as sophisticated materials, e.g. as specifically interacting fluorescent probes for labeling and analytical purpose and chemical libraries [12, 13, 33, 35, 36, 38, 45, 46, 68, 89, 91, 136, 146, 149, 150, 163, 164].

Nucleic acids on gold nanoparticles were developed initially because of their ease of production and handling. These hybrid particles provided highly specific tools for DNA-based bioanalysis [32-34, 36-38, 164].

Proteins have also been used to extend the binding capabilities of these inorganic nanoparticles. These supramolecular composites were mostly used as in vivo or in vitro fluorescent probes for cell imaging or biotechnology assays applications [44, 144, 145, 147, 148, 162]. For this purpose, many type of coating molecules such as simple thiol-ligands, polyelectrolyte, and amphiphile polymers were used which allow subsequent specific interactions with other biomolecules or small analytes.

In chapter 3, a versatile novel method was developed to coat TOPO-NCs with a lipid monolayer and thereby solubilize the NCs in water. Functionalization for the specific interaction with biomolecules was achieved via the addition of functionalized-lipids in the lipid mixture used for solubilization of the NC. For this purpose, commercially available or homemade functionalized lipids (biotin, NTA, hexahistidine-tag) were used.

To check binding affinity of the resulting functionalized-NCs, FRET experiments were carried out to test the specificity of interactions with their complementary recognition element. To demonstrate the possibility of decorating the NCs with more than one kind of functionality, a double-functionalization of the lipid-NC was achieved using biotin and NTA simultaneously. A multiple FRET experiment was then achieved between a NC and two different proteins attached to it; the NC acting here as a local **nano-excitation source** and as **nano-template** for immobilization of two initially non-interacting proteins.

Such supramolecular assemblies can be applied for analytical assays, as was recently shown for the detection of maltose [146] using maltose binding protein adsorbed on NCs.

In the next part the basis of FRET is explained as far as it is required for the evaluation of our experimental data. The specific interactions via the different functionalities (histidine-tag, biotin and NTA) are presented subsequently.

4.1 Intermolecular optical interactions

4.1.1 Förster Resonance Energy Transfer

Fluorescence or Förster resonance energy transfer FRET is a nonradiative energy transfer between a donor molecule and an acceptor molecule. The donor fluorescence spectrum

overlaps with the absorption spectrum of the acceptor. FRET results in long-range dipole-dipole interactions between donor and acceptor [165].

The following is referred to figure 4.1.1. Upon excitation the donor (D) absorbs the photon $h\nu_0$ and relaxes to the singlet excited state $S_1(D)$. The excitation energy of the donor can be released via fluorescence emission $h\nu_D$; the rate constant of this process is k_D. If there are allowed resonance optical transitions in donor and acceptor (A) electronic structures, the excitation energy can be nonradiatively transferred to the singlet excited state of the acceptor $S_1(A)$ with the rate constant $k_{D/A}$. For an efficient transfer ($k_{D/A} > k_D$) the energy of the excited state of the donor and acceptor states should be in resonance, i.e. the fluorescence spectrum of the donor and the absorption spectrum of the acceptor should overlap. Finally the acceptor can emit a photon $h\nu_A$.
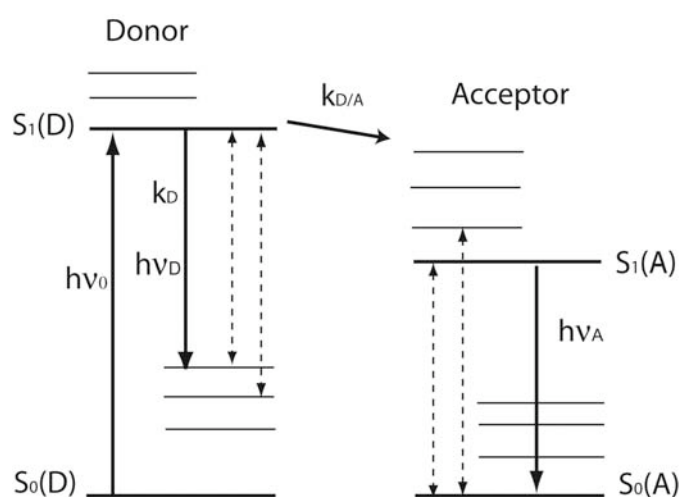
Figure 4.1.1: Energy diagram for the nonradiative energy transfer. $S_0(D)$ and $S_1(D)$ are the ground and first excited singlet states of the donor; k_D and $k_{D/A}$ are the rate constants for the radiative and nonradiative energy transfer processes, respectively. Solid lines depict photon participated transitions, dashed lines depict resonant transitions in the electronic structures of the donor and acceptor [165].

The rate of energy transfer depend on the overlap of the fluorescence spectrum of the donor and the absorption spectrum of the acceptor, the quantum yield of the donor, the relative orientation of the donor and acceptor transition dipoles, and the distance between D and A. This allows to measure (i) interaction between molecules, for example: between proteins, between a protein and a ligand, or (ii) distances between two sites in a macromolecule. If

there is a single donor and acceptor, and if D-A distance does not change during excited-state lifetime, the D-A distance can be calculated from the FRET efficiency.

The rate of energy transfer for a single D-A pair separated by a distance r can be expressed using the Förster formalism introducing the Förster radius R_0 which is the distance between the donor and acceptor at which the rate of the nonradiative energy transfer is equal to the rate of radiative fluorescence of the donor. We can express the rate of energy transfer as

$$k_{D/A} = \left(\frac{1}{\tau_D}\right) \times \left(\frac{R_0}{r}\right)^6 = \frac{B \times QY_D J}{\tau_D r^6} \tag{4.1}$$

where QY_D is the quantum yield of the donor and τ_D is the excited-state lifetime of the donor; the constant B is a function of the refractive index of the medium n_d, the Avogadro's number N_A and a parameter κ_p that depends on the relative orientation of the donor and acceptor dipoles [138] as

$$B = \frac{\left[9000 \times (\ln 10)\right]\kappa_p^2}{128\pi^5 n_d^4 N_A} \tag{4.2}$$

κ_p^2 = 2/3 for randomly oriented dipoles and varies between 0 and 4 for the cases of orthogonal and parallel dipoles, respectively. The overlap integral, J, defined as

$$J = \int_0^\infty PL_{D-corr}(\lambda)\varepsilon_A(\lambda)\lambda^4 d\lambda \tag{4.3}$$

is a quantitative measurement of the donor-acceptor spectra overlap over wavelengths λ. It is a function of the normalized donor emission spectrum PL_{D-corr} and the acceptor absorption spectrum expressed by the extinction coefficient ε_A.

The FRET efficiency E is defined as

$$E = \frac{k_{D/A}}{k_{D/A} + \tau_D^{-1}} = \frac{R_0^6}{R_0^6 + r^6} \tag{4.4}$$

And the Förster radius as

$$R_0 = (BQY_D J)^{1/6} = \left(\frac{9000(\ln 10)\kappa_p^2 QY_D}{N_A 128\pi^5 n_d^4} J\right)^{1/6} \tag{4.5}$$

This distance is typically in the range of 20 to 80 Å.

In our case, a CdSe NC acts as donor, to which several acceptors are bound. To account FRET between one donor and several acceptors equation 4.4 can be modified as

$$E = \frac{nR_0^6}{nR_0^6 + r^6} \qquad\qquad 4.6$$

assuming equivalent distances between donor and each acceptor. Here n is the average number of acceptor molecules interacting with one donor. Thus the presence of more than one acceptor increases the rate of FRET.

By measuring the emission spectrum of the donor in the absence and in the presence of the acceptor, the FRET efficiency can be calculated as

$$E = 1 - \frac{F_{DA}}{F_D} \qquad\qquad 4.7$$

where F_{DA} is the fluorescence intensity of the donor in the presence of the acceptor and F_D is the fluorescence intensity in the absence of the acceptor.

Rearranging equation 4.6 to gives an expression for the donor-acceptor distance r as a function of n

$$r_n = \left(\frac{nR_0^6(1-E)}{E}\right)^{1/6} = R_0\left(\frac{n(1-E)}{E}\right)^{1/6} \qquad\qquad 4.8$$

As R_0, n and E can be determined and estimated from experimental data, the donor-acceptor distance r can in turn be obtained.

Equation 4.8 is used to evaluate the donor-acceptor distance r from FRET knowing the values of R_0, n, E. This treatment assumes an exciton with a symmetric wave function around the NC center, which may not be appropriate for this case [138]. Moreover it treats the NC and the acceptors molecule as points, but the NC and the proteins are quite large particles. Nevertheless, it is the best treatment available for these type of experiments and gives a good idea on the specificity and distances between the energy transfer partners.

4.2   Experimental section

4.2.1   Materials

Lipids as POPC, POPG and 1,2-dioleoyl-sn-glycero-3-[N-(5-amino-1-carboxypentyl) iminodiacetic acid succinyl] nickel salt (Ni-NTA-DOGS) were provided by Avanti Polar Lipids, USA. N-((6-(biotinoyl)amino)hexanoyl)-1,2-dihexadecanoyl-sn-glycero-3-phosphoethanolamine, triethylammonium salt (DHPE-X-biotin), streptavidin, streptavidin-Alexa568 and 633 were supplied by Molecular Probes, USA. All these substences were aliquoted and stored at –20°C. Biotin, octylglucopyranoside (OG), phosphate buffer saline (PBS) and ethylenediamine tetraacetate (EDTA) were purchased from Sigma, Switzerland. Ni-NTA-Magnetic Agarose beads were from Qiagen, Germany.

Hexahistidine tagged lipids were synthesized as described elsewhere [151]. EqFP611- His_6 proteins were produced by bacteria expression. The protein plasmid was provided by J. Wiedenmann and culture and purification were done as described [166].

4.2.2   Lipid-coating of NCs

A typical procedure for coating and bio-functionalization of NCs started with the precipitation of the NCs from 1 ml of a 10 μM toluene solution by addition of 4 ml of methanol, pelletted by centrifugation (4000 rpm, 5 min), and dispersed in 2 ml of a lipid solution (1 mg/ml) in chloroform. The lipid mixture used for preparing lipid-NCs consisted of 80 wt% POPC, 10 wt% POPG and 10 wt% of the functionalized lipid (His_6-lipid, DHPE-X-biotin, Ni-NTA-DOGS or equimolar mixture of DHPE-X-biotin and Ni-NTA-DOGS for double-functionalization), to produce His_6-NCs, biotin-NCs or NTA-NCs, or biotin/NTA-NCs, respectively. 4 ml of 26.4 mM OG in water was added, the mixture was then slowly concentrated by evaporating the chloroform using a rotary evaporator. The resulting solution containing the coated NCs was filtered via syringe-filter 0.2 μm; (Nalgene, USA) and dialyzed against water or PBS buffer (1:2000 volume, changed 2 times for 12h) to remove detergent.

4.2.3   Optical measurements

See chapter 2

4.2.4   Specific interactions

Binding to magnetic beads: Ni-NTA-functionalized magnetic agarose beads in a 5% suspension from Qiagen, Germany were used for binding of His_6-NCs. The solution of beads was initially washed three times with deionized water. The beads were then incubated in 500 μl solution of His_6-NCs 1 μM under continuous stirring. Absorption spectra were recorded after the magnetic beads were removed from the solution by magnet. The solution was then reincubated with the magnetic beads and stirred for another period.

FRET experiments: The specific interaction of functionalized-NCs with the particular proteins was investigated by measuring FRET between the NCs as donor and Texas Red-NTA (for His_6-NCs), Alexa568 labeled streptavidin (for biotin-NCs) or eqFP611-His_6 a red fluorescent protein (for NTA-NCs) as FRET acceptor. In the case of biotin/NTA-NCs, both Alexa633-labelled streptavidin and eqFP611-His_6 were used. Increasing amounts of acceptor were added to the NCs solution (for details on the solutions see the different results). The fluorescence emission was measured in a 500 μl quartz cuvette. Control experiments were performed with non-functionalized lipid-NC and with functionalized-NCs in the presence of excess biotin or EDTA in the case of biotin-NCs or NTA-NCs, respectively.

Calculations of Förster distances: The Förster radius is determined from the absorption and emission spectra of D and A. First the FRET efficiencies were estimated using equation 4.5, the number of acceptors per donor was estimated as well. Finally the calculation of r was possible using equation 4.5 and 4.8, respectively. The value of 2/3 was taken for κ_p^2 in all cases. The refractive index was taken as 1.4 for the hydrated protein layer at the NC surface. Values of the extinction coefficient of the various dyes were taken from literature and supporting information from the suppliers.

4.3   Results for mono-functionalized NCs

A study of the interactions between mono-functionalized-NCs with their respective complementary biological recognition elements was carried out for different functionalities: histidine-tag, biotin and NTA-Ni chelator.

4.3.1 His$_6$-functionalized NCs

For protein purification and functional studies, poly-histidine tags (histag) are often fused to recombinant proteins, as it is a simple and well-established approach for introducing an affinity group in the protein structure. The histag bind reversibly and with high affinity divalent transition metal ions (e.g. Zn^{2+}, Co^{2+}, Ni^{2+} or Cu^{2+}) complexed by nitriloacetic acid (NTA). By adding a strong chelating agent as EDTA as competitor, the metal ion is removed from the NTA-polyhistidine complex, which is thus disrupted. This approach is widely used in biology, for example in immobilized metal ion affinity chromatography (IMAC) for protein purification [167, 168]. Figure 4.3.1 shows schematically how a functionalized surface interacts with a poly-histidine tagged protein.
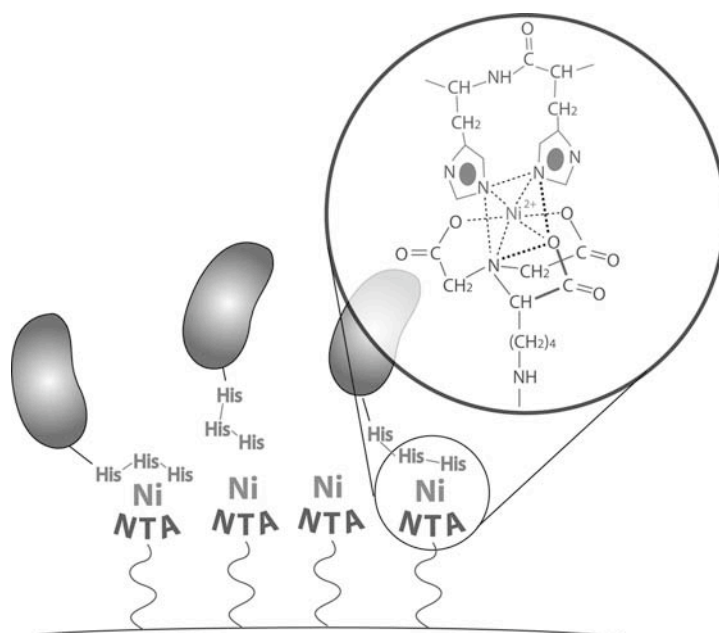
Figure 4.3.1: Schematic representation of the binding of His-tagged proteins to a surface functionalized with NTA. The Blow up region shows the chemical interaction of the NTA, Nickel ion and histidines.

The Ni-ion mediated apparent binding affinity between polyhistidine sequences and NTA-comprising molecules depends on several factors such as the length of the polyhistidine sequence, the environment and, when reactions at interfaces are considered, on the surface concentration of the immobilized binding partner. Guignet et al. have shown recently that Ni-NTA binds with an apparent K_D of about 5 μM to hexahistidine sequences and with 150 nM to decahistidine sequences [169]. This was sufficient for investigation of biomolecular

interactions in living cells. On NTA-modified surfaces the apparent affinity of this interaction is enhanced by several orders of magnitude resulting in a stable (>4h) complex formation [170]. This is due to the high surface concentration of binding sites. A practical example is the NTA-polyHis interactions in surface reactions used for surface plasmon resonance (SPR) in commercial "Biacore" instruments. The situation on the surface of an SPR chip is close to that on the surface of our QDs, where a high surface concentration of either polyhistidines or NTA reduces considerably the off-rates of the corresponding complementary bound partner and thus decrease the apparent K_D and thereby stabilize the NTA-polyhistidine complex.

Histag-functionalized NCs, named as His_6-NCs were produced via inclusion of 10% of His_6-lipid in the lipid mixture for NC coating (see [151] for details for His_6-lipids). The presence of His_6-lipids in the NC coating generated the potential to bind any NTA-labeled species. To test if they are available for specific binding, first a simple binding experiment using Ni-NTA labeled magnetic micro-beads was done. Then a FRET assay was performed using Texas Red dye functionalized with NTA-group (made by Emmanuel Guignet), possessing matching spectral domains with the NC used to allow FRET analysis.

Binding on NTA-functionalized magnetic beads

First the binding of His_6-NCs to NTA-functionalized magnetic beads was investigated. A His_6-NCs solution was added to the magnetic bead solution, incubated for a particular time, and then specific binding of the His_6-NCs to NTA-magnetic bead was measured by first separating the magnetic beads from the solution using a magnet, followed by measuring the solution optical density (OD). Binding of the His_6-NCs on the NTA-decorated magnetic beads results in a diminution of the solution optical density due to the decrease in the amount of NCs in solution. Figure 4.3.2 shows the OD at the beginning of the reaction when the His_6-NCs are mixed with the beads dispersion and at the end of experiment when no more changes were observed. As we can see, a drastic decrease of the His_6-NCs absorption is visible when the magnetic NTA-beads are present. A binding efficiency of 90% can be estimated from the data. A negative control was then carried out to test whether the interaction was specific via histag/NTA interaction, or due to a nonspecific binding (NSB). Therefore the same experiment was repeated but now using lipid-NC solution devoid of His_6-lipid. This control

experiment showed no changes in the OD with time compared to the initial value, this meant no interactions with the beads thus no NSB (clear bars in the figure 4.3.2).
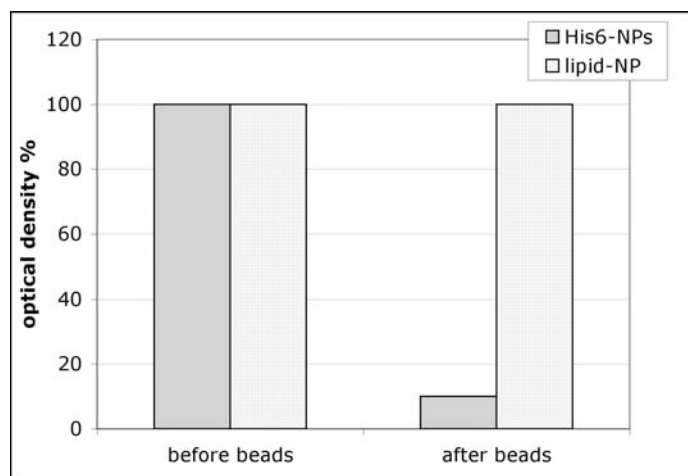

Figure 4.3.2: Graph of the optical density (at 524 nm) of the solution before addition of the NTA-labeled magnetic beads and after stirring the solution with the magnetic beads for one hour and isolating the beads before measurement. This was done for the His$_6$-NCs solution (clear grey) and for the control experiment using lipid-NC devoid of His-tag groups (dark grey).

This straightforward binding experiment demonstrated that His$_6$-NCs binds specifically to NTA-beads. Addition of EDTA resulted in a total release of the bound His$_6$-NCs into the solution. These His$_6$-NCs could easily be reused for specific labeling of any NTA-containing compound.

FRET experiment

Next, we measured by FRET the interaction between His$_6$-NCs (donor) and NTA-Texas Red acceptor; the absorption spectrum of Texas Red (TR) suitably overlaps with the fluorescent spectrum of the NCs. Fluorescence emission spectra were measured for 1 µM His$_6$-NC solutions in water without and with increasing concentration of the NTA-TR. The figure 4.3.3 shows a scheme of the two interacting systems, the overlapping spectral domain of the NC and Texas Red and results of the FRET experiment. In the case of binding, FRET should occur between the donor and acceptor. Indeed the addition of successive amount of NTA-Texas Red until saturation resulted in a decrease of the NCs emission and increase of the TR emission.
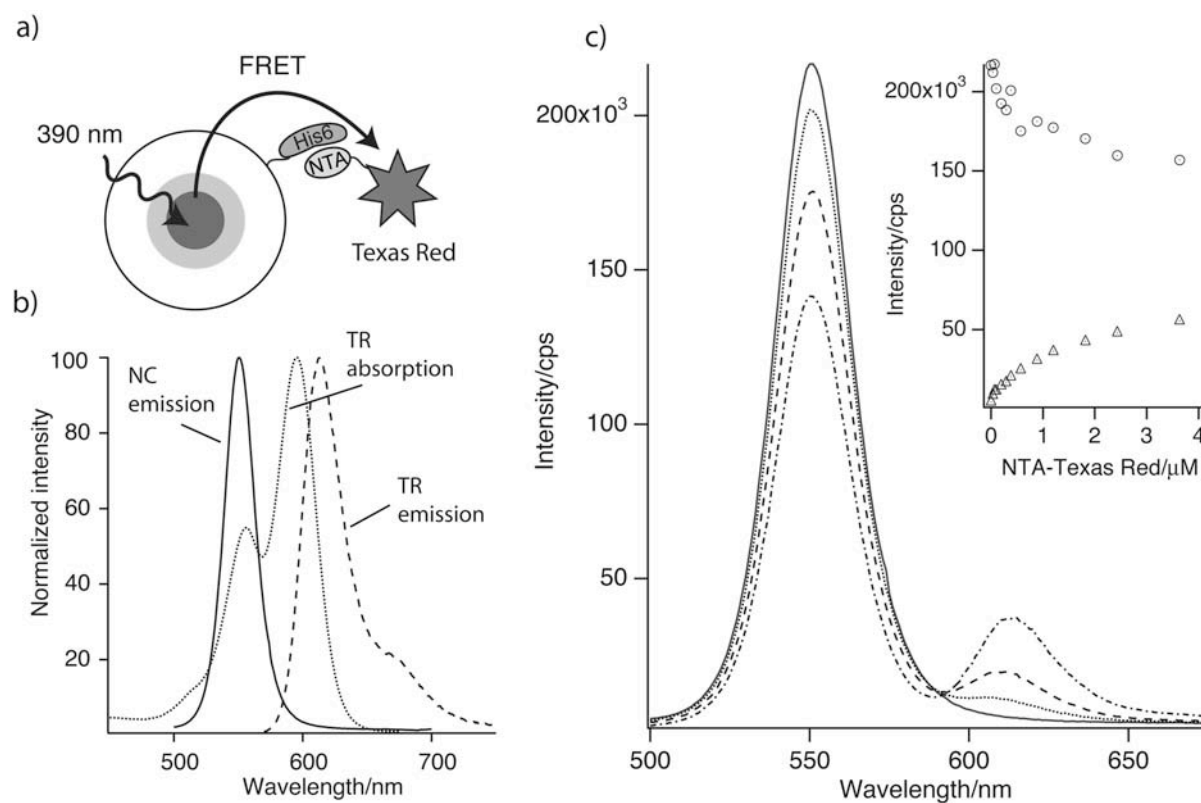
Figure 4.3.3: FRET experiment between the His_6-NC and NTA-Texas Red. a) Scheme of the two interacting FRET couple His-NC and NTA-Texas Red. b) Spectral overlap of the interacting couple, R_0 of 6.6 ± 0.2 nm. c) FRET experiment; with increasing concentration of acceptor, spectra are corrected from direct excitation of TR. The insert shows emission intensities of the different NTA-TR concentrations for the NC peak at 550 nm (○), the TR peak at 610 nm in the presence of His-NC (△) and in absence of the His-NC (▲). Excitation was performed at 390 nm ± 1.8 nm, the spectra of TR were corrected from direct excitation.

Saturation of the His_6-NC binding sites was estimated from experiment and was achieved when a ratio of 5 NTA-Texas Red to NC was reached. As 10% of the lipid mixture used for NC coating possess a histag group, more than one NTA-Texas Red can bind on the NC surface, resulting in FRET between one donor (the NC) and more than one acceptor. Moreover this value correlates well with the average number of functionalities per NC estimated in chapter 3.

A control experiment was achieved to test the specificity of the interaction observed by repeating the same FRET experiment but using lipid-NC devoid of hexahistidine tag instead of His_6-NCs. Here neither a change of NC fluorescence intensity nor an increase in acceptor fluorescence was observed allowing us to conclude that the interaction observed before was specific and no nonspecific interaction occurred. Furthermore, the addition of EDTA resulted

in a complete release of the NTA-Texas Red bound to His_6-NCs, reveling the reversible His_6-NTA interaction and another proof of the specificity of the interaction observed.

The FRET results and Förster distance R_0 of 6.6 ± 0.2 nm allowed us to calculate the distance r for the donor acceptor pair, taking n the amount of acceptors per donor "molecules" equal to 5 and a FRET efficiency of 0.35. Using equation 4.8 we found a value of r = 7.3 ± 0.3 nm. This value is reasonable, considering the radius of the lipid-NC to be 4.5 nm and the length of hexahistidine linker plus NTA-Texas Red around 2.5 nm.

4.3.2 Biotin-functionalized NCs

Biotin was also chosen to decorate the NC surface. Biotin associates to streptavidin with a high affinity and specificity. Streptavidin is a 60,000-dalton tetrameric protein possessing 4 binding sites for biotin making it a highly attractive agent in bioanalytics and nanotechnology [171].

We introduced biotin on the NC surface by inclusion of biotinylated-lipids during the NCs coating procedures resulting in the formation of biotin-NCs. To demonstrate both the presence of biotin moieties exposed on the surface of the NCs and their ability for specific molecular recognition, the binding of a fluorescently labeled streptavidin to these particles was examined using a FRET assay. Streptavidin-Alexa568 was chosen as a FRET acceptor possessing an acceptable overlap of absorption spectra with NC emission.

Addition of increasing concentrations of streptavidin-Alexa568 to 1 μM biotin-NCs solution in PBS buffer should result in a progressive diminution of the biotin-NC fluorescence intensity at 560 nm and a simultaneous increase of the Alexa568 emission intensity at 601 nm. This would indicate the direct interaction between NC and streptavidin. This is indeed observed in figure 4.3.4. Higher concentrations of streptavidin (not shown) resulted in aggregation of the biotin-NCs/streptavidin due to the multivalent binding capability of streptavidin and the several biotins present on one NC. This effect prevented reaching higher concentrations and thus binding-sites saturation.
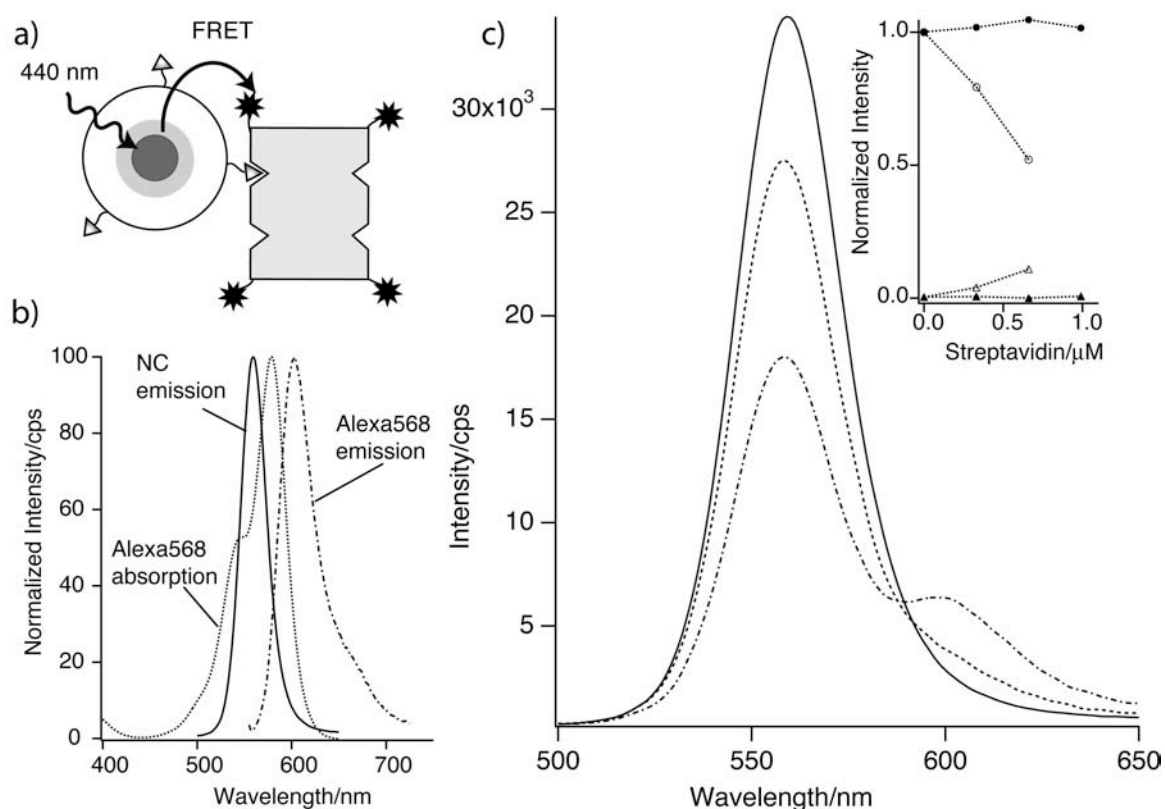
Figure 4.3.4: FRET experiment between biotin-NC and Streptavidin Alexa568. a) Scheme of the interacting FRET couple biotin-NC and streptavidin Alexa568. b) Spectral overlap of the interacting couple, $R_0 = 5.8 \pm 0.2$ nm. c) Fluorescence emission spectra of biotin-NCs emission in the absence (full line) or presence (dashed & dotted lines) of increasing concentrations of streptavidin Alexa568. Insert: Intensities at the maxima of emission of biotin-NCs (at 560 nm, ○) and Alexa568 (at 601 nm, △) and for control using lipid-NCs (●, at 560 nm) and (▲, at 601 nm). Excitation was performed at 440 nm ± 1.8 nm and spectra were corrected from direct excitation of streptavidin Alexa568

To check the specificity of the interaction, the same experiment was performed with lipid-NC devoid of biotinylated-lipids and addition of streptavidin Alexa568 showed neither a decrease of the fluorescence emission of the NC nor an increase of the fluorescence emission of Alexa568, indicating that no nonspecific interaction occurred between the partners. This experiment proves the specificity of the biotin-NCs interaction with streptavidin through the biotin moiety.

Calculation of the Förster distance for the couple biotin-NC/streptavidin Alexa568, resulted in $R_0 = 5.8 \pm 0.2$ nm. We obtained a FRET efficiency of 0.5 for a ratio of 2 streptavidins per

NC. To calculate the distance r between the NC center and the protein, we used equation 4.8 describing r_n. As we couldn't reach saturation of streptavidin Alexa568, we can only estimate a value for r with respect to the amount of streptavidin per NC. We could obtain values of r = 5.5 to 6 nm taking n = 2 to 4. The resulting value for the biotin-NC and streptavidin distance correlates well with the geometric distance, which can be estimated from molecular size estimates of the NC, the linker and the streptavidin fluorophore.

The binding of streptavidin to biotin-NCs resulted in a small blue shift of the NC emission, as can be seen on the successive spectra with increasing streptavidin Alexa568 concentration. This might be due to changes in the electrostatic environment of NCs caused by the proximity of negatively charged streptavidin at this pH, such shift is observed as well in the presence of non-labeled streptavidin and with the streptavidin used in the multi-functionalized NC. No further investigation of this effect was carried out.

4.3.3 NTA-functionalized NCs

NTA groups at the surface of the NCs offer a convenient possibility to bind proteins, which comprise oligo-histidine tags.

Here, we prepared NTA-NCs by adding 10% of Ni-NTA functionalized lipids to the lipid mixture. Specific binding of poly-histidine tagged proteins to NTA-NCs was demonstrated using a red fluorescent protein with a N-terminal hexahistidine called eqFP611-His$_6$ [166]. This protein possesses matching spectral properties with the donor NCs. Interaction between the NTA-NCs and eqFP611-His$_6$ could be investigated using a FRET experiment (figure 4.3.5).

For FRET experiments, addition of increasing concentrations of eqFP611-His$_6$ to 50 nM NTA-NCs solution in PBS buffer was completed and resulted in a progressive quenching of the NC fluorescence and a concomitant increase of the eqFP611-His$_6$ emission due to FRET (see figure 4.3.5). To prove specificity of the interaction observed, a control experiment was also realized using lipid-NCs devoid of NTA and indeed showed no interaction between the lipid-NCs and eqFP611-His$_6$ on the solutions emission spectra. This indicates that eqFP611-His$_6$ interacts specifically with the NTA-NCs through the NTA-moieties and no NSB was observed. Addition of EDTA after binding of NTA-NCs with the protein eqFP611-His$_6$ resulted in their dissociation and a recovery of the NC emission and a fading of the eqFP611-His$_6$ emission, proving again specificity of the interaction.
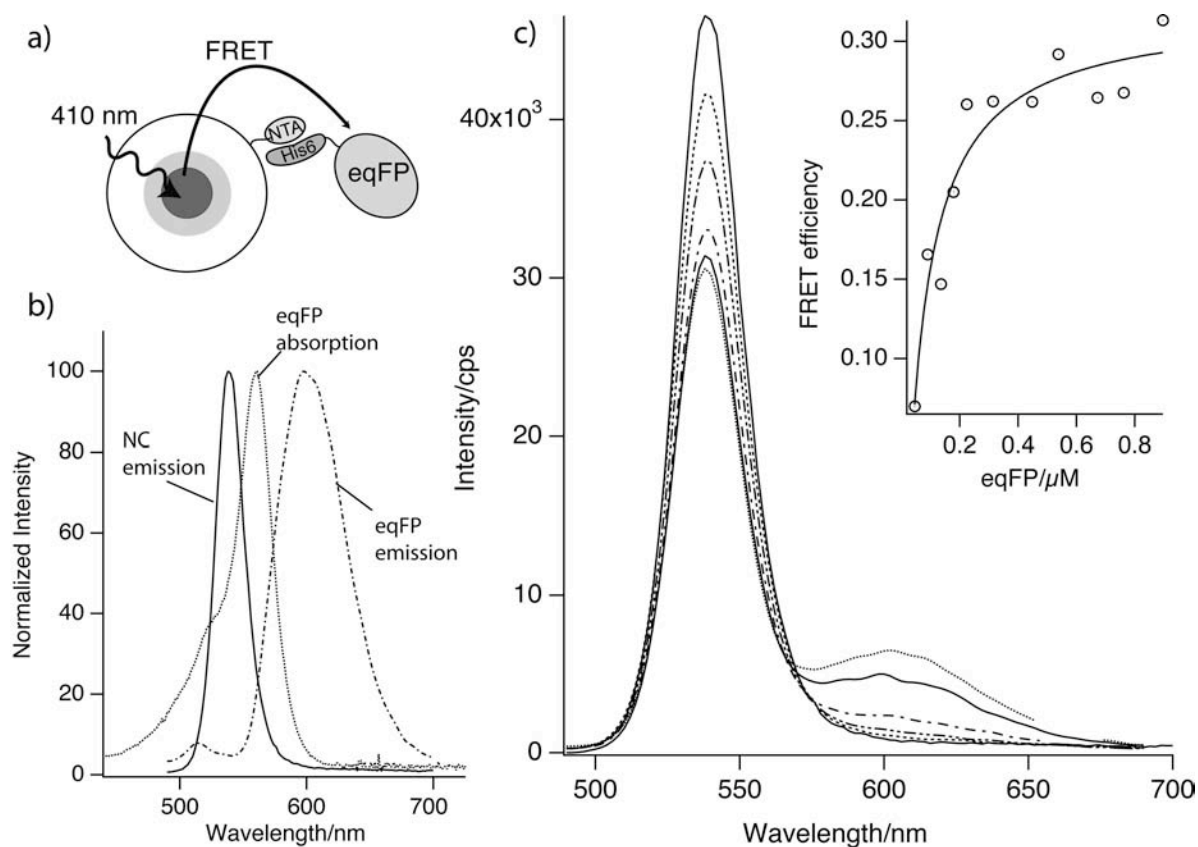
Figure 4.3.5: FRET experiment between NTA-NC and eqFP611- His$_6$. a) Scheme of the interaction between the NCs and the protein. b) Spectral overlap of the interacting FRET players, R$_0$ = 6.5 ± 0.3 nm. c) Emission fluorescence spectra of NTA-NCs at 550 nm in the absence (full line) or presence (grey, dashed & dotted lines) of increasing concentrations of eqFP611-His$_6$ emitting at 601 nm (for clarity not all the spectra are shown). Insert: FRET efficiency versus eqFP611-His$_6$ concentration fitted with a Langmuir binding isotherm. A maximal stoichiometry of 4 to 5 eqFP611 per NC can be estimated from this graph. Excitation was performed at 410 nm ± 1.8nm and spectra were corrected from direct excitation of eqFP611-His$_6$.

A maximal stoichiometry of 5 fluorescent proteins per NC could be estimated from the concentration dependence of the FRET efficiency (figure 4.3.5 c) referring to saturation. This correlates also well with the amount of functionalities on one NC estimated in chapter 3. A maximum FRET efficiency of 0.3 was derived from data. The Förster radius R$_0$ was calculated to be 6.5 ± 0.3 nm, using equation 4.8. A distance r between the two fluorophores of 8.5 ± 0.3 nm was calculated for n = 5. This value is compatible with the distance estimated by the geometry of the NC, the linker and the protein eqFP611-His$_6$, assuming fluorescence from the center.

4.4   Results for multi-functionalization

Here we describe the formation of supramolecular assemblies of higher complexity using the nanocrystals coated with lipids, functionalized with biotin and NTA. To achieve this double-functionalization, we added 5% of each biotin-lipid and NTA-lipid (1:1) to the lipid mixture for coating the NC.

The presence of both functional groups on the same NC was shown by FRET between the NC, eqFP611-His$_6$ and Alexa633-labelled streptavidin. The two proteins were chosen so that the optical overlap of the eqFP611-His$_6$ absorption with NC emission, the eqFP611-His$_6$ emission with Alexa633 absorption were optimal for FRET observation, but FRET could also occur between the NC and Alexa633, since the later has a significant extinction coefficient even at the NC emission position (figure 4.4.1). The FRET assay was achieved upon the addition of the streptavidin Alexa633 protein to biotin/NTA-NCs pre-incubated with a certain amount of eqFP611-His$_6$. This experiment showed energy transfer between the NC and eqFP611-His$_6$, the NC and streptavidin Alexa633 and/or eqFP611-His$_6$ with streptavidin Alexa633. In the later case, the emission of eqFP611-His$_6$ is enhanced via FRET between the NC and eqFP611-His$_6$, and then reduced by further addition of the streptavidin Alexa633. This effect could be due to FRET from eqFP611-His$_6$ towards Alexa633 but could also be due to direct FRET between the NC and streptavidin Alexa633-His$_6$ competing for the relaxation channel between NCs and eqFP611-His$_6$.
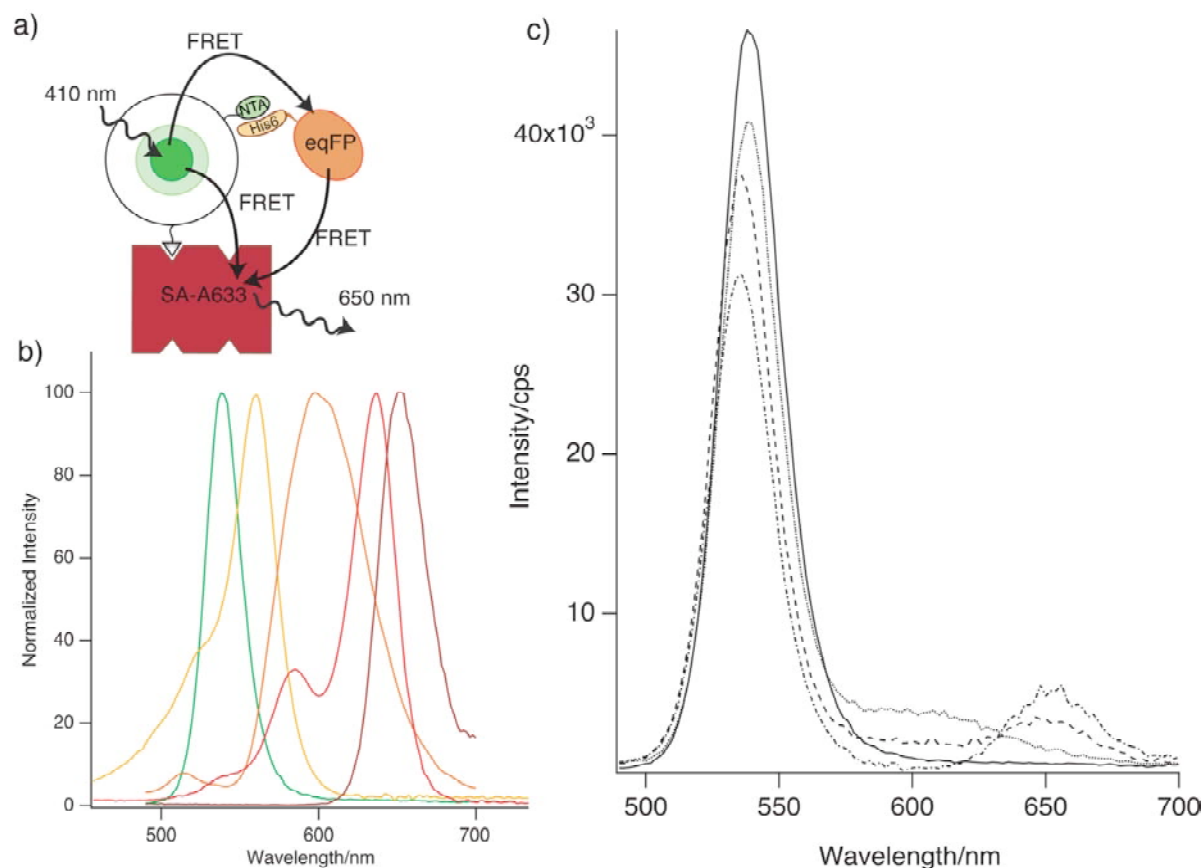
Figure 4.4.1: Bi-functionalization of the NCs. a) This shows a scheme of the interaction of biotin/NTA-NCs with eqFP611-His$_6$ and with streptavidin Alexa633. b) Spectral overlap of the interacting FRET players. The colors correspond to the scheme color key. The values of R$_0$ for the FRET couples NC/eqFP611-His$_6$, NC/streptavidin Alexa633 and eqFP611-His$_6$/streptavidin Alexa633 are 6.5 ± 0.2 nm, 5.1 ± 0.2 nm and 10.2 ± 0.2 nm, respectively. c) The graph shows fluorescence emission spectra of biotin/NTA-NCs of 100nM at 540 nm in the absence (line), or presence of 0.4 μM eqFP611-His$_6$ (dotted lines) emitting at 601 nm, with addition of various concentrations of streptavidin Alexa633: 47 nM (dashed line) and 156 nM (dot-dashed line) emitting at 650 nm. Excitation was at 410 nm ± 1.8 nm. The spectra were corrected from direct excitation.

A control experiment showed that eqFP611-His$_6$ and Alexa633-labelled streptavidin did not interact with each other in the absence of biotin/NTA-NCs and did not interact with non-functionalized NCs. These results indicate that only specific interactions occurred between the biotin/NTA-NC and the two proteins.

Calculation of the different R$_0$ for the three energy transfer couples (see figure legend), allowed us to estimate the radii r between the probes: NC, eqFP611-His$_6$ and streptavidin Alexa633. Taking the amount of protein per NC as 4 eqFP611-His$_6$ and 1.5 streptavidin, the following results were obtained: 8 nm for the NC/eqFP611-His$_6$ distance, 7 nm for

NC/streptavidin Alexa633 and 10 nm for eqFP611-His$_6$/streptavidin Alexa633. These values are in reasonable agreement with the estimated geometric assumptions of the interacting partners (figure 4.4.2). For NC/streptavidin distance, the value is a bit higher than what was calculated for the experiment in 4.3.2. These values are not taking in account the presence of a third actor, thus they are not reliable but give just a qualitative idea.
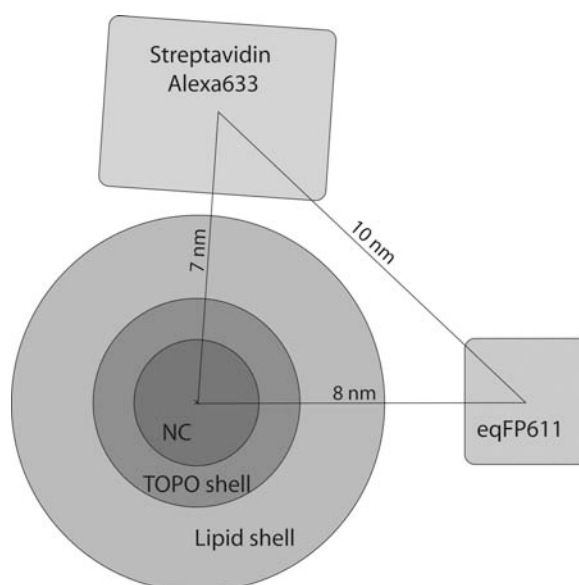

Figure 4.4.2: In scale schematic representation of the different participants of the multiple FRET experiment, the drawing is in scale and the distance come from the r calculation using FRET data obtained. As we can see the calculated distances correlate well with the estimated ones considering the dimensions of the proteins and NC.

This experiment demonstrates that a bi-functionalized NC acts as a local excitation source through FRET for bound proteins, but also as a scaffold for the immobilization of mutually non-interacting proteins. The lipid-coated NCs are versatile systems were in a one step modification any functionalities or even several types of functionalities can be added on their surface.

4.5   Conclusions

The functionalized lipid-coated NCs were tested for specific interactions via FRET assays. To demonstrate the versatility of the coating method, functionalized-NCs decorated with different groups, hexahistidine tag, biotin and NTA were tested. The study of their interaction with complementary proteins or molecules illustrated their specificity.

Saturations of acceptor molecules binding on one NC were found to be approximately 4-5 per nanocrystals for the His_6-NCs and NTA-NCs, which correlates well with amount of functionalities found in chapter 3.

The achievement of multi-functionalization of NCs demonstrated two important features. First, the multi-functionalized-NCs (MF-NCs) can act as nanometer sized scaffolds for the confined self-assembly of non-interacting macromolecules. Secondly, they serve as local excitation sources transmitting sequentially their excitation energy over a FRET range of distances (up to tens of nanometers) to specifically bound components within the supramolecular nano-assemblies. The possibility of the multi-functionalization of fluorescent bodies such as the nanocrystals can lead to a large variety of sensing applications. An example of the use of the multi-functionalities and fluorescence of the MF-NCs is shown in chapter 6 with sandwich immobilization.

These functionalized-NCs are interesting as fluorescent and specific tools for probing, tracking or imaging of biomolecules.

5 Protein-lipid interaction at the surface of lipid-NCs

Membrane protein can be classified as either peripheral or integral membrane proteins. Integral membrane proteins traverse the lipid bilayer membrane; detergents are required to solubilize them. In contrast, peripheral membrane proteins are bound to the surface of a membrane, primarily by electrostatic and hydrogen-bonding interactions. These polar interactions can be disrupted by addition of salt or changing pH. Many peripheral membrane proteins are bound to the surface of an integral protein, either on the cytosolic or extracellular side of the membrane. Others are anchored to the lipid bilayer by covalently attached hydrophobic chains, such as fatty acids [172].

Although peripheral membrane proteins are abundant in cells and participate in diverse important cellular functions, the molecular function related to specific lipid-protein interactions have received only limited attention. To understand how peripheral membrane proteins interact with membranes is of considerable interest, as reversible adsorption on the membrane surfaces offers an excellent means for regulatory purposes.

In order to investigate whether peripheral membrane proteins can bind to our lipid-coated NCs and whether this lipid coat acts like a biological lipid membrane, experiments were performed to investigate the interaction of lipid-NCs with cytochrome c (cyt c) a well characterized mitochondrial peripheral membrane protein and possessing suitable absorption feature for acting as acceptor for the NCs.

Our experiments were inspired from researches carried out on the interaction of cyt c with lipid vesicles [173-177].

5.1 Cytochrome c

Cytochrome c is a small cationic peripheral membrane protein of 13 kDa, which mediates single-electron transfer in the respiratory chain between cyt c reductase and cytochrome c oxidase of the inner mitochondrial membrane via its heme group. Cyt c is present in all organisms having mitochondrial respiration chains, such as in plants, animals and eukaryotic microorganisms. This electron-carrier evolved more than 1.5 billon years ago, before the divergence of plants and animals. Its function has been conserved throughout this period. This was evidenced by the fact that the cyt c of any eukaryotic species reacts in vitro with the cytochrome c oxidase of any other spices tested so far.

It has also been shown that it is a key component in apoptosis. Its release from mitochondria apparently representing the rate-limiting step in the commitment of a cell into the death program [178-180].

Binding of cyt c to lipid vesicles was pratically observed by a concomitant quenching of the fluorescence of a membrane dye and the increase of the tryptophan residue of the protein due to conformational changes. Cyt c associates only weakly to zwitterionic phospholipids as phosphalidylcholine [181, 182], whereas an increased affinity is observed when acidic phospholipids are present (the inner mitochondrial membrane is rich in acidic lipids, thus also negatively charged). Membrane binding was shown to induce conformational alterations in the protein and the phospholipids, together with a change in the conformation and coordination of the heme group [183-190]

It was first thought that interaction of cytochrome c with the lipid-bilayer was electrostatic as almost no binding occurred if less than 5% of negatively charged PG lipids were present in the liposomes. Furthermore, it was dissociated from the lipid membrane by increasing the ionic strength [191]. However, hydrophobic interactions were also reported later, as the binding of cyt c was associated to conformational changes in the protein as well as in the lipid bilayer [190].

Some researchers [184, 189, 192] believe that the binding on the lipid membrane induces a destabilization and a loosening of the tertiary structure, this has been observed via circular

dichroism for example [192]. The secondary structure is apparently not perturbated, but the tertiary structure of the protein is modified or defolded ("molten globule") and the heme position as well.

Recently E. J. Choi et al. made atomic force microscopy studies on the binding of cytochrome c to a supported lipid bilayers and realized that the protein in fact incorporates into the bilayer. They also observed that this insertion induced changes in the tertiary structure of the proteins (defolding) as well as in the bilayers properties [193].

In opposition to the majority view, Kinnunen et al. believed that an acyl chain of the di-acyl phospholipid penetrates inside a hydrophobic cavity in the protein leading to the heme. For lipids containing unsaturation, when the curvature of the membrane is large it causes frustrated lipid phase. To minimize this stress energy, it can allow the so-called extended conformation, in which one of the acyl chains extends out of the bilayer while the other remains within the bilayer. This extended acyl chain enters the protein cavity producing a more efficient binding of the peripheral protein. Thus association depends as well on the curvature of the liposomes, the more curved the surface the easiest cytochrome c associates [190].
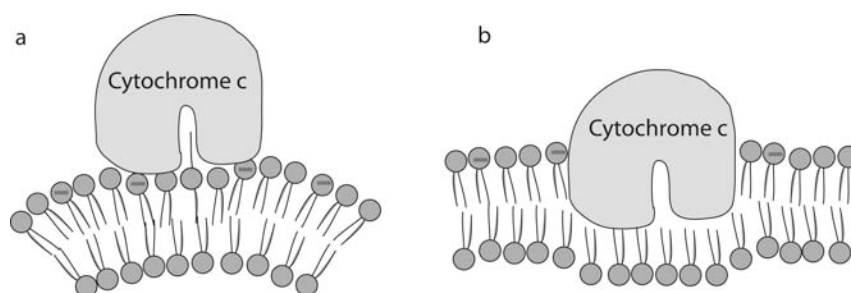

Figure 5.1.1: Scheme of the two different models proposed for the explanation of the cytochrome c binding to lipid membranes. All agree that conformational changes of the protein and the lipid membrane occur, but the mode of interaction with lipids is different in the different models. a) Kinnunen et al. [190] imagined a slight incorporation of the protein and a lipid chain in an extended form entering the protein cavity. b) Choi et al. [193] experienced an incorporation of the protein into the bilayer hydrophobic core with bilayer properties modifications in addition to protein unfolding.

Conformational changes can be monitored by observation of the tryptophan fluorescence at 360 nm. The fluorescence is normally quenched by the proximity of the heme group of the protein. But the interaction of the protein with the lipid bilayer induces conformational

changes accompanied by an increase of the distance between the tryptophan residue and the heme, leading to an increase of the fluorescence at 360 nm [177].

5.2 Experimental section

5.2.1 Materials

Cytochrome c in the oxidized form and from horse heart was purchased from Sigma, Switzerland. It was reduced using vitamin C.

5.2.2 Optical measurements

See chapter 2

5.2.3 Cytochrome c binding to lipid-NCs

Solutions of lipid-NCs, coated with a lipid mixture of POPC and POPG 0, 3, 10 and 20%, of concentration 0.5 µM in Hepes buffer 10 mM pH 7.4 were put into a fluorescence cuvette and emission spectra measured for the NC at 547 nm and for tryptophan emission at 350 nm. Fluorescence intensity of the NCs was measured at increasing concentrations of cyt c. The experiments were repeated for the three different lipid-NCs possessing various amounts of POPG on the NCs surface to see if it influences the adsorption properties of cyt c.

For calculation of the Förster radius R_0 and the distance r between quenching substances, the relations described by the Förster formalism (part 4.1.1) were used. First the FRET efficiencies were estimated for the lipid-NC and the cyt c in the oxidized and reduced form using equation 4.4. The amount of acceptor per donor was estimated as well and finally the calculation of R_0 and r were done using equation 4.4 and 4.8 respectively. The value of κ_p^2 was taken to be 2/3 for all cases, and the NC quantum yield 0.1. The refractive index was taken as 1.4 for the water/protein mixture.

Graphs allowed the estimation of the dissociation constant of the cyt c toward the lipid-NCs via a standard Langmuir binding isotherm.

5.3   Results on lipid-NCs and cytochrome c interaction

The NCs were chosen (530/547) such that their fluorescence emission matched the absorption spectra of the protein in order to perform FRET. The absorption spectra of the oxidized and reduced form of cyt c and fluorescence spectrum of the NCs are shown in figure 5.3.1.
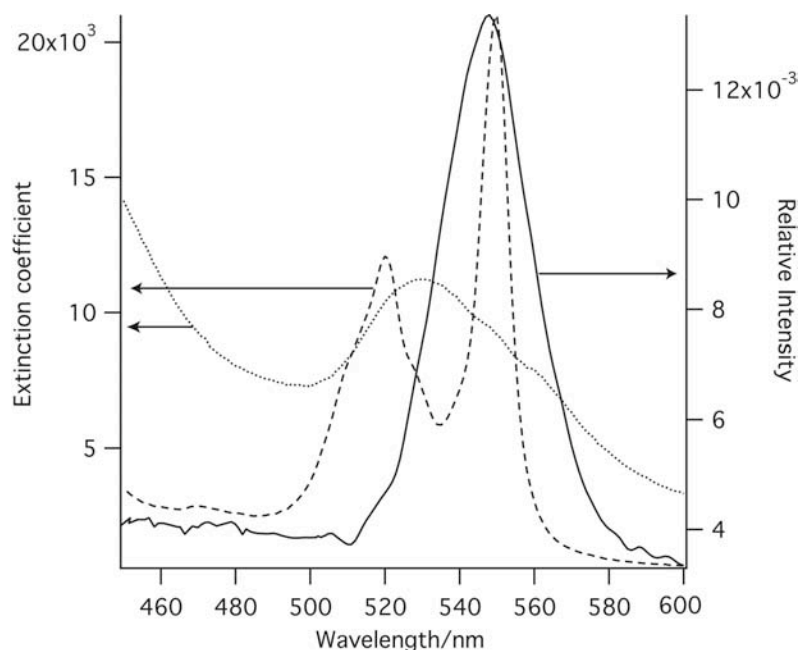

Figure 5.3.1: Optical overlap of the cytochrome c absorption spectra and emission spectra for the lipid-NC. The dotted curve for the oxidized form of cyt c, the dashed curve for reduced form of cyt c (left axis) and the plain curve for the emission of the NC (right axis).

The cyt c taken for the binding experiment was the reduced form. The cyt c adsorption on the NC surface was monitored by following the variations of the NC fluorescence intensity with increasing concentration of cyt c. The adsorption was also studied by observing the increase of tryptophan emission at 350 nm due to conformational changes.

We varied the amount of PG on the NC lipid layer to see if the amount of PG were influencing the proteins binding. We thus prepared different lipid-NCs solutions containing the following percentage of negatively charged lipids PG: 0, 3, 10 and 20%. Increasing amount of cytochrome c was added to the 0.5 μM solutions in the low ionic strength buffer Hepes pH 7.4, and binding was monitored by the NC fluorescence quenching at 547 nm and the tryptophan fluorescence "dequenching" at 350 nm. The results are plotted in the

following figures for the different concentration of cytochrome c, together with lipid-NCs containing 0, 3, 10 and 20% of negatively charged lipids (PG).
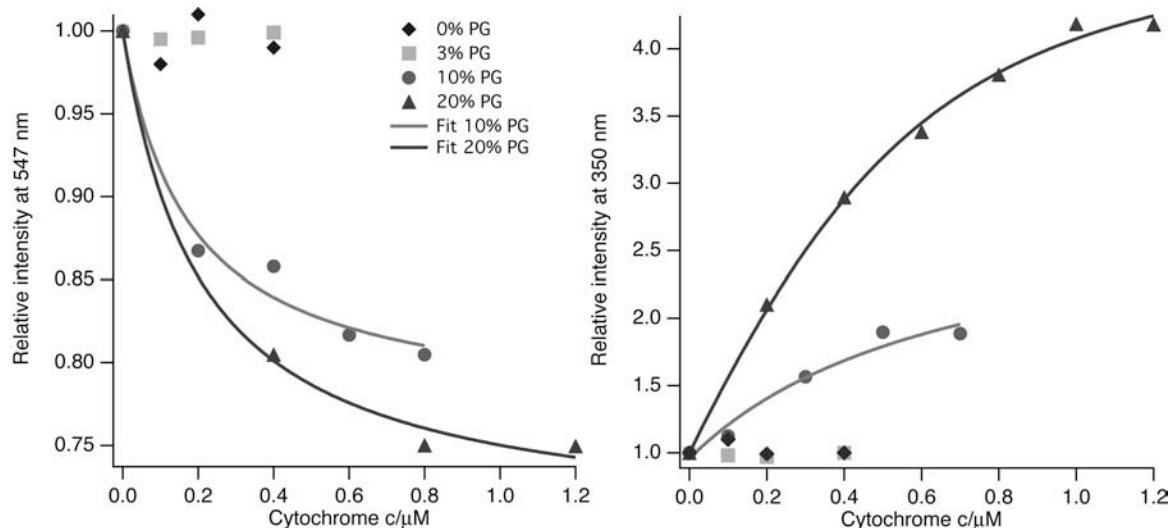

Figure 5.3.2: Interaction between lipid-NC and reduced cytochrome c. The relative fluorescence intensity of the NCs at 547 nm and tryptophan from cytochrome c r at 350 nm are shown with increasing concentration of cyt c. The adsorption of the protein on the lipid layer induces a quenching of the NC fluorescence (left graph), and a simultaneous increase of the tryptophan fluorescence due to conformational changes (right graph). Diamonds for lipid-NCs with for 0% PG in the lipid mixture, squares 3% PG, circles for 10% PG and triangles for 20% PG. Langmuir fit are visible for 10% and 20% for the calculation of K_D. A average of 0.2 μM was found for K_D.

As we can see from the graphs above, there is an interaction between the lipid-NC and cytochrome c proteins. If we compare the different curves shown relating to different amount of PG, we can see that the interaction depends on the amount of PG present on the surface of the lipid layer. Indeed with 0% and 3% of PG no interaction occurs, but with 10 and 20% the interaction increases, demonstrating the electrostatic character of the interaction. Looking on the right graph, the increase in the tryptophan emission intensity in the presence of more than 3% PG illustrates the defolding of the protein due to the interaction with the lipid layer. This effect is due to a conformational change through defolding and a partial incorporation into the lipid layer. This will be confirmed by distances r between the NC center and the cytochrome c calculated with the Förster formalism.

From the fluorescence quenching data (left graph), the intensity of the decrease is not linear, meaning the effect for 20% PG containing lipid-NCs is not double of that of 10% PG. The addition of a second protein induces a smaller quenching. But looking at the data representing

the defolding of the protein (right graph), the intensities increase is not proportional to the amount of PG. If more PG is present the defolding effect is much larger than for 10% PG, resulting from higher fluorescence increase for 20% compared to 10% PG. This could be explained by a deeper interaction between the lipid-NC and the protein if more negative charges are present, resulting in a stronger defolding.

From the graphs, we can estimate the saturation of proteins on the nanocrystals to be one cytochrome c per lipid-NC if 10% of PG is present, but two cyt c per lipid-NC if 20% of PG is used. This linear relation correlates with results obtained by M. Rytömaa et al. [176] where they obtained a linear relation between the percentage of PG and the saturation concentration of cytochrome c. These estimations correlate also well with the size of the protein and the lipid-NC.

The dissociation constant K_D could be estimated from the different graphs via a Langmuir binding isotherm fit and the average value was found to be 0.2 μM for the cytochrome c/lipid-NCs binding. This value is lower than the referred values from Jordi et al. [194] of 1 to 5 μM.

As the interaction is mostly electrostatic, the addition of salt such as NaCl in the solution resulted in a 70% detachment of the protein accompanied by a recovery of the NC fluorescence and a decrease of the tryptophan emission (see graph below) due to refolding of the cytochrome c in solution.
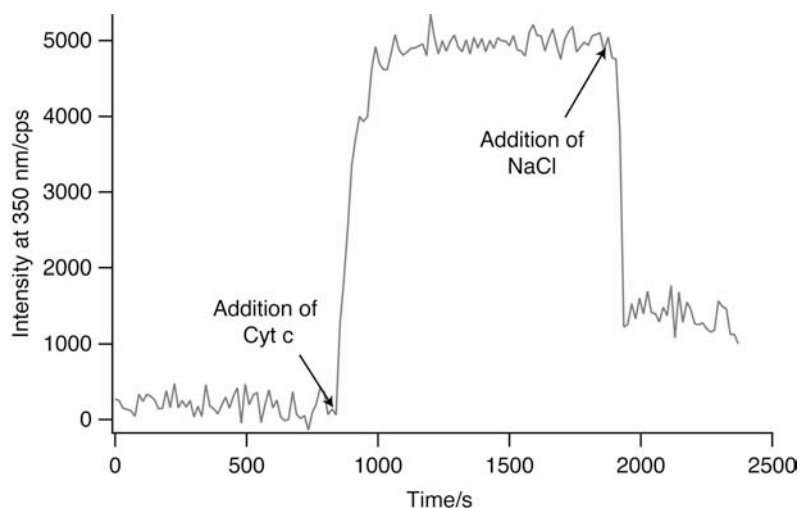
Figure 5.3.3: Time trace of fluorescence emission: Variation of the emission intensity at 350 nm for a lipid-NC solution with 10% PG (0.5 µM) before and after addition of cytochrome c (final concentration 0.5 µM). The addition of NaCl engenders a decrease of the intensity characteristic to for desorption of the cytochrome c from the NC surface. As we can see desorption is not total, 30% of the intensity remains after NaCl addition.

This confirmed the reversibility of the interaction and the partly electrostatic character. However 30% of the intensity remained. This residual fluorescence could be due to a partial amount of the protein remaining on the lipid-NC surface due to higher hydrophobic interactions. The hydrophobic interaction is maybe more favorable in our example compared to vesicles because of the huge curvature of the lipid layer on the NC.

Control experiments were carried out with the addition of cytochrome c to Hepes buffer devoid of NCs and observing the fluorescence at 350 nm, but no increase in fluorescence intensity could be observed. The lipid-NCs were also exposed to high salt concentration to see if any effect on the fluorescence intensity could be observed, but here as well no changes occurred. If neutral lipid-NCs were used and cyt c added, no increase of tryptophan emission could be observed (data for 0% PG).

These results indicate that the lipid layer on the NC surface act as model membrane as they behave similarly with the peripheral protein cytochrome c as lipid vesicles.

For information, the R_0 calculated with the Förster formalism introduced in the previous chapter gave the following: 2.8 nm ± 0.2 nm for reduced cyt c and 3 nm ± 0.2 nm for oxidized cyt c. The calculation of the distance r between the heme and the NC center gave: 3.8 nm ± 0.3 nm and 4.1 nm ± 0.3 nm respectively for reduced and oxidized form, taking two cyt c per NC.

The averaged distance r between the NC center and the heme is 4 nm (FRET estimation). The radius of the lipid-NC being geometrically estimated as 4.5 nm, the value of r would agree with the theory of a partial incorporation of the protein into the lipid layer. This is illustrated in the figure 5.3.4.
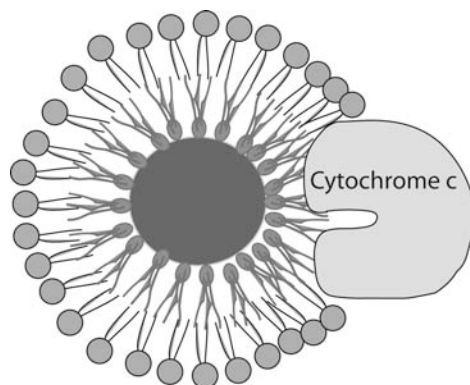

Figure 5.3.4: illustration of the interaction of the lipid-layer on the NC and the protein cytochrome c. This illustration is consistent with descriptions from E. J. Choi et al [193].

Another purpose for adsorbing cyt c onto the lipid-NC surface was the hope of observing a different NC fluorescence intensity (through quenching) if reduced and oxidized cyt c were added. It would therefore be possible to follow the redox cycles by observation of the NC fluorescence with single molecule spectroscopy. Immobilization of the NCs, then addition of the cyt c could yield a potential surface sensor for redox substances. Unfortunately the Förster radius of cytochrome c of reduced and oxidized form is very similar and consequently the redox cycle is not clearly visible by observing the NC fluorescence intensity.

5.4   Conclusions

The peripheral protein cytochrome c interacts with the negatively charged lipid-coated NCs in a very similar way as its interaction with lipid vesicle or the inner mitochondrial membrane. The lipid-NC is thus believed to mimic natural lipid bilayers. The interaction of the lipid-NCs with the cyt c engendered a successive quenching of the NC fluorescence with increasing cyt c amount. The conformational changes were confirmed by variations of the fluorescence at 350 nm for the tryptophan residue of the cyt c. The amount of negative

charges on the lipid layer were also influencing the binding, showing a very low to no adhesion if 0 to 3% of PG were used, and increasing affinity with 10% and 20% PG content. Additionally to specific interactions via functional groups (as mentioned in chapter 4), we can also induce electrostatic interaction with the lipid-NCs by addition of PG around it. This shows ones again the variability and versatile usability of the lipid-NCs developed in this thesis.

These findings are interesting properties as any specific peripheral protein should adsorb on the NC surface and some sensing applications would be possible if changes in the NC fluorescence could be observed. This opens a wide field of applications for study of those proteins or bioassays development.

6   Immobilization on surfaces

This chapter describes the immobilization of the functionalized NCs on predefined surfaces. The immobilization of the NCs was achieved by means of a specific interaction with an immobilized protein layer and was monitored using total internal reflection fluorescence TIRF a surface-specific optical technique.

The creation of micrometer-sized patterns on a surface allows the creation of active surfaces for biosensor applications, improved detection and resolution of fluorescence images using functionalized-NCs as a local FRET sources.

6.1   Experimental section

6.1.1   Materials

The solvents were of puriss. grade and the ethylenediamine tetraacetate (EDTA) were from Fluka, Switzerland. PBS buffer was 1% in water to give a pH of 7.4, from Sigma, Switzerland. BSA-biotin (1:8 mole/mole) were purchased from Sigma, fluorescent and non-fluorescent streptavidins were from Molecular Probes, USA, and BSA (MW 67 kDa) from Fluka, Switzerland. All were aliquoted in water solutions and stored at -20°C. EqFP611, was produced following the protocol described in [166].

6.1.2   TIRF apparatus

Here we used a home-built TIRF microscope (PhD thesis # 1970, Lausanne-CH, EPFL, 1998) [168, 195]. A schematic drawing of the measurement cell is found on figure 6.1.1. The substrate was a quartz microscope slide (25×40×1 mm^3, n= 1.467 at 488 nm, Wisag, Zürich, Switzerland). The slide was mounted on a Teflon sample holder, the bottom of the cell was a

thin 0.1 mm glass coverslip (25×40 mm^2). The Teflon spacer defined a volume of 30 µl between the two plates (20 mm^2 of quartz surface accessible). The cell was held together by two anodized aluminum frames tightened with screws. A new cleaned quartz surface and glass slide was used for each measurement. A quartz prism with an internal angle of 72 degrees (Krug, Switzerland) was used to couple the light into the cell. The prism was kept in optical contact with the substrate by index matching fluid (Cargill, Cedar Groove, NJ, USA). The laser beam passed through the air/quartz interface with an incidence angle of 0 degree, which avoided any distortion of the beam profile. The cell was mounted onto the x-y-translation stage of an inverted fluorescence microscope (Axiovert 100, Zeiss, Oberkochen, Germany) with a high-aperture water immersion objective (0.75 NA, 40×, Zeiss).
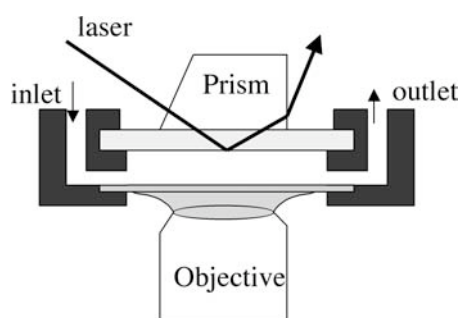

Figure 6.1.1: TIRF measurement cell (not to scale). From top to bottom: Quartz prism, quartz slide, chamber, glass coverslip, water and objective. For maximum collection efficiency, water was always kept between the water immersion objective and the coverslip.

Laser, optical elements and microscope were mounted on an optical table (Newport, Schlieren, Switzerland). A forced air-cooled argon-ion laser (532-AP, Omnichrome, Chino, CA, USA) was used as light source giving the following output lines: 476 nm, 488 nm (suitable for nanocrystals) and 514 nm. A polarizer was used to regulate laser light intensity to 10 µW, as checked manually with a powermeter (Newport). A computer-controlled shutter protected the sample from light in-between the measurements exposure to avoid photobleaching. An f = 600 mm achromatic converging lens focused the laser down to a 2×10^3 µm^2 spot onto the sample. The coupling mirror to the prism was mounted on a goniometer to allow the precise alignment of the laser beam into the microscope. A fluorescence filter rejected all scattered excitation light (available filters: band pass 515-565 nm (used for NCs emission), cut-off 590 nm (for Alexa568)). The emitted fluorescence was

collected via a photomultiplier (R928 Hamamatsu, Bridgewater, NJ, USA)) operated in photon-counting mode and controlled by a PC with standard fluorometer software (DM3000, Spex, Middlesex, U.K.).

Preparation of the surfaces:

1. The quartz slide was washed extensively with multiple cycles of detergent-sonication, methanol-sonication and rinsing steps, and finally stored in water in closed slide holders. Always new quartz and glass slides are used for the experiments.

2. The glass coverslip is incubated with BSA solution of 0.1 mg/ml in PBS for 10 min, and then washed. This treatment avoids further binding of the BSA-biotin and thus the binding of the analyte of interest on the wrong surface.

3. The two slides are put on the Teflon spacer and closed with the aluminum window and tightened to obtain a liquid tight chamber. Then the chamber were filled with a BSA solution

4. The chamber is then incubated with a solution of BSA/BSA-biotin 0.05 mg/ml each (1 ml), for 30 minutes. After incubation, the chamber is rinsed with 10 ml PBS buffer.

5. 1 ml of a 0.5 mg/ml solution of streptavidin with 1% fluorescein-labeled streptavidin is then introduced in the chamber and the binding can be followed from fluorescence signal changes, due to the presence of fluorescein-labeled streptavidin.

6. The surface is then washed with 10 ml buffer to eliminate excess protein. The fluorescence signal of the surface is again measured to check for surface stability.

7. The surface is at this point ready for immobilization of the biotinylated nanocrystals, by addition of 1 ml biotin-NCs of concentration 2 nM. This can be monitored again by the increase of fluorescence on the screen (the filter setting adapted for the NCs).

8. After binding the chamber is washed with 10 ml PBS buffer to remove excess NCs, and the fluorescence signal measured again to check for the stability of the bound NCs.

9. In this experiment, we added a second layer of streptavidin on the biotin-NC surface, as the NCs possess several functionalities on their surface. For this 1 ml of a solution of streptavidin 1 mg/ml with 1% streptavidin Alexa568 was injected in the chamber and the fluorescence signal was measured, this time changing the collection filter for observation of red fluorescence without signal of the fluorescein and NCs (filters cut-off 590).

6.1.3 Stamping for micropatterning

Round glass slides of 22 mm diameter were used together with homemade holders. The stamps were made out of commercially available polymer blend (Sylgard 184, Dow Corning, Midland), and were kindly donated by E. Delamarche, IBM Zurich. The successive steps of stamping are listed below.

1. First the glass slides are thoroughly cleaned in several wash/sonication cycles before use. They are first rinsed 10 times with Milli-Q pure water, then washed with detergent, typically Helmanex 2%, and sonified for 10 minutes. The glass slides are then intensively rinsed with water to remove all detergent traces. They are sonified one more time in methanol and stored in methanol.

2. Before stamping, the glass slide is dried in a stream of N_2.

3. A small piece of the poly(dimethylsiloxane) (PDMS) stamp is cut and rinsed with ethanol under slight pressure and left to dry under a stream of nitrogen for 3-5 min.

4. For the adsorption of proteins (here BSA-biotin), the stamp surface is incubated with a solution of 0.2 mg/ml for more than 10 minutes.

5. The inked stamp is then rinsed several times with PBS buffer 1% and dried with nitrogen.

6. The inked stamp is delicately put into contact with the glass slide and left for a few seconds. The stamp manipulation is done using thin tweezers and minimal pressure is made on the stamp toward the surface.

7. After stamping, the stamped glass slide is incorporated into the slide holder liquid cell and incubated with a streptavidin solution of 0.025 mg/ml in PBS buffer for at least 10 minutes. The surface is finally ready for fluorescence imaging with the confocal microscope, to observe the biotin-NCs or biotin/NTA-NCs binding on the patterned surface.

6.1.4 Laser scanning confocal microscopy

Laser-scanning confocal micographs were recorded using Argon (458 and 488 nm) and 543 nm HeNe laser lines on a Zeiss LSM 510 microscope (Zeiss, Germany) equipped with a 63x water (1.2 numerical aperture) objective. Detection and distinction of fluorescence signals was achieved by appropriate filter sets using a multitracking mode. Scanning speed and laser

intensity were adjusted to avoid photobleaching of the fluorescent proteins. This problem is not encountered with the NCs as they are much more photostable.

6.2   Results on immobilization on surface, a TIRF study

6.2.1   Surface-based method: TIRF

Total internal Reflection Fluorescence (TIRF) is an elegant and efficient surface method for specific interactions investigation. The principle of TIRF is based on the total internal reflection of a laser beam at a glass-water interface [196]. Total reflection is originally illustrated in the figure below. When the incident light (polarized laser beam) hits the interface between an optically dense (e.g. quartz) medium and an optically less dense medium (e.g. aqueous solution) with an angle higher than the critical angle θ_c (or Brewster angle), the beam is totally reflected back into the dense medium and a standing electromagnetic wave is generated at the interface. The maximum of the electric field is located at the interface between the two different media, as shown in the figure 6.2.1. An exponentially decayed electromagnetic wave (evanescent wave) penetrates into the aqueous solution. The depth of penetration depends on the angle, wavelength, and ratio of refractive indexes. Typically the penetration depth of the evanescent wave is in the range of 100-400 nm (<100 nm for our setup).

This evanescent wave provides a surface selective illumination of the molecules. The fluorophores which will absorb or bind on a pre-treated surface will be excited, as the non-binding ones present in the solution will be out of the excitation field and thus not visible.
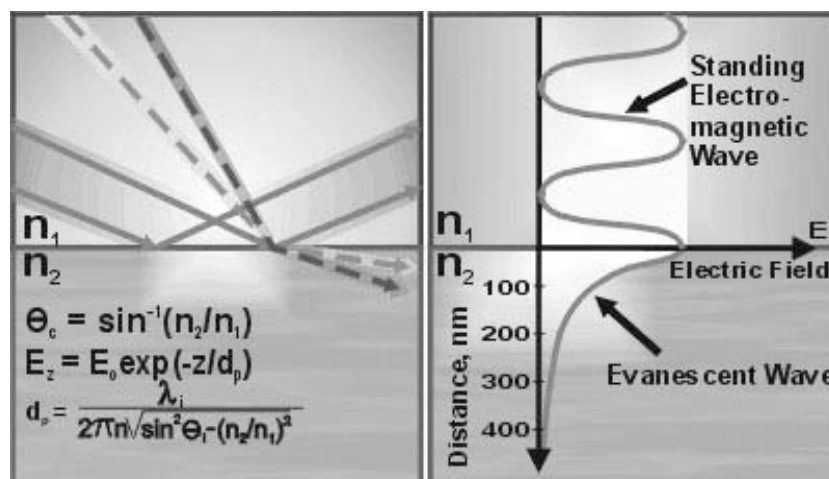
Figure 6.2.1: Scheme of the behavior of a incident light beam on a interface between two media of different density. It shows the importance of the incident angle when it hits the interface, and the case of total internal reflection that creates an evanescent wave. (Taken from www)

In the case of proteins, TIRF allows reliable detection of single molecules at the TIRF sensor surface. This method is a powerful tool for the interaction and analysis with a high sensitivity, which can allow single molecule detection as well as microscopy imaging [197-199].

Our TIRF systems provide measurement of real time kinetics of bioanalyte binding to a surface immobilized sensor molecule. TIRF is a fast, non-destructive, sensitive and versatile technique that is well suited for monitoring biomolecular interactions. TIRF allows monitoring conformational changes, orientation and lateral mobility of biomolecules. The sensitivity of TIRF is more than 10,000 times better than that of biosensor systems based on surface plasmon resonance (but with requirement of fluorescent analytes). Any analyte, such as proteins, peptides, DNA, or small therapeutically active molecules that fluoresces can be detected using TIRF.

6.2.2   Results

TIRF was used in our case to investigate whether the functionalized-NCs were binding on prestructured surfaces. The binding of biotin-NCs (chapter 3) to a pretreated glass surface incubated with streptavidin were monitored in-situ using TIRF. This allows optical excitation of the nanocrystals only in the proximity of the surface meaning the bound NCs.

Following figure 6.2.2, after incubation with BSA-biotin the holder was placed on the microscope and the fluorescence intensity (filter setting BP 515-565) measured to get the

background intensity (step 1). The streptavidin solution (containing fluorescein-streptavidin) was then injected into the chamber and the fluorescence intensity measured simultaneously to observe the protein binding on the BSA-biotin surface (step 2), followed by washing the excess protein with PBS (step 3). The surface is now ready for binding of biotin-NCs. The increase of the fluorescence intensity indicated the attachment of the biotinylated nanocrystals to the streptavidin layer on the surface via a binding curve (step 4). Rinsing with a PBS buffer solution caused no change in the fluorescence intensity meaning that the nanoparticles are specifically bound to the surface and in a stable way (step 5).

As the biotin-NCs are decorated with several biotin-groups, the addition of a fluorescently labeled streptavidin should be possible. We injected in the chamber a solution of streptavidin Alexa568, and observed the fluorescence increase due to binding on the surface with another filter setting (cut-off 590) to observe only the Alexa568 fluorescence (step 7). Indeed a binding curve appeared and the rinsing with buffer did not disrupt the bound proteins. The change of the emission setting to observe the NCs (filter setting BP 515-565) showed that the NCs are still on the surface.

In addition to this experiment, control experiments were carried out. First with the use of lipid-NCs devoid of biotin, second with biotin-NCs on the streptavidin surface pre-incubated with biotin to saturate the binding sites. Both controls showed no nonspecific binding of the biotin-NCs to the surface proving specificity of the interactions.
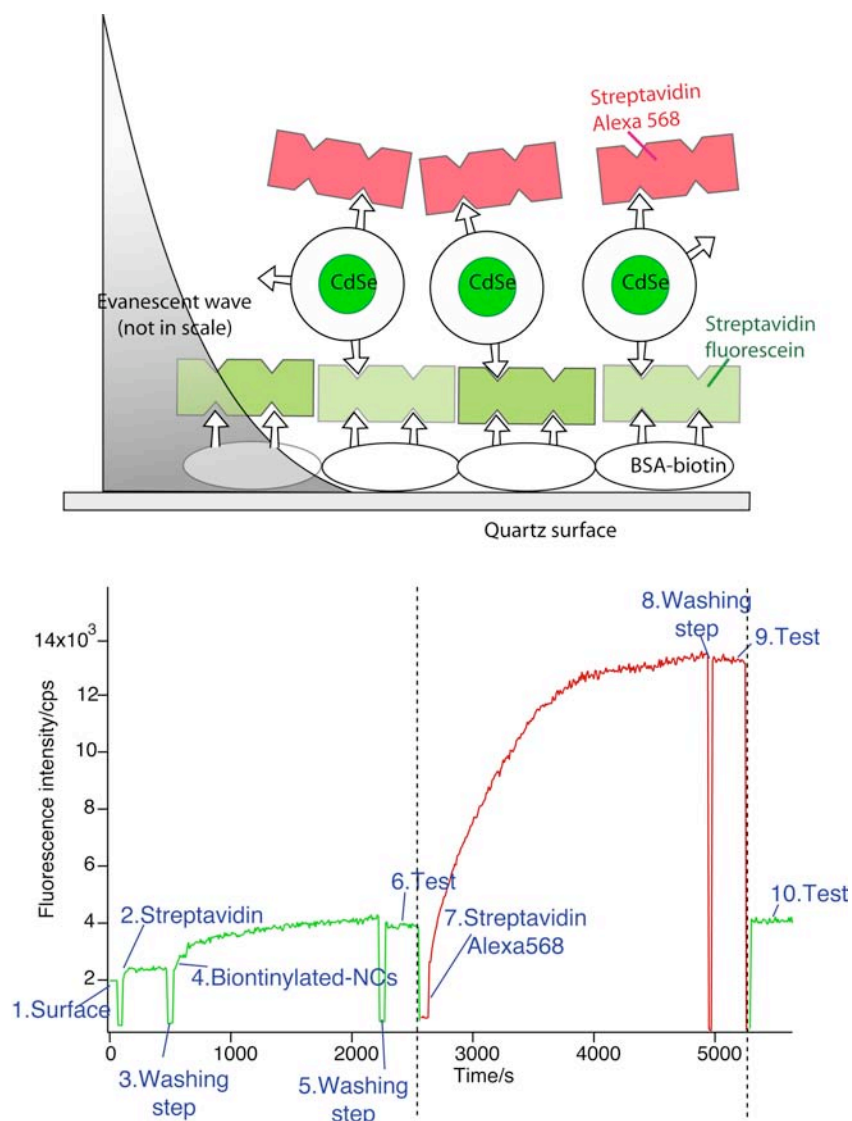
Figure 6.2.2: Scheme of the immobilization of biotinylated nanoparticles on the glass substrate (left). Time course of the TIR fluorescence signal due to the specific binding of CdSe nanoparticles to the streptavidin coated quartz substrate, followed by binding of a second layer of streptavidin on the NC layer (right). The successive binding steps on the graph of biotin-NCs to the surface are listed below: Excitation wavelength was 488 nm. 1. The surface was first incubated with BSA-biotin/BSA and the surface fluorescence measured for a baseline. 2. The chamber was then incubated with streptavidin/fluorescein-labeled streptavidin solution and the binding trace followed on the graph. 3. Washing step with PBS buffer to remove unbound streptavidin. 4. Biotinylated-NCs were then loaded into the measuring chamber, on the binding curve could be followed in real time. 5. Washing step to remove unbound NCs. 6. Test to see if biotin-NCs still present on the surface after washing. Indeed the intensity stays constant, meaning stable binding. 7. Change filter settings for visualization of Alexa568 only, cut-off 590. Addition of streptavidin Alexa568/streptavidin solution and binding curve followed on the graph. 9. Washing to remove unbound streptavidin. Test to see if streptavidin layer still present after washing. 10. Test to see if NCs still present by changing filter settings again to BP 515-565.

As seen on the graph above, the NCs bind specifically to the surface pre-incubated with streptavidin. As more than one functionality is present on the NC surface, experiment was done to see if an additional layer of streptavidin could be specifically bound to the surface. Indeed, a second streptavidin layer could bind to the biotin-NC one, forming a sandwich-like structure.

This kind of measurement was not followed up as we observed for some samples FPB effect (introduced in chapter 3). The binding of the biotin-NCs was observed but a continuous increase of the fluorescence intensity prevented us from observing any kind of binding. We thus decided to stop this kind of experiments.

As the biotin-NCs can bind specifically to a pre-treated surface with streptavidin, as shown above, we went further on to produce micropatterned surfaces for surface specific interactions via FRET with a sandwich bound protein.

6.3   Results on immobilization on micropatterns

Biologically addressable surfaces were used for specific immobilization of the functionalized lipid-NCs. The streptavidin-biotin model recognition couple was used for the specific anchoring of biotin/NTA-NCs on defined streptavidin micro-contact printed lines on a surface. The use of the doubly functionalized biotin/NTA-NCs as introduced in chapter 4 allowed us to immobilize the NCs in a specific way on predefined micro-domains, and allowed further binding of a biomolecule of interest. More interesting are the fluorescence properties of the NC, producing stable fluorescent micropatterns (slow photobleaching and high intensities if pre-illuminated), which can then act as local (tens of nanometers) excitation source of bound compounds. This will be exposed for the red fluorescent protein eqFP611-His$_6$ introduced in chapter 4.

6.3.1   Proteins micro-contact printing

Biomolecules on surfaces have applications that range from medical diagnostics, analytical chemistry, and for specific protein binding studies. Producing micro-patterns of proteins on surfaces is challenging considering the fragility and complexity of these molecules. It was quickly realized that photolithography methods could not be applied for proteins, thus novel approaches to pattern proteins were developed to maintain the protein functionality. Here

microcontact printing was used, where the proteins are applied like ink to the surface of a stamp and transferred to a substrate by printing. Microcontact printing was first developed by Whitesides and coworkers for printing alkanethiols on gold with spatial control [200]. Later many variants of microcontact printing were developed and collectively termed "soft-lithography" [201].

The central element is the preformed stamp, which is a silicon-based elastomer that is microstructured by curing liquid prepolymer of poly(dimethylsiloxane) (PDMS) on a lithographically fabricated master or mold. Then the stamp is peeled off the mold by hand, the stamp then bearing an inverted pattern of that of the master. The softness of the stamp allows it to follow the contours of a surface onto which it is applied. The contact between the elastomer and the substrate occurs at the molecular scale, it ensures the homogeneous transfer of ink from the stamp to the printed areas of the substrate. See chapters from Delamarche, Niemeyer and Mirkin in "Nanobiotechnology" [161].

In the immobilization experiment shown below, we used the microcontact printing method for creation of fluorescent micropatterns of functionalized-NCs.

Microcontact printing was chosen because it was well developed in the group. It can pattern down to the micron scale (0.1-10 μm range over cm^2 areas) in a reliable, inexpensive and in a rapid manner [201].

An important advantage of this method is the high contrast of the produced patterns. This is due to the fact that the desired material is deposited exclusively in selective areas due to the contact. If the stamping is done in a proper way, no material will be found outside of the patterns on the substrate.
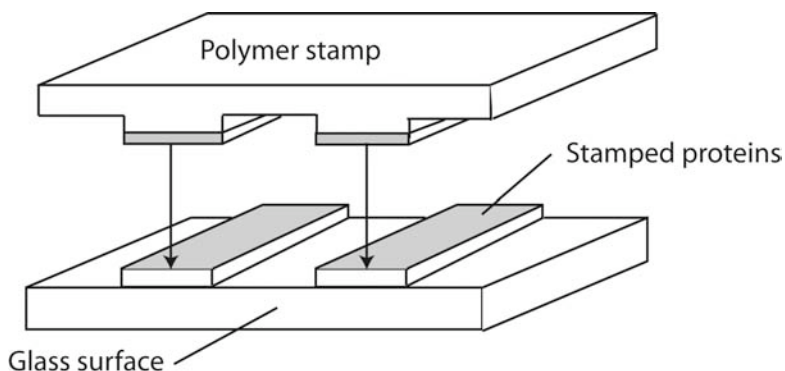
Figure 6.3.1: Scheme of the microcontact printing process. A polymer stamp (PDMS in most cases) is pre-incubated with a solution of the molecule to be stamped. Once the stamp is washed and dried, contact between stamp and substrate will deliver the adsorbing molecule in a defined and selective manner, producing patterns of this molecule.

Like conventional stamping, microcontact printing transfers material from one surface to another by region-selective conformal contact. Many molecules can be printed on surfaces [201, 202]. Bernard et al. [203] were the first to stamp proteins on surfaces; this approach is followed here for the patterned bio-functionalization of our surfaces.

It is our experience that immobilization of BSA-biotin and further coupling of streptavidin from a solution enhanced the affinity of streptavidin binding-sites or binding-sites number compared to a direct stamping of streptavidin. To avoid non-specific adsorption of proteins on the outside of the micropatterns at the surface, the surface can be incubated with BSA, a plasma protein that has a high adsorbing capacity on glass.

6.3.2 Results

Our goal was to micropattern NCs at the micrometer scale. Since, the functionalized-NCs comprise multiple binding-sites, additional proteins could be bound onto the NC patterns.

Typically, the following procedure was used for stamping: the PDMS stamp was incubated with a BSA-biotin solution, washed and printed on a glass slide. The surface was successively incubated with a BSA solution for surface passivation, rinsed, and finally incubated with a biotin-NCs solution resulting in a pattern of NCs.

The micropatterned surfaces were imaged with confocal microscope before and after addition of the fluorescent biotin-NC solution, to observe the binding, as well as after washing out the

non-bound molecules. The images shown here are the final steps, where the surface was washed with buffer to eliminate unbound substances.

The experiment using stamped surfaces treated with BSA to avoid non-specific binding (NSB) the NSB of biotin-NCs was high in the presence of BSA, up to 30% NSB. The lipid-NCs adsorb apparently a lot on BSA.

As we can see very clearly from the two images from figure 6.3.2, the treatment of the surface outside the patterns with BSA engendered a lot of NSB of the biotin-NCs. Moreover the stamp used for these experiments was giving rise to inhomogeneous line patterns.
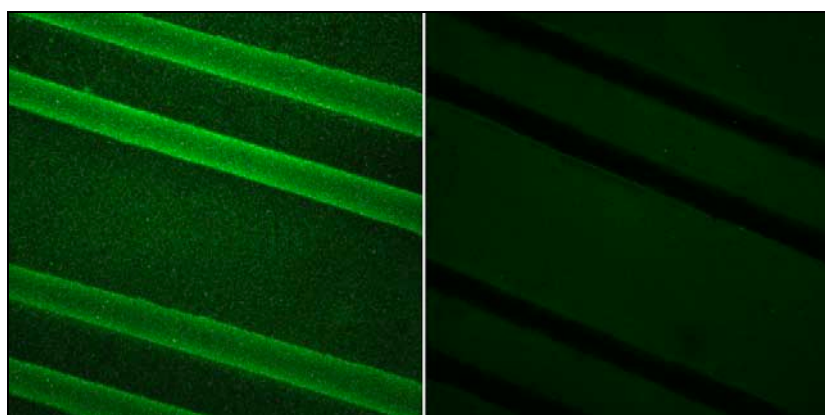

Figure 6.3.2: Confocal images of stamped surfaces. The left image is a positive image of bound biotin-NCs to a BSA-biotin/streptavidin patterning and surface protected by BSA. As we can see here the stamp is not homogeneous and a lot of NSB is visible. To show NSB even clearly, the right image is the control experiment where the streptavidin on patterns were incubated with excess biotin, thus no binding of biotin-NC occurred. But it is well visible that NSB is present as the green background outside the lines. Stamp of 10 μm thick lines.

The use of a new stamp improved the homogeneity of the patterned lines, as seen in the following experiment. This time the experiment was done using double functionalized biotin/NTA-NCs to allow sandwich immobilization of the NCs followed by a fluorescent protein eqFP611-His$_6$. This experiment is illustrated in the scheme below for better understanding.

The different steps of the stamping are illustrated in the figure 6.3.3. As we can see on the following scheme, we avoided this time the incubation with BSA, because in our previous case the results showed more NSB with BSA than without. This contrasted with the conclusions made earlier by D. Stamou (PhD thesis n°2163 EPFL 2000).
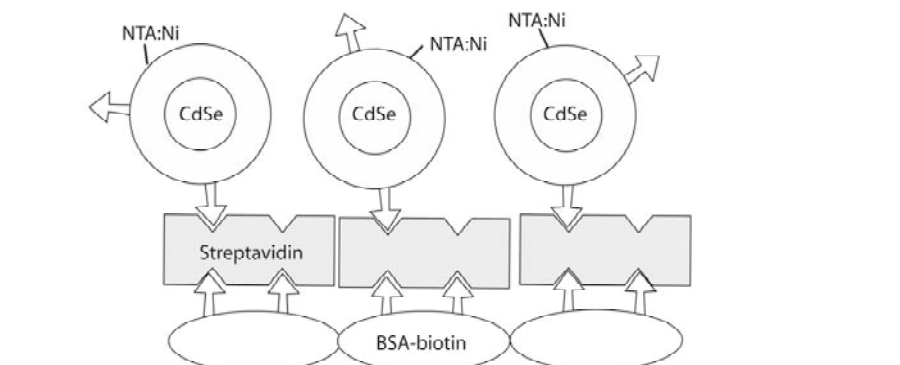
1. Stamping of BSA-biotin

Polymer Stamp incubated with BSA-biotin

BSA-biotin
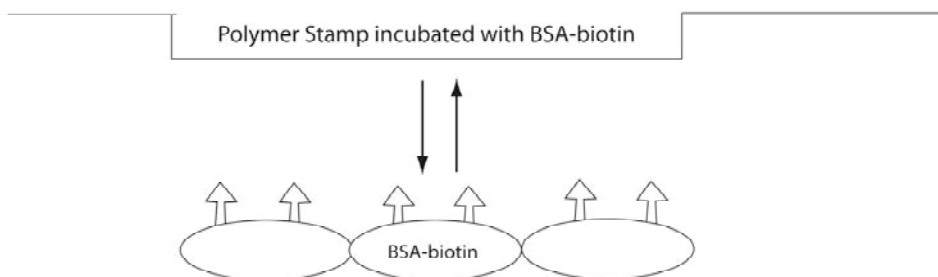
2. Incubation with a streptavidin solution

Streptavidin

BSA-biotin
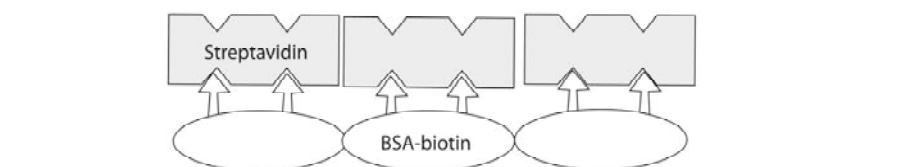
3. Incubation with biotin/NTA-functionalized NCs

NTA:Ni

NTA:Ni

NTA:Ni

CdSe

CdSe

CdSe

Streptavidin

BSA-biotin

4. Incubation with the His-taged red fluorescent protein eqFP611

eqFP611

eqFP611

eqFP611

6His
NTA:Ni

6His
NTA:Ni

6His
NTA:Ni

CdSe
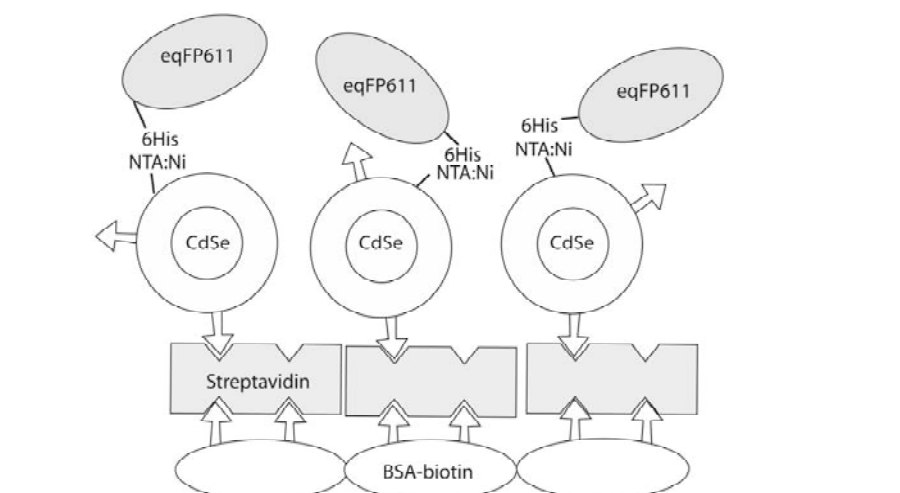
CdSe

CdSe

Streptavidin

BSA-biotin

Figure 6.3.3: Scheme for the successive steps for immobilization of NCs on micropatterns (3), and additional immobilization of a fluorescent protein on top of the NC micropatterns. 1. First BSA-biotin is incubated on the polymer stamp, the polymer is then washed and the stamp deposited on the glass slide. 2. Streptavidin is then incubated on the stamped BSA-biotin, and the surface washed to eliminate excess streptavidin. 3. A biotin/NTA-functionalized NCs solution can then be incubated for specific binding of the NCs through biotin on patterned proteins; the excess is washed away. 4. Incubation with a His-tagged fluorescent protein eqFP611-His$_6$ through his$_6$-groups.

The resulting surfaces of experiments following the different steps of this scheme are imaged (figure 6.4.3) with the confocal microscope at the two following steps; before the addition of the eqFP611-His$_6$ (step 3, figure 6.3.3) and after its binding (step 4, figure 6.3.3). The left graph of figure 6.3.4 images the NC fluorescence. The left image shows the bound eqFP611-His$_6$ fluorescence but with the same excitation wavelength as for the NCs. We thus see here the emission of eqFP611-His$_6$ due to FRET from the NC toward the red fluorescent protein.
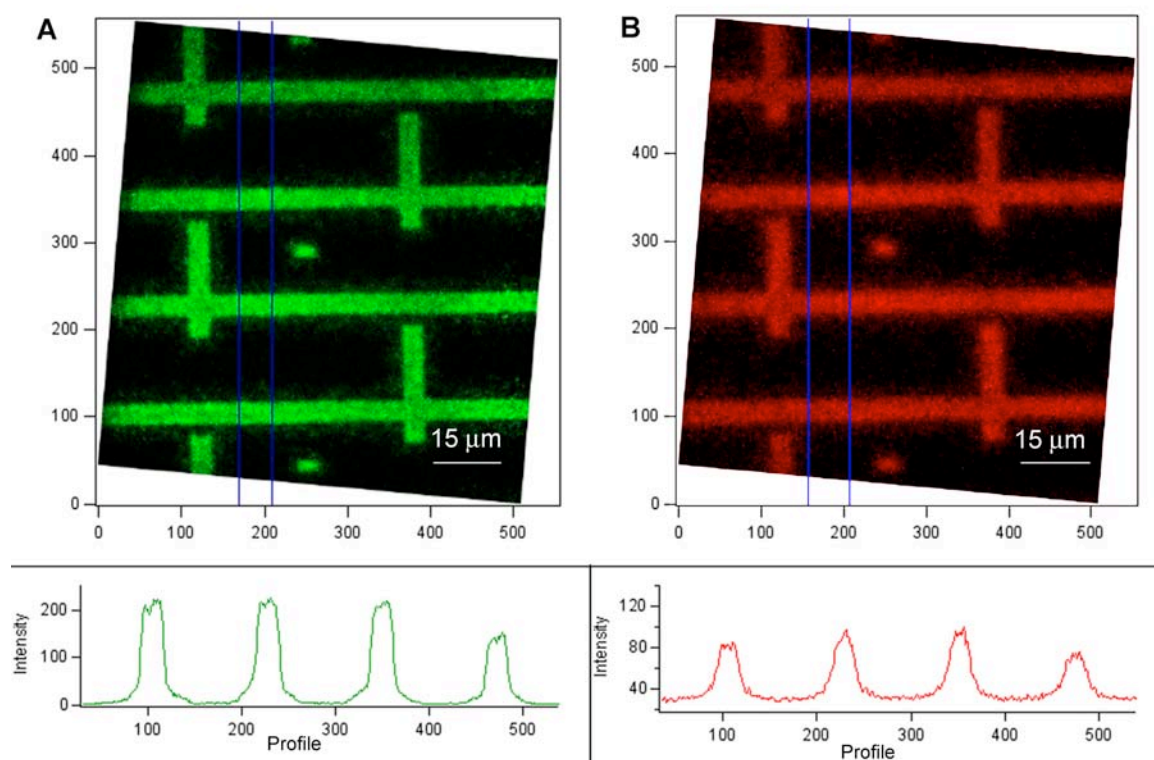
Figure 6.3.4: Confocal images of the patterned NCs (A) and the red-fluorescent protein eqFP611 on the NCs (B). (A) Excitation was at 458 nm, and observation filter BP 505-565 was used for observation of the NC fluorescence. (B) This picture represents step 4 of figure 6.3.3: Excitation is at 458 nm, and observation filter is LP 585 for observation of the eqFP611 fluorescence; the fluorescence seen here originates from FRET between the NC and the protein. Below the fluorescence images are the line profile graphs along the perpendicular blue lines visible on the fluorescent images. The intensity ratio of NSB to specific binding is 5% for the NCs binding. The patterned features are 4 μm thick lines.

As we can see on the fluorescence confocal image above (left), the immobilization of the NCs is specifically localized on the pre-printed BSA-biotin/streptavidin lines, with low NSB. This was achieved in the absence of BSA passivation outside the patterns (see graph profiles under the fluorescence image). The nonspecific to specific binding was less than 5%. The pattered lines were also homogeneous and well defined as can be seen from the profiles. To test binding specificity of the biotin/NTA-NCs toward streptavidin, control experiments were performed on a surface patterned the same way but using this time non-biotinylated NCs (lipid-NC devoid of biotin-lipids). No binding could be observed on the patterned features, proving that specific immobilization on the streptavidin lines is achieved through biotin-streptavidin recognition. As a second control, the addition of an excess of biotin on the

patterned surface before addition of the biotin/NTA-NCs also prevented binding of the NCs, confirming the specific interactions as well.

The immobilized NCs through biotin possessed another binding functionality on their surface, NTA chelator. To test specific immobilization of a his-tagged protein on it, we incubated the surface with eqFP611-His$_6$, the his-tagged red fluorescing protein previously used for solution binding experiment, using FRET. Its immobilization on the NCs micron-thick lines is observed. Here some NSB of the protein was present. But this effect was overcome with the advantage that the NCs were used as a local excitation source. Only the proteins on the patterns are excited through FRET (figure 6.3.4, right image), thus reducing the signal to noise ratio problem if the proteins of interest or analytes possess a less specific adsorbing property towards surfaces. The eqFP611-His$_6$ remained immobilized on the surface-patterned nanostructures even after multiple washing with buffer, but was released after adding EDTA, showing that the interaction between oligo-histidine sequences and the NTA groups is stable and fully reversible. EDTA displaces the Nickel ion from the complex made of oligo-histidine and NTA group resulting in disruption of binding of the red-fluorescent protein.

6.4   Conclusions

Possessing functionalized fluorescent nanocrystals, which are specific toward the complementary protein, an interesting approach is to immobilize them on predefined surfaces. For this purpose, first a surface-specific fluorescent method were used named TIRF. This method allowed us to follow the binding of the biotin-NCs on a surface pretreated with BSA-biotin and streptavidin, a biotin specific protein. Control experiments demonstrated the specificity of the interaction. An additional layer of streptavidin Alexa568 could be attached to the biotin-NC layer through specific binding, as the NCs possess more than one binding site. We thus produced sandwich supramolecular assemblies on a surface.

A similar approach was then used to produce micropatterns of functionalized-NCs, via microcontact printing of BSA-biotin, and further binding of streptavidin. The binding of biotin/NTA-NCs was successful, and we achieved good specificity. The presence of NTA functionalities on the NC allowed the attachment of any histidine-tag-protein in a reversible way. Here the binding was tested with eqFP-His$_6$.

These patterns of fluorescent and functionalized NCs introduce a surface specific method through specific interactions of biomolecules with the patterns and observation was achieved using FRET with confocal microscopy. These surfaces are potential biosensing surfaces for minimizing the amount of analyte through micro and maybe nanopatterning as a subsequent step.

A good advantage of the NCs patterns is that they can act as local source of illumination, avoiding problems of non-specific binding of proteins, via FRET observation of the local dots or lines and not the proteins adsorbed outside of the pattern. Patterned nanometer-sized local light sources offer attractive possibilities for applications, e.g. for DNA or protein arrays, where nonspecific binding of labeled analyte molecules impairs high sensitivity using standard illumination techniques (resolution 100's of nm). The NCs, as a local light source, would only excite specifically bound analyte molecules within the FRET range (about 10 nm), enhancing signal to noise ratio.

7   Outlook

The well-known TOP/TOPO method allowed the production of fluorescent, stable and nearly monodisperse nanocrystals (NCs) in solution. Because this procedure delivers hydrophobic NCs, it is necessary to modify the NC surface for further interactions with biomolecules. Here we have presented a versatile method to solubilize and simultaneously functionalize the NCs via lipid coating, while minimizing non-specific interactions, all this in a one step procedure. The specific interaction of these functionalized-NCs with complementary biomolecules was observed by FRET. Specific interaction between NCs and different proteins through multiple high affinity binding sites enabled site-selective controlled formation of supramolecular assemblies. The multi-functional NCs served as local light sources, which could, within supramolecular assemblies be positioned with nanometer precision and there exchanged energy over distances from 1 to more than 10 nm, again controlled with nanometer precision (FRET distances). Such concepts might be of importance for the development of biotechnology and bioanalytics at a nanometer or attoliter scale. Challenging examples are the use of single NCs for investigating substrate tunneling on multi-enzyme complexes or (bio)chemical syntheses and biomolecular reactions in sub-micrometer-sized containers [204, 205].

The presence of a lipid monolayer on the NCs enabled us to use the NCs to sense the interactions with peripheral membrane proteins or for incorporation of proteins into the lipid layer. We studied the adsorption of cytochrome c, a peripheral membrane protein, on negatively charged lipid-NCs and obtained similar interactions as published for vesicles. Further studies could be carried out in the future as for example the displacement of cytochrome c in the presence of Histone H1, a protein related to cell apoptosis. During apoptosis, H1 plays an important role in the release of cytochrome c from mitochondria into

the cytosol [206]. Another example is myelin basic protein (MBP), which adsorbs [207] in form of multi-layers on lipid membranes from nerves. Their adsorption on the lipid-NCs would allow us to study the destruction mechanism of the MBP layers during multiple sclerosis [208], by monitoring the NC fluorescence at different conditions.

We succeeded in micropatterning the functionalized NCs on pretreated surfaces allowing the specific immobilization of selected proteins. This would be useful for the development of biosensor surfaces. Another interesting topic would be to achieve nanometer-scale patterning of the desired NCs with desired functionalities. This would allow immobilization of single functionalized-NCs on nanometer-sized patterns. The immobilization of single NCs would make it possible to investigate molecular interactions at a single molecule level directly on the NC.

We also produced detergent-coated NCs, which could be incorporated into vesicular lipid bilayer. The interesting point is that the NCs could then act as membrane dyes for cell imaging.

The creation of hybrid supramolecular assemblies of NCs and biomolecules is a field gaining much interest, mostly due to the unusual properties of the resulting assemblies allowing their application in many different domains.

Reference List

[1]   A. Henglein, *Chem. Rev*. **1989**, *89*, 1861.
[2]   H. Weller, *Adv. Mater*. **1993**, *5*, 88.
[3]   H. Weller, *Angew. Chem. Int. Ed. Engl*. **1993**, *32*, 41.
[4]   L. M. Liz-Marzan, D. J. Norris, M. G. Bawendi, T. Betley, H. Doyle, P. Guyot-Sionnest, V. I. Klimov, N. A. Kotov, P. Mulvaney, C. B. Murray, D. J. Schiffrin, M. Shin, S. Sun, C. Wang, *Editorial for MRS Bulletin* **2001**, *26*, 981.
[5]   M. C. Schlamp, X. Peng, A. P. Alivisatos, *J. Appl. Phys*. **1997**, *82*, 5837.
[6]   N. C. Greenham, X. Peng, A. P. Alivisatos, *Phys. Rev. B* **1996**, *54*, 17628.
[7]   S. Coe, W. K. Woo, M. G. Bawendi, V. Bulovic, *Nature* **2002**, *420*.
[8]   W. U. Huynh, J. J. Dittmer, W. C. Libby, G. L. Whiting, A. P. Alivisatos, *Adv. Func. Mater*. **2003**, *13*, 73.
[9]   V. I. Klimov, *J. Phys. Chem. B* **2000**, *104*, 6112.
[10]   N. Suzuki, Y. Tomita, T. Kojima, *Appl. Phys. Lett*. **2002**, *81*, 4121.
[11]   R. J. Walters, P. G. Kik, J. D. Casperson, H. A. Atwater, R. Lindstedt, M. Giorgi, G. Bourianoff, *Appl. Phys. Lett*. **2004**, *85*, 2622.
[12]   M. Bruchez, M. Moronne, P. Gin, S. Weiss, A. P. Alivisatos, *Science* **1998**, *281*, 2013.
[13]   B. Dubertret, P. Skourides, D. J. Norris, V. Noireaux, A. H. Brivanlou, A. Libchaber, *Science* **2002**, *298*, 1759.
[14]   A. P. Alivisatos, *Science* **1996**, *271*, 933.
[15]   C. M. Niemeyer, *Angewandte Chemie-International Edition* **2001**, *40*, 4128.
[16]   C. M. Niemeyer, *Angewandte Chemie-International Edition* **2003**, *42*, 5796.
[17]   R. L. Whetten, J. T. Khoury, M. M. Alvarez, S. Murthy, I. Vezmar, Z. L. Wang, P. W. Stephens, C. L. Cleveland, W. D. Luedtke, U. Landman, *Adv. Mater*. **1996**, *8*, 428.
[18]   Y. Yin, Z.-Y. Li, Z. Zhong, B. Gates, Y. Xia, S. Venkateswaran, *J. Mater. Chem*. **2002**, *12*, 522–527.
[19]   D. W. Bahnemann, M. R. H. C. Kormann, *J. Phys. Chem*. **1987**, *91*, 3789.
[20]   W. L. Wilson, *science* **1993**, *262*, 1242.
[21]   Z. A. Peng, X. Peng, *J. Am. Chem. Soc*. **2001**, *123*, 183.
[22]   T. Vossmeyer, M. G. L. Katsikas, I.G. Popovic, K. Diesner, A. Chemseddine, A. Eychmüller, H. Weller, *J. Phys. Chem*. **1994**, *98*, 7665.
[23]   C. B. Murray, D. J. Norris, M. G. Bawendi, *Journal of the American Chemical Society* **1993**, *115*, 8706.
[24]   A. L. Rogach, *Ber. Bunsenges. Phys. Chem*. **1996**, *100*, 1772.
[25]   N. Kumbhojkar, *NanoStructured Mat*. **1998**, *10*, 117.
[26]   R. L. Wells, W. L. Gladfelter, *J. Cluster Science* **1997**, *8*, 217.
[27]   O. I. Micic, *j. Luminesc*. **1996**, *70*, 95.
[28]   H. Uchida, *J. Phys. Chem*. **1991**, *95*, 5382.
[29]   M. A. Malik, P. O'Brien, S. Norager, J. Smith, *J. Mater. Chem*. **2003**, *13*, 2591–2595.

[30]   O. I. Micic, *J. Phys. Chem.* **1994**, *98*, 4966.

[31]   T. Schneider, A. K. M. Haase, S. Naused, H. Weller, *Ber. Bundesges. Phys. Chem.* **1997**, *101*, 1654.

[32]   M. Himmelhaus, H. Takei, *Sensors and Actuators B* **2000**, *63*, 24.

[33]   D. J. Maxwell, J. R. Taylor, S. Nie, *J. Am. Chem. Soc.* **2002**, *124*, 9606.

[34]   C. A. Mirkin, R. L. Letsinger, R. C. Mucic, J. J. Storhoff, *Nature* **1996**, *382*, 607.

[35]   J.-M. Nam, S.-J. Park, C. A. Mirkin, *J. Am. Chem. Soc.* **2002**, *124*, 3820.

[36]   S. G. Penn, L. He, M. J. Natan, *Current Opinion Chem. Biol.* **2003**, *7*, 609.

[37]   J. J. Storhoff, R. Elghanian, R. C. Mucic, C. A. Mirkin, R. L. Letsinger, *J. Am. Chem. Soc.* **1998**, *120*, 1959.

[38]   T. A. Taton, C. A. Mirkin, R. L. Letsinger, *Science* **2000**, *289*, 1757.

[39]   M. Grätzel, *J. of Photochemistry and Photobiology C: Photochemistry Reviews* **2003**, *4*, 145.

[40]   M. Grätzel, *Nature* **2003**, *421*, 586.

[41]   T. Fukumura, Z. Jin, A. Ohtomo, H. Koinuma, M. Kawasaki, *Appl. Phys. Lett.* **1999**, *75*, 3366.

[42]   S. B. Orlinskii, J. Schmidt, P. G. Baranov, D. M. Hofmann, C. d. M. Donega, A. Meijerink, *Phys. Rev. Lett.* **2004**, *92*, 047603.

[43]   A. P. Alivisatos, *Abstracts of Papers of the American Chemical Society* **1998**, *216*, U337.

[44]   J. K. Jaiswal, H. Mattoussi, J. M. Mauro, S. M. Simon, *Nature Biotechnology* **2003**, *21*, 47.

[45]   E. R. Goldman, A. R. Clapp, G. P. Anderson, H. T. Uyeda, J. M. Mauro, I. L. Medintz, H. Mattoussi, *Analytical Chemistry* **2004**, *76*, 684.

[46]   X. Wu, H. Lui, J. Lui, K. N. Haley, J. A. Treadway, J. P. Larson, G. Ge, F. Peale, M. P. Bruchez, *Nature Biotechnology* **2003**, *21*, 41.

[47]   M. Dahan, S. Lévi, C. Luccardini, P. Rostaing, B. Riveau, A. Triller, *Science* **2003**, *302*, 442.

[48]   W. Schroter, *Handbook of semiconductor technology: Electronic structure and properties of semiconductors*, Wiley VCH, Weinheim, **2000**.

[49]   A. P. Alivisatos, *J. Phys. Chem.* **1996**, *100*, 13226.

[50]   A. I. Ekimov, A. A. Onushchenko, *Sov. Phys. Semicond.* **1982**, *16*, 775.

[51]   A. L. Efros, A. L. Efros, *Sov. Phys. Semicond.* **1982**, *16*, 772.

[52]   G. C. Papavassiliou, *J. Solid State Chem.* **1981**, *40*, 330.

[53]   L. Brus, *Appl. Phys.* **1991**, *A 53*, 465.

[54]   L. E. Brus, *J. Chem. Phys.* **1984**, *80*, 4403.

[55]   M. V. Rama Krishna, R. A. Friesner, *J. Chem. Phys.* **1991**, *95*, 8309.

[56]   A. D. Yoffe, *Adv. Phys.* **2001**, *50*, 1.

[57]   H. Fu, L.-W. Wang, A. Zunger, *Phys. Rev. B* **1998**, *57*, 9971.

[58]   J. H. Davies, *The physics of low-dimensional semiconductors: an introduction*, Cambridge University press, **1998**.

[59]   V. Mohan, J. B. Anderson, *Chem. Phys. Lett.* **1989**, *156*, 520.

[60]   R. J. Dwayne Miller, G. L. McLendon, A. J. Nozik, W. Schmickler, *Surface Electron transfer processes*, Wiley VCH, **1995**.

[61]   H. Weller, H. M. Schmidt, U. Koch, A. Fojtik, S. Baral, A. Heinglein, W. Kunath, K. Weiss, E. Dieman, *Chem. Phys. Lett.* **1986**, *124*, 557.

[62]   A. Henglein, *Ber. Bunsenges. Phys. Chem.* **1974**, *78*, 1078.

[63]   S. V. Gaponenko, *Optical Properties of Semiconductor Nanocrystals*, Cambridge, **1998**.

[64]   S. M. Sze, *Physics of semiconductor devices*, New-York, **1981**.

[65]   P. E. Lippens, M. Lannoo, *Phys. Rev.* **1990**, *B41*, 6079.

[66]   P. E. Lippens, M. Lannoo, *Phys. Rev.* **1989**, *B39*, 10935.

[67]   N. F. Johnson, H. Ehrenreich, K. C. Hass, T. C. McGill, *Phys. Rev. Lett.* **1987**, *59*, 2352.

[68]   A. P. Alivisatos, *Endeavour* **1997**, *21*, 56.

[69]   K. E. Drexler, *Proc. Natl. Acad. Sci.* **1981**, *78*, 5275.

[70]   L. E. Brus, A. I. Efros, T. J. Itoh, *Luminesc. 70, R7* **1996**, *70*, R7.

[71]   L.-S. Li, J. Hu, W. Yang, A. P. Alivisatos, *Nanolett.* **2001**, *1*, 349.

[72]   C. A. Leatherdale, M. G. Bawendi, *Phys. Rev. B* **2001**, *6316*, 165315.

[73]   P. Guyot-Sionnest, M. Shim, C. Matranga, M. Hines, *Phys. Rev. B* **1999**, *60*, R2181.

[74]   O. Schmelz, A. Mews, T. Basche, A. Herrmann, K. Mullen, *Langmuir* **2001**, *17*, 2861.

[75]   A. Striolo, J. Waed, J. M. Prausnitz, W. J. Parak, D. Zanchet, D. Gerion, D. Milliron, A. P. Alivisatos, *J. Phys. Chem. B* **2002**, *106*, 5500.

[76]   C. A. Leatherdale, W. K. Woo, F. A. Mikulec, M. G. Bawendi, *J. Phys. Chem.* **2002**, *106*, 7619.

[77]   W. W. Yu, L. Qu, W. Guo, X. Peng, **2003**, *2854*.

[78]   O. Schmelz, Diplomarbeit thesis, Johannes-Gutenberg Universität (Mainz), **1999**.

[79]   F. Seker, K. Meeker, T. F. Kuech, A. B. Ellis, *Chem. Rev.* **2000**, *100*, 2505.

[80]   L. E. Brus, *J. Phys. Chem.* **1986**, *90*, 2555.

[81]   T. D. Krauss, L. Brus, *Phys. Rev. Lett.* **1999**, *83*, 4840.

[82]   V. I. Klimov, D. W. Mcbranch, C. A. Leatherdale, M. G. Bawendi, *Phys. Rev. B* **1999**, *60*, 13740.

[83]   F. Koberling, A. Mews, T. Basché, *Adv. Mater.* **2001**, *13*, 672.

[84]   M. Nirmal, L. Brus, *Acc. Chem. Res.* **1999**, *32*, 407.

[85]   X. Peng, L. Manna, W. D. Yang, J. Wickham, E. Scher, A. Kadavanish, A. P. Alivisatos, *Nature* **2000**, *404*, 59.

[86]   J. E. B. Katari, V. L. Colvin, A. P. Alivisatos, *J. Phys. Chem.* **1994**, *98*, 4109.

[87]   I. Potapova, R. Mruk, S. Prehl, R. Zentel, T. Basche, A. Mews, *J. Am. Chem. Soc.* **2003**, *125*, 320.

[88]   X. Michalet, F. Pinaud, T. D. Lacoste, M. Dahan, M. P. Bruchez, A. P. Alivisatos, S. Weiss, *Single Mol.* **2001**, *2*, 261.

[89]   W. J. Parak, D. Gerion, T. Pellegrino, D. Zanchet, C. Micheel, S. C. Williams, R. Boudreau, M. A. Le Gros, C. A. Larabell, A. P. Alivisatos, *Nanotechnology* **2003**, *14*, R15.

[90]   E. Katz, I. Willner, *Angew. Chem. Int. Ed.* **2004**, *43*, 2.

[91]   W. C. W. Chan, S. M. Nie, *Science* **1998**, *281*, 2016.

[92]   A. P. Alivisatos, K. P. Johnson, X. Peng, T. E. Wilson, C. J. Loweth, M. P. Bruchez, P. G. Schulz, *Science* **1996**, *382*, 609.

[93]   D. Gerion, F. Pinaud, S. C. Williams, W. J. Parak, D. Zanchet, S. Weiss, A. P. Alivisatos, *J. Phys. Chem. B* **2001**, *105*, 8861.

[94]   M. A. Correa-Duarte, *Chem. Phys. Lett.* **1998**, *286*, 497.

[95]   P. Reiss, J. Bleuse, A. Pron, *Nano Lett.* **2002**, *2*, 781.

[96]   G. Schmid, *Nanoparticles*, **2004**.

138

[97] U. Simon, G. Schön, *Handbook of Nanostructured Materials and Nanotechnology*, Academic Press, **2000**.

[98] C. D. Dushkin, S. Saita, K. Yoshie, Y. Yamaguchi, *Adv. Colloid Interface Sci.* **2000**, *88*, 37.

[99] A. I. Ekimov, *J. Lumin.* **1996**, *70*, 1.

[100] E. M. Wong, J. E. Bonevish, P. C. Seraon, *J. Phys. Chem. B* **1998**, *102*, 7770.

[101] H.-C. Youn, S. Baral, J. H. Fendler, *J. Phys. Chem.* **1988**, *92*, 6320.

[102] J. H. Fendler, *Chem. Rev.* **1987**, *87*, 877.

[103] S. Mahamuni, A. A. khosravi, M. Kundu, *J. Appl. Phys.* **1993**, *73*, 5237.

[104] J. P. Yang, S. B. Qadri, B. R. Ratna, *J. Phys. Chem.* **1996**, *100*, 17255.

[105] F. Gindele, R. Westhäling, U. Woggon, L. Spanhel, V. Platschek, *Appl. Phys. Lett.* **1997**, *71*, 2181.

[106] C. B. Murray, C. R. Kagan, M. G. Bawendi, *Annu. Rev. Mater. Sci.* **2000**, *30*, 545.

[107] Y. De Smet, L. Derimaeker, R. Finsy, *Langmuir* **1997**, *13*, 6884.

[108] H. Grätz, *Scr. Mat.* **1997**, *37*, 9.

[109] H. Reiss, *J. Phys. Chem.* **1951**, *19*.

[110] X. Peng, J. Wickham, A. P. Alivisatos, *J. Am. Chem. Soc.* **1998**, *120*, 5343.

[111] D. V. Talapin, A. L. Rogach, A. Kornowski, M. Hasse, H. Weller, *Nanolett.* **2001**, *1*, 207.

[112] T. Sugimoto, *Adv. Colloid Interface Sci.* **1987**, *28*, 65.

[113] M. L. Steigerwald, *J. Am. Chem. Soc.* **1988**, *110*, 3046.

[114] N. P. Gaponik, D. V. Talapin, A. L. Rogach, A. Eychmüller, H. Weller, *Nanolett.* **2002**, *2*, 803.

[115] J. Aldana, Y. A. Wang, X. Peng, *J. Am. Chem. Soc.* **2002**, *123*, 8844.

[116] P. T. Tran, E. R. Goldman, G. P. Anderson, J. M. Mauro, H. Mattoussi, *Phys. Status Solidi B* **2002**, *229*, 427.

[117] C. B. Murray, M. G. Bawendi, *Abstracts of Papers of the American Chemical Society* **1993**, *205*, 136.

[118] C. H. Fischer, H. Weller, A. Fojtik, C. Lume-Pereira, E. Janata, A. Heinglein, *Ber. Bundesges. Phys. Chem.* **1986**, *90*, 46.

[119] J. P. Wilcoxon, J. E. Martin, F. Parsapour, B. Wiedenman, D. B. Kelly, *J. Chem. Phys.* **1998**, *108*, 9137.

[120] D. Zanchet, C. M. Micheel, W. J. Parak, D. Gerion, S. C. Williams, A. P. Alivisatos, *J. Phys. Chem. B* **2002**, *106*.

[121] D. Zanchet, C. M. Micheel, W. J. Parak, D. Gerion, A. P. Alivisatos, *Nanolett.* **2001**, *1*, 32.

[122] D. Gerion, W. J. Parak, S. C. Williams, D. Zanchet, C. M. Micheel, A. P. Alivisatos, *J. Am. Chem. Soc.* **2002**, *124*, 7070.

[123] W. J. Parak, D. Gerion, D. Zanchet, A. S. Woerz, T. Pellegrino, C. M. Micheel, S. C. Williams, M. Seitz, R. E. Bruehl, Z. Bryant, C. Bustamante, C. R. Bertozzi, A. P. Alivisatos, *Chem. Mater.* **2002**, *14*, 2113.

[124] J. Hofkens, L. Latterini, G. De Belder, T. Gensch, M. Maus, T. Vosch, Y. Karni, G. Schweitzer, F. C. De Schryver, A. Hermann, K. Müllen, *Chem. Phys. Lett.* **1999**, *304*, 1.

[125] R. Eckert, PhD thesis, University of Basel (CH) (Basel), **2001**.

[126] M. B. Mohamed, C. Burda, M. A. El-Sayed, *Nanolett.* **2001**, *1*, 589.

[127] W. C. W. Chan, D. J. Maxwell, X. H. Gao, R. E. Bailey, M. Y. Han, S. M. Nie, *Current Opinion in Biotechnology* **2002**, *13*, 40.

[128] M. A. Hines, P. Guyot-Sionnest, *J. Phys. Chem. B* **1998**, *102*, 3655.

[129] M. Kuno, D. P. Fromm, H. F. Hamann, A. Gallagher, D. J. Nesbitt, *J. Chem. Phys.* **2001**, *115*, 1028.

[130] S. A. Empedocles, D. J. Norris, M. G. Bawendi, *Phys. Rev. Lett.* **1996**, *77*, 3873.

[131] M. Nirmal, B. O. Dabbousi, M. G. Bawendi, J. J. Macklin, J. K. Trautman, T. D. Harris, L. E. Brus, *Nature* **1996**, *383*, 802.

[132] J. Tittel, W. Göhde, F. Koberling, A. Mews, A. Kornowski, H. Weller, A. Eychmüller, T. Basche, *Ber. Bundesges. Phys. Chem.* **1997**, *101*, 1626.

[133] K. T. Shimizu, R. G. Neuhauser, C. A. Leatherdale, S. A. Empedocles, W. K. Woo, M. G. Bawendi, *Phys. Rev. B* **2001**, *63*, 205316.

[134] J. Hu, L. Li, W. Yang, L. Manna, L. Wang, A. P. Alivisatos, *Science* **2001**, *292*, 2060.

[135] W. C. W. Chan, S. Nie, *Science* **1998**, *281*, 2016.

[136] S. J. Rosenthal, I. Tomlinson, E. M. Adkins, S. Schroeter, S. Adams, L. Swafford, J. McBride, Y. Wang, L. J. DeFelice, R. D. Blakely, *J. Am. Chem. Soc.* **2002**, *124*, 4586.

[137] H. Mattoussi, J. M. Mauro, E. R. Goldman, G. P. Anderson, V. C. Sundar, F. V. Mikulec, M. G. Bawendi, *Journal of the American Chemical Society* **2000**, *122*, 12142.

[138] A. R. Clapp, I. L. Medintz, J. M. Mauro, B. R. Fisher, M. G. Bawendi, H. Mattoussi, *Journal of the American Chemical Society* **2004**, *126*, 301.

[139] L. L. Erskine, T. Emrick, A. P. Alivisatos, J. M. J. Frechet, *Abst. Pap. Am. Chem. Soc.* **2000**, *219*, U413.

[140] A. S. Susha, F. Caruso, A. L. Rogach, G. B. Sukhorukov, A. Kornowski, H. Mohwald, M. Giersig, A. Eychmüller, H. Weller, *Colloid Surf.* **2000**, *163*, 39.

[141] W. J. Yang, D. Trau, R. Renneberg, N. T. Yu, F. Caruso, *J. Colloid Interf. Sci.* **2001**, *234*, 356.

[142] N. P. Gaponik, I. L. Radtchenko, G. B. Sukhorukov, H. Weller, A. L. Rogach, *Adv. Mater.* **2002**, *14*, 879.

[143] M. Y. Han, G. X., J. Z. Su, S. M. Nie, *Nat. Biotech.* **2001**, *19*, 631.

[144] E. R. Goldman, G. P. Anderson, P. T. Tran, H. Mattoussi, P. T. Charles, J. M. Mauro, *Analytical Chemistry* **2002**, *74*, 841.

[145] A. R. Clapp, I. L. Medintz, J. M. Mauro, H. Mattoussi, *Abstracts of Papers of the American Chemical Society* **2003**, *226*, U490.

[146] I. L. Medintz, A. R. Clapp, H. Mattoussi, E. R. Goldman, B. Fisher, J. M. Mauro, *Nature Materials* **2003**, *2*, 630.

[147] N. O. Fischer, A. Verma, C. M. Goodman, J. M. Simard, V. M. Rotello, *Journal of the American Chemical Society* **2003**, *125*, 13387.

[148] D. M. Willard, L. L. Carillo, J. Jung, A. Van Orden, *Nano Letters* **2001**, *1*, 469.

[149] A. Sukhanova, M. Devy, L. Venteo, H. Kaplan, M. Artemyev, V. Oleinikov, D. Klinov, M. Pluot, J. H. M. Cohen, I. Nabiev, *Analytical Biochemistry* **2004**, *324*, 60.

[150] F. Pinaud, D. King, H.-P. Moore, S. Weiss, *J. Am. Chem. Soc.* **2004**, *126*, 6115.

[151] T. Stora, Z. Dienes, H. Vogel, C. Duschl, *Langmuir* **2000**, *16*, 5471.

[152] D. D. Lasic, *Liposomes: from physics to applications*, Elsevier, Amsterdam, **1993**.

[153] M. Jones, J. Nedeljkovic, R. J. Ellingson, A. J. Nozik, G. Rumbles, *J. Phys. Chem. B* **2003**, *107*, 11346.

[154] S. Maenosono, C. D. Dushkin, S. Saita, Y. Yamaguchi, *Jpn. J. Appl. Phys.* **2000**, *39*, 4006.

[155] S. Maenosono, N. Eiha, Y. Yamaguchi, *J. Phys. Chem. B* **2003**, *107*, 2645.

[156] S. R. Cordero, P. J. Carson, R. A. Estabrook, G. F. Strouse, S. K. Buratto, *J. Phys. Chem. B* **2000**, *104*, 12137.

[157] H. Asami, Y. Abe, T. Ohtsu, I. Kamiya, M. Hara, *J. Phys. Chem. B* **2003**, *107*, 12566.

[158] L. M. Fiske, Y. Subbarow, *J Biol chem* **1925**, *66*, 375.

[159] J. E. Bowen Katari, V. L. Colvin, A. A. P., *J. Phys. Chem* **1994**, *98*, 4109.

[160] S. F. Wuistler, A. Van Houselt, C. de Mello Donega, D. Vanmaekelbergh, A. Meijerink, *Angew. Chem. Int. Ed.* **2004**, *43*, 3029.

[161] C. M. Niemeyer, C. A. Mirkin, *Nanobiotechnology: Concepts, Applications and Perspectives*, Wiley-VCH, Weinheim, **2004**.

[162] M. Bäumle, D. Stamou, J.-M. Segura, R. Hovius, H. Vogel, *Langmuir* **2004**, *20*, 3828.

[163] K. E. Sapsford, I. L. Medintz, J. P. Golden, J. R. Deschamps, H. T. Uyeda, H. Mattoussi, *Langmuir* **2004**, *20*, 7720.

[164] J.-M. Nam, C. S. Thaxton, C. A. Mirkin, *Science* **2003**, *301*, 1884.

[165] J. R. Lakowicz, *Principles of fluorescence spectroscopy*, 2nd ed., Klumer Academic, New York, **1999**.

[166] J. Wiedenmann, A. Schenk, C. Rocker, A. Girod, K. D. Spindler, G. U. Nienhaus, *Proceedings of the National Academy of Sciences of the United States of America* **2002**, *99*, 11646.

[167] J. Porath, *Protein Purif. Expression* **1992**, *3*, 263.

[168] E. L. Schmid, T. A. Keller, Z. Dienes, H. Vogel, *Anal. Chem.* **1997**, *69*, 1979.

[169] E. G. Guignet, R. Hovius, H. Vogel, *Nature Biotechnology* **2004**, *22*, 440.

[170] S. A. Lauer, J. P. Nolan, *Cytometry* **2002**, *48*, 136.

[171] M. Wilchek, *Trends in Biol. Sci.* **1989**, *14*, 408.

[172] L. Stryer, *Biochemistry*, W. H. Freeman and Company, New York, **1995**.

[173] M. Rytömaa, P. K. J. Kinnunen, *J. Bio. Chem* **1995**, *270*, 3197.

[174] M. Subramanian, A. Jutila, P. K. J. Kinnunen, *Biochemistry* **1998**, *37*, 1394.

[175] P. Mustonen, J. A. Virtanen, P. J. Somerharju, P. K. J. Kinnunen, *Biochemistry* **1987**, *26*, 2991.

[176] M. Rytömaa, P. K. J. Kinnunen, *Biochemistry* **1996**, *35*, 4529.

[177] U. Kim, Y. S. Kim, S. Han, *Bull. Korean Chem. Soc.* **2000**, *21*, 412.

[178] J. Yang, X. Liu, K. Bhalla, C. N. Kim, A. M. Ibrado, J. Cai, T. Peng, D. P. Jones, X. Wang, *Science* **1997**, *275*, 1129.

[179] X. Liu, C. N. Kim, J. Yang, R. Jemmerson, X. Wang, *Cell* **1996**, *86*, 147.

[180] R. M. Kluck, E. Bossy-Wetzel, D. R. Green, D. D. Newmeyer, *Science* **1997**, *275*, 1132.

[181] P. Mustonen, J. Lehtonen, A. Köiv, P. K. J. Kinnunen, *Biochemistry* **1993**, *32*, 5373.

[182] P. Nicholls, *Biochim. Biophys. Acta* **1974**, *346*, 261.

[183] J. S. Vincent, H. Kon, I. W. Levin, *Biochemistry* **1987**, *26*, 2312.

[184] A. Muga, H. H. Mantsch, W. K. Surewicz, *Biochemistry* **1991**, *30*, 7219.

[185] P. J. R. Spooner, A. Watts, *Biochemistry* **1992**, *31*, 10129.

[186] P. J. R. Spooner, A. Watts, *Biochemistry* **1991**, *30*.

[187] P. J. R. Spooner, A. Watts, *Biochemistry* **1991**, *30*, 3871.

[188] T. J. T. Pinheiro, A. Watts, *Biochemistry* **1994**, *33*, 2451.

[189] H. H. J. de Jongh, T. Ritsema, A. Killian, *FEBS Lett.* **1995**, *360*, 255.

[190] P. K. J. Kinnunen, *Chem. Phys. Lipids* **1996**, *81*, 151.
[191] M. Rytömaa, P. Mustonen, P. K. J. Kinnunen, *J. Bio. Chem.* **1992**, *267*, 22243.
[192] I. L. Nantes, M. R. Zucchi, O. R. Nascimento, A. Faljoni-Alario, *J. Bio. Chem* **2001**, *276*, 153.
[193] E. J. Choi, E. Dimitriadis, *Biophys. J.* **2004**, *87*, 3234.
[194] W. Jordi, Rijks University (Utrecht), **1990**.
[195] R. Hovius, E. L. Schmid, A. P. Tairi, H. Vogel, *J. Receptor and Signal Trans. Research* **1999**, *19*, 533.
[196] D. Axelrod, T. P. Burghardt, N. L. Thompson, *Annu. Rev. Biophys. Bioengin.* **1984**, *13*, 247.
[197] D. Axelrod, *Meth. Enzymo.* **2003**, *361*, 1.
[198] N. L. Thompson, K. H. Pearce, H. V. Hsieh, *Eur. Biophys. J. Biophys. Lett.* **1993**, *22*, 367.
[199] M. Toriumi, H. Masuhara, *Spectrochimica acta reviews* **1991**, *14*, 353.
[200] A. Kumar, H. A. Biebuyck, G. M. Whitesides, *Langmuir* **1994**, *10*, 1498.
[201] Y. Xia, G. M. Whitesides, *Angew. Chem. Int. Ed. Engl.* **1998**, *37*, 550.
[202] A. Kumar, G. M. Whitesides, *Appl. Phys. Lett.* **1993**, *63*, 2002.
[203] A. Bernard, E. Delamarche, H. Schmid, B. Michel, H. R. Bosshard, H. Biebuyck, *Langmuir* **1998**, *14*, 2225.
[204] D. Stamou, C. Duschl, E. Delamarche, H. Vogel, *Angewandte Chemie-International Edition* **2003**, *42*, 5580.
[205] P.-Y. Bolinger, D. Stamou, H. Vogel, *J. Am. Chem. Soc.* **2004**, *126*, 8594.
[206] N. Yan, Y. Shi, *Nature struct. Bio.* **2003**, *10*, 983.
[207] H. Mueller, H.-J. Butt, E. Bamberg, *J. Phys. Chem. B* **2000**, *104*, 4552.
[208] B. Mazzanti, M. Vergelli, P. Riccio, R. Martin, H. F. McFarland, G. M. Liuzzi, L. Amaducci, L. Massacesi, *Journal of Neuroimmunology* **1998**, *82*, 96.
[209] J. Petersen, P. G. Wilmann, T. Beddoe, A. J. Oakley, R. J. Devenish, M. Prescott, J. Rossjohn, *J. Biol. Chem.* **2003**, *278*, 44626
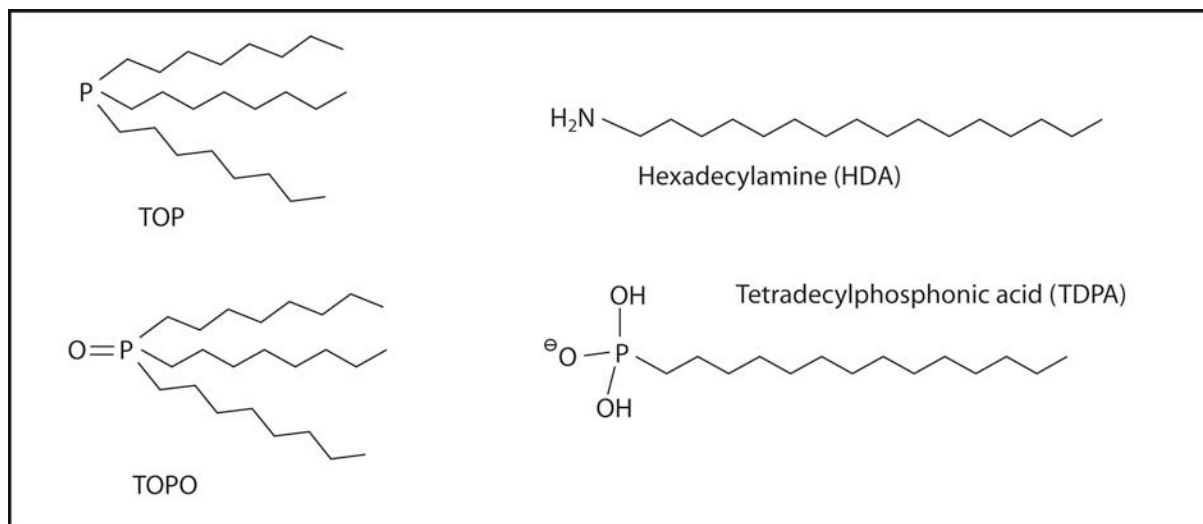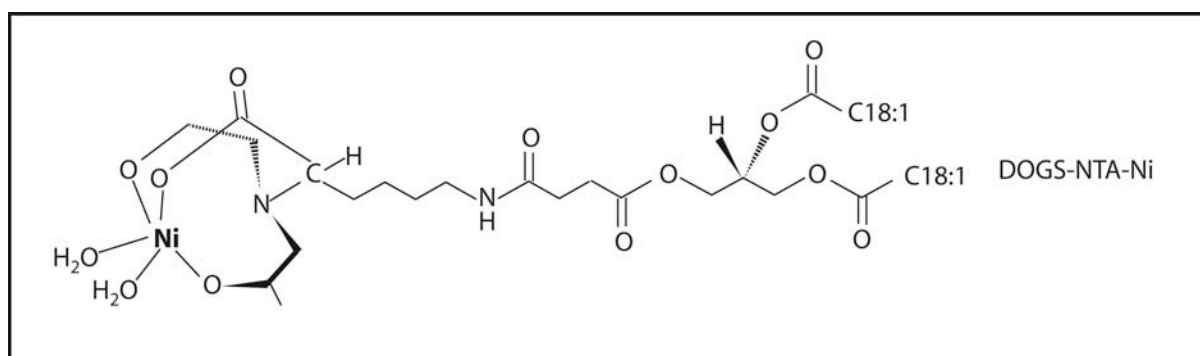
Abbreviation List
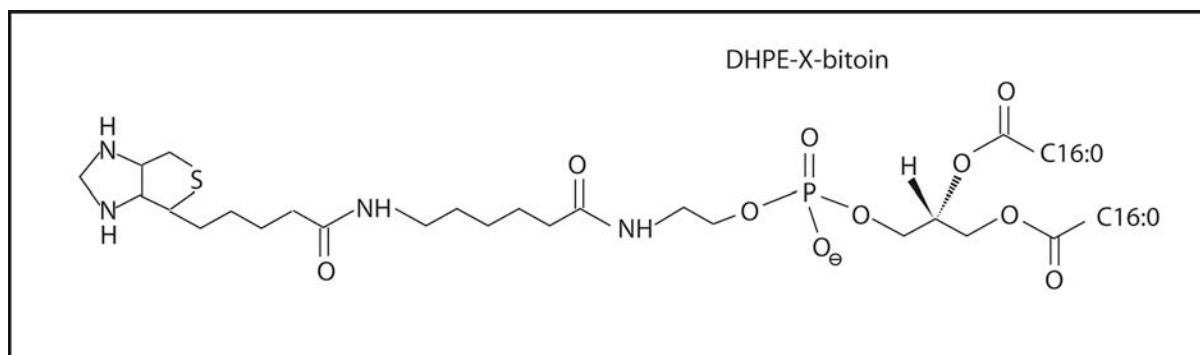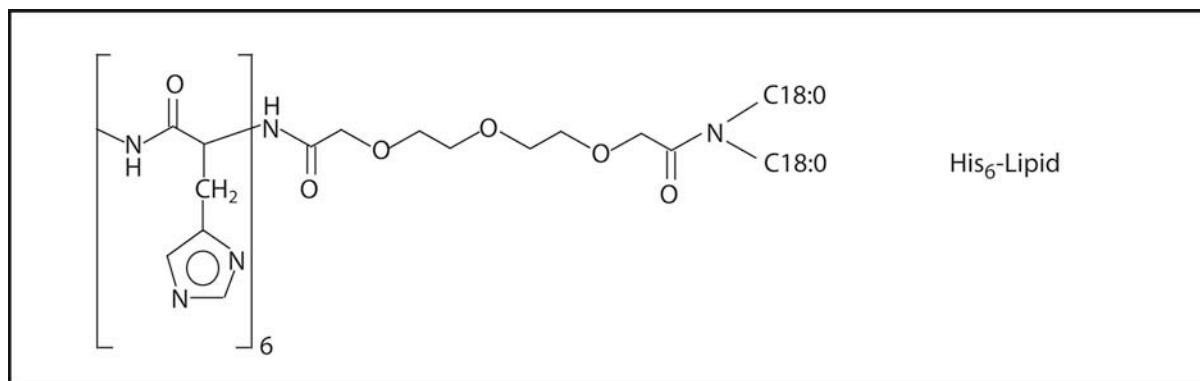
A	Acceptor
Å	Angstrom
biotin-NCs	Biotin functionalized NCs
biotin/NTA-NCs	Biotin and NTA functionalized NCs
BSA	Bovin Serum Albumin
BSA-biotin	Biontinylated Bovin Serum Albumin
$Cd(Me)_2$	Dimethyl cadmium
CM	Confocal Microscopy
CMC	Critical Micellar Concentration
CSEM	Centre Suisse d'Electronique et Microtechnique
Cryo-EM	Cryogenic Electron Microscopy
Cyt c	Cytochrome c
D	Donor
DHPE-X-biotin	N-((6-(biotinoyl)amino)hexanoyl)-1,2-dihexadecanoyl-sn-glycero-3-phosphoethanolamine, triethylammonium salt
DOS	Density of states
DPPC	Dipalmitoyl phosphatidyl choline
EDTA	Ethylenediamine tetraacetate
eV	Electron Volt
FPB	Fluorescence Photobrightening
FRET	Fluorescence Resonnance Energy Transfer
FTIR	Fourier Transformed Infrared spectroscopy
Functionalized-NCs	Nanocrystals decorated with functionalized lipids
FWHM	Full Width at Half Maximum
HDA	Hexadecyl amine
Histag	Polyhistidine tag
His_6-NCs	Hexahistidine-functionalized NCs
HOMO	Highest Occupied Molecular Orbital

144

HPA	Hexadecylphosphonic acid
IR	Infrared
Lipid-NCs	Lipid coated nanoparticles
LUMO	Lowest Unoccupied Molecular Orbital
LSM	Laser scanning confocal microscopy
M	Mol/l
MF-NCs	Multi-functionalized NCs
mMPG	Monomiristoyl phosphatidyl glycerol
mPPG	Monopalmitoyl phosphatidyl glycerol
NC	Nanocrystal
Ni-NTA-DOGS	1,2-dioleoyl-sn-glycero-3-[N-(5-amino-1-carboxypentyl)iminodiacetic acid succinyl] nickel salt
nm	Nanometer
NP	Nanoparticle
NSB	Nonspecific binding
NTA-NC	NTA-functionalized NCs
NTA	Nitrilotriacetic acid
OD	Optical Density
OG	Octylglucopyranoside
OPA	Octylphosphonic acid
PA	Phosphonic acid
PBS	Phosphate Buffer Saline
PDMS	Poly(dimethylsiloxane)
PEG	Polyethyleneglycol
PEG-PC	Polyethyleneglycol-functionalized phosphatidyl choline
PG	Phosphatidyl glycerol lipid
PL	Photoluminescence
PMMA	Poly(methylmethacrylate)
POPC	Palmitoyloleyl phosphatidyl choline
POPG	Palmitoyloleyl phosphatidyl glycerol
QD	Quantum dot (Qdots)
QY	Quantum Yield
SA	Stearic acid
Se:TOP	TOP complexed Selenium

SM	Single Molecule Spectroscopy
SPR	Surface plasmon resonance
TBP	Tributylphosphine
TDPA	Tetradecylphosphonic acid
TEM	Transition Electron Microscopy
TIRF	Total Internal Reflection Fluorescence
Tof-SIMS	Time of Flight Second Ion Mass Spectroscopy
TOP	Trioctylphosphine
TOPO	Trioctylphosphin oxide
TOPO-NC	TOPO-coated nanocrystal
UV	Ultra violet
XPS	X-rays Photoelectron Spectroscopy

Chemical structures

TOP

Hexadecylamine (HDA)

Tetradecylphosphonic acid (TDPA)

TOPO

Octyl-β-D-glucopyranoside (OG)

POPC

POPG

His₆-Lipid

DHPE-X-bitoin

DOGS-NTA-Ni
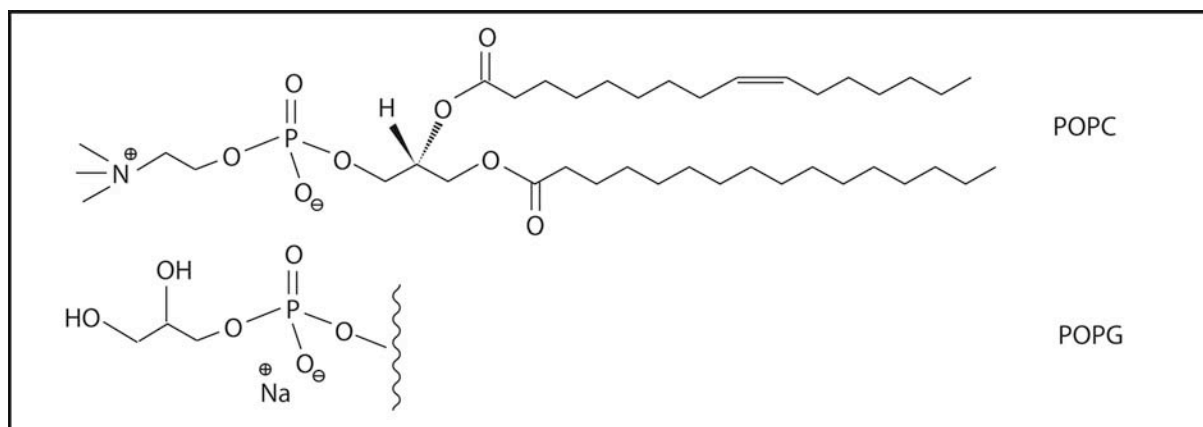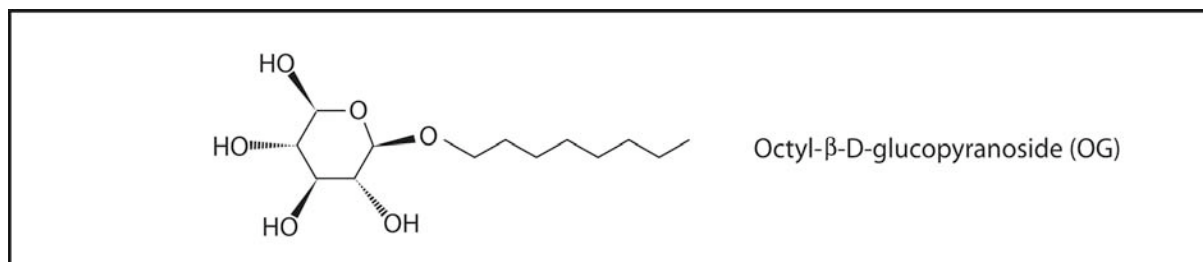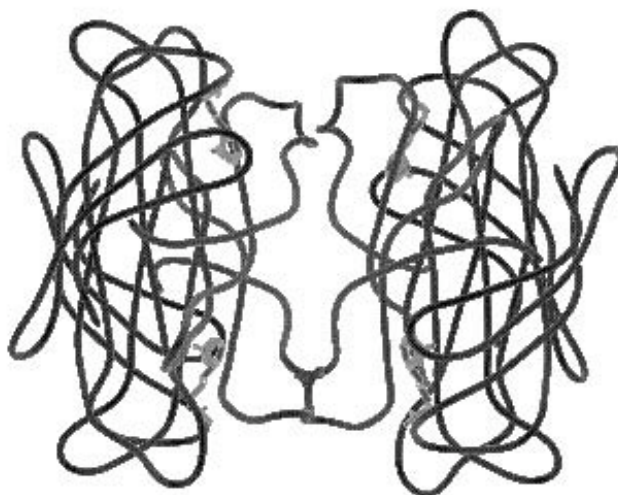
Schematic structure of streptavidin, the four biotins binding sites are represented in gray with a molecular weight of 60 kDa (taken from www).
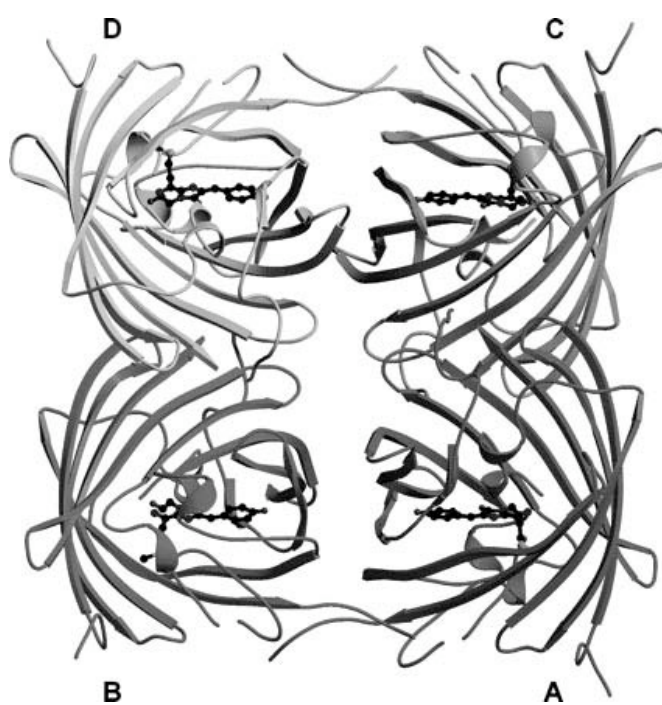
Schematic structure of the protein eqFP611-His$_6$ with molecular weight of 26 kDa [209].
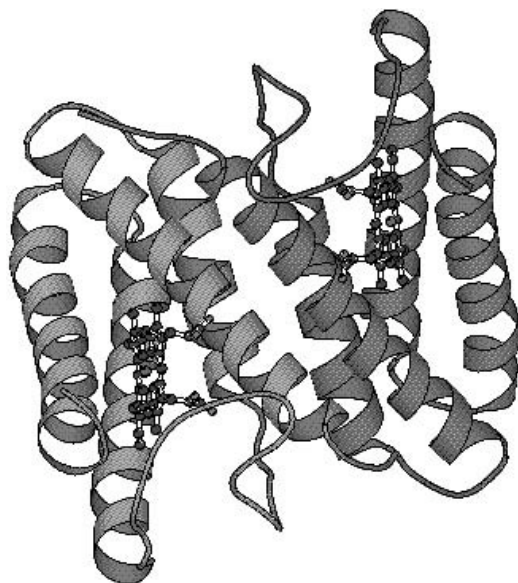
Schematic structure of cytochrome c with a molecular weight of 13 kDa (Taken from the www).

Acknowledgements

A special thank to **Hervé** and **Pascal** who shared the same office for 3 years and supported my work frustrations, but also for the good moments of fun! And to **Bernard** and **Raphael** for good company!

A special thank to the secretaries **Mme Tabet, Mme Gontier and Mme Gourdou**, I was lucky to have them for any required help and more...

A great thank to my favorite lunch partners, **Ashwini, Maja** and **Nam Hee**!!

But I also want to thank all **my friends** for the good moments outside of EPFL, my **family** who always supported me in everything I do, and finally **Tobias** for all his psychological support.

Curriculum Vitae

Isabelle Geissbühler Bärlocher

César Roux, 26   16.02.1975

1005 Lausanne   Married

Tel: ++41 216933113   Nationality: Swiss, French

E-mail: isabelle.geissbuehler@epfl.ch

Education

2000-present	Swiss Federal Institute of Technology Lausanne (EPFL), **PhD** in Chemistry. Domain: semiconductor nanoparticles: Surface modification and functionalization for specific interactions with biomolecules and immobilization on micropatterns.
1994-1999	University of Lausanne (UniL), Chemistry. **Chemist Diploma.** Diploma-work on synthesis of novel organometallic molecules for Organic Light Emitting Diodes (OLED).
1993-1994	EPFL, Special mathematics course, **Federal Maturity Equivalence.**
June 1993	**French Baccalauréat scientific section** (Annemasse, France)

Publications

I. Geissbuehler, R. Hovius, K. L. Martinez, M. Adrian, K. R. Thampi and H. Vogel, Lipid-Coated Nanocrystals as Multifunctionalized Luminescent Scaffolds for Supramolecular Biological Assemblies, *Angew. Chem. Intl. Ed.*, 2005, **44**, 1388-1392.

C. Minelli, I. Geissbuehler, R. Eckert, H. Vogel, H. Heinzelmann and M. Liley, Organization of nanoscale objects via polymer demixing, *Colloid. Polym. Sci.* (2004) **282**, 1274-1278.

I. Geissbuehler, R. Hovius and H. Vogel, Lipid-Coated Nanocrystals as Fluorescent Model Membranes. Interaction with the Peripheral Protein Cytochrome c, in preparation.

Professional experiences

2000   **Teaching** in <u>Centre Doret</u> in Vevey, chemistry and physics, **4 months**.

1998   **Internship** in <u>R&D Nestlé</u>, Vers-Chez-les-Blancs. Comparison of different analytical methods for frying oil degradation; development of a new method using infrared spectroscopy, **2 months**.

Languages

French   mother tongue
English   good oral and written
German   medium level   *Swiss German:* oral
Spanish   medium level